Spin phenomena in semiconductor quantum dots

Jorge Luis Puebla Nunez

Department of Physics and Astronomy

University of Sheffield

A thesis submitted for the degree of

Doctor of Philosophy

December 2012

I would like to dedicate this thesis to the most important co-authors of my life... To my loving parents:

Fernando Puebla y Ma. Transito Nuñez

Sisters and brothers:

Elsa, Aurora, Hector y Carlos

"What is an electron, anyway? Physicists see them, primarily, as great criminals. Perverse and canny little subjects who, after committing countless atrocities, somehow manage to slip away. No doubt there are clever types, and every effort to track them down only encourage them to perform the most devilish escape tactics. With the skill of trapeze artists, they are capable to leaping from one place to another without us even realising it. They fire away mercilessly when they see the enemy approaching, and they always keep an alibi ready to sabotage any investigations. Some observes have even come to believe that they don't operate alone, but rather in gangs of like-minded villains. Either that, or they possess something akin to a manipulate personality disorder. The individual electron behaves not as a single entity but as a team, a swarm of desires and appetites, a storm cloud of violent emotions that blasts through the wide reaches of space, swirling around the objective at its mercy"[1].

Jorge Volpi

[1]In Search for Klingsor - Jorge Volpi. English version first published in 2004, first original version in Spanish published 1999

Acknowledgements

It has been my pleasure to work in the LDSD group in Sheffield during my PhD project. And I would like to acknowledge first at all to my supervisor Alexander Tartakovskii (Sasha) who has been excellent guide and advisor during my whole PhD. I would also like to thanks to Prof. Maurice Skolnick, whose dedication for research is a great motivation for the whole group. I would also like to express a great thanks to Odilon for incredible support and hard work, I could not have any better college and friend during the first part of my PhD. I would also like to say a big thank you to Evgeny, who is a brilliant physicist and hard worker, for all his help and constructive criticism during all this time, I have learned a lot from you. I would also like to thank Claire Elliot and N. Babazedah for all the support during my first weeks in the department.

I would like to thank Andrew Ramsay, Tim for give me the opportunity of taking part as device processing support of the coherent control project and for your invaluable friendship. Many thanks to all the group members of the LDSD, in particular: D.J. Mowbray, A.M. Fox, D.M. Whittaker, P. Kok, D.N. Krizhanovskii, L.R. Wilson, I.J. Luxmoore, M.N. Makhonin, D. Sarkar, F. Fras, P. M. Walker, Ehsaneh, Maksym, Osvaldo, Lloyd, Rikki, Nathan, Daniel, Andrew, Romain, John, Kuru, Chris, P. Commin, Rob, the staff of the EPSRC National Centre for III-V Technologies in particular: Rob Airey, Andrey Krysa, M. Hopkinson, K. Kennedy, Paul Fry, John Milner, the cryogenics and workshop staff for the hard work, in particular: C. Vickers, P. Robinson, P. Kemp-Russell, Simon Dixon. Many thanks to all the staff from the departmental office. Thanks to our collaborators P. Senellart and A. Lematre from CNRS (France), A.M. Sanchez

and R. Beanland from University of Warwick, K.V. Kavokin from Ioffe Institute (Russia). Finally enormous thank you to CONACyT (Mexico) for the PhD funding.

Many thanks to all my friends back home in Mexico and here in UK, in particular during this journey: Miriam, Marta, Javier, Obed, Corina and Liz Diskin, Lizz Cedillo for the time we shared living together, rest of the mexican crowd and internationals... Cheers!

Massive thanks to my family: my Mum, Dad, Sisters, Brothers without all your support this could not happen. MUCHAS GRACIAS!

Jorge Puebla

Sheffield, December 2012.

Abstract

This thesis discusses development of new semiconductor quantum dot (QD) devices and materials. Optical spectroscopy of single QDs is employed in order to investigate electronic structure and magnetic properties of these materials. First we realise self-assembled InP/GaInP QDs embedded in Schottky diode structures, with the aim to realise charge control in these nanostructures, which recently provided an important test-bed for spin phenomena on the nano-scale. By varying the bias applied to the diode, we achieve accurate control of charge states in individual QDs, and also characterise the electron-hole alignment and the lateral extent of the exciton wavefunction. Second part of the thesis explores optimum regimes for optically induced dynamic nuclear polarization (DNP) in neutral InGaAs/GaAs QDs. Very efficient DNP under ultra low optical excitation is demonstrated, and its mechanism is explained as the electron-nuclear flip-flop occurring in the second order process of the dark exciton recombination. The final part of the thesis reports on magneto-optical studies of novel individual InPAs/GaInP quantum dots studied in this work for the first time. Here the long-term aim is to realise strong carrier confinement potentially suitable for QD operation at elevated temperatures, e.g. as a single photon emitter. Here we lay foundations for future structural studies of these dots using optically detected nuclear magnetic resonance, and explore regimes for efficient DNP in InPAs dots emitting in a wide range of wavelength 690-920 nm.

Contents

Contents **vi**

List of Figures **ix**

Nomenclature **xv**

1 Introduction **1**

1.1 Background and motivation 1

1.2 Self-assembled quantum dots - fabrication 5

1.2.1 Epitaxial methods for fabrication of self-assembled quantum dots 8

1.2.1.1 Molecular beam epitaxy 8

1.2.1.2 Metal organic chemical vapor deposition 10

1.3 Optical techniques for studies of QDs 11

1.3.1 Non-resonant optical excitation 12

1.3.2 Resonant optical excitation 14

1.4 Electron-hole complexes in quantum dots 15

1.5 Conclusions 19

2 Charge control in InP/GaInP single quantum dots embedded in Schottky diodes **29**

2.1 Introduction 29

2.2 Experimental 32

2.3 Results 33

2.3.1 Ensemble characterization 33

2.3.2 Single dot properties 35
2.3.3 Exciton wavefunction 38
2.3.4 Photocurrent of single dots 44
2.4 Conclusions 45

3 Dynamic nuclear polarization in InGaAs/GaAs quantum dots under non-resonant ultra-low power optical excitation 51
3.1 Introduction 51
3.2 Techniques and samples 53
3.3 Photoluminescence spectroscopy of dark and bright exciton states in neutral quantum dots 54
3.4 Dynamic nuclear polarisation in neutral quantum dots at ultra-low excitation power 58
3.4.1 Detection of nuclear spin polarisation in quantum dots . . 58
3.4.2 Dynamic nuclear polarisation at ultra-low optical powers in InGaAs quantum dots 60
3.5 Conclusions 68

4 Magneto - spectroscopy and dynamic nuclear polarisation of InPAs/GaInP quantum dots 73
4.1 Introduction 73
4.2 Techniques and samples 75
4.2.1 Transmission electron microscopy characterization 77
4.3 Photoluminescence spectroscopy of InPAs/GaInP quantum dots . 77
4.3.1 Photoluminescence detection of single InPAs/GaInP quantum dots 80
4.4 Magneto - spectroscopy of individual InPAs/GaInP quantum dots 82
4.4.1 Using magneto-optics for determination of the QD charging 84
4.4.2 Dynamic nuclear polarisation in InPAs/GaInP quantum dots 86
4.5 Conclusions 94

5 Conclusions and future work 99
5.1 Conclusions 99
5.2 Future work 101

5.2.1 Coherent control in InP/GaInP quantum dots 101
5.2.2 Voltage control of nuclear spin polarisation 102
5.2.3 Inverse nuclear magnetic resonance for material characterization 102

Appdx A **105**
.1 Quantum dot Schottky diode structure 105
.1.1 Device processing 106

Appdx B **109**
.2 CCD Detection System 109

List of Figures

1.1 Stranski - Krastanov formation of quantum dots. a) GaAs substrate, b) InAs monoatomic layer deposition, c) Formation of InAs nano-islands, d) GaAs capping layer on top of InAs QDs. The inset on the left hand side, shows the strain form by the difference in lattice constants of the two semiconductor materials. In the upper inset typical TEM image of a Stranski-Krastanov QD is shown. . 7
1.2 Schematic of principal elements of molecular beam epitaxy reactor (MBE). 9
1.3 Schematic of principal elements of metal organic chemical vapor deposition system (MOCVD) 10
1.4 Optical excitation techniques. Top panel shows non-resonant optical excitation which creates carriers in the barriers. Bottom panel shows resonant optical excitation which generates e-h pairs in the dot transitions. 12
1.5 Comparison of a PL spectra of a QD ensemble under optical excitation with a laser beam diameter of $\sim 100\mu m$ (gray spectrum), and $\mu - PL$ spectra of a QD ensemble (black spectrum) under optical excitation with a laser beam diameter of $\sim 2\mu m$ and nano-apertures for optical access $\sim 400nm$ (inset). 13
1.6 A typical micro-photoluminescence (micro-PL) set-up including the sample attached to a three-dimensional piezo-positioner with electrical connections, which is immersed into a superconducting magnet. The laser beam is focused in a $\approx 2\mu$m spot on the sample by the lens with a short focal length. 14

1.7 Principle of photocurrent detection. QD embedded in a Schottky diode structure. (a) Resonant excitation with an optical transition creates an electron-hole pair. (b) When applied electric field the carriers scape from the dot and are detected as a change in photocurrent. 16

1.8 Exciton complexes in semiconductor quantum dots. Photon-generated carriers are represented by blue solid (electron) and open (hole) circles, while resident carrier are red solid (electron) and open (hole) circles. From left to right hand we have neutral exciton (X^0), negative exciton (X^{-1}), positive exciton (X^{+1}) and biexciton (XX^0). 18

1.9 Charging of a quantum dot embedded in a Schottky diode structure. Top panel shows the charging control of a single hole under forward bias. The bottom panel shows a typical PL spectra of a InGaAs neutral and singly positive charge exciton (left), and ratio of X^+/X^0 under applied bias. 20

2.1 μPL spectra of InP/GaInP QD ensembles measured with HeNe laser (λ=632 nm). Spectra for samples with d_{InP} varying from 1.65Å to 4.4 Å are shown for laser excitation powers: (a) $P = 5\mu$W and (b) $P = 0.15\mu$W. (c) Spectrum of a QD ensemble grown with d_{InP}=11Å measured at $P = 15\mu$W. 34

2.2 (a) Single QD μPL as a function of the bias applied between the n and Schottky contacts. (b) Linear polarisation resolved PL measured at -2.55 V for the X_0 and X^{-1} lines shown on (a). The black and red lines represent polarisation parallel to the [110] and [1$\bar{1}$0] crystallographic directions, respectively. (c) Negatively charged exciton (X^{-1}) binding energy for samples A (black dots) and B (empty squares) against E_0, the energy of the neutral exciton at zero field. (d) Distribution of the X^{-1} binding energy. (e) Neutral-exciton energy E_{X0} as a function of the applied electric field F_z. Inset shows the values of p and β obtained from the fit to the data (solid curve). 37

2.3 (a) Permanent dipole moment p and (b) polarisability β plotted against the neutral exciton energy E_0 for samples A (dots) and B (empty squares). In (a), the inset shows the distribution of the electron-hole separation r. In (b), the inset shows the extent of the hole wavefunction along **z** direction ($L_{h,z}$) for sample A. (c) Permanent dipole moment p against polarisability β for samples A and B. Solid lines are linear fits to the data. 39

2.4 Photocurrent a neutral exciton state X_0 measured in a single InP QD for different excitation-laser energies. The 2D-plot inset shows, for comparison, the μPL bias dependence of X_0 for the same single QD. The upper inset illustrates the measurement procedure, where the laser is fixed at different excitation energies E_{LD}, and the QD energy is tuned by the applied bias and brought in resonance with the laser, as described in the text. 42

3.1 PL spectrum of neutral InGaAs QD1, measured in external magnetic field applied along the sample growth axis $B_Z = 8T$. Two spectra are shown: at ultra-low optical excitation power $P_{exc} = 11nW$ (bottom spectrum) and at high power $P_{exc} = 3\mu W$ (top spectrum). In a neutral quantum dot heavy holes $(\Uparrow, \Downarrow)$ and electrons $(\uparrow, \downarrow)$ with spins parallel (antiparallel) can form optically allowed "bright" states ($|\Uparrow, \downarrow>$,$|\Downarrow, \uparrow>$) and forbidden "dark" states ($|\Uparrow, \uparrow>$,$|\Downarrow, \downarrow>$) with total spin projections $J_Z = |+1>(|-1>)$ and $J_Z = |+2>(|-2>)$ respectively. At ultra low excitation power all four (bright and dark) excitons are observed in PL spectrum. At high power, PL of dark states is saturated and only bright states are observed. 55

3.2 Magnetic - field dependence of exciton PL energies in InGaAs QD2. Open symbols represent bright states $|\Uparrow, \downarrow>$ (circles) and $|\Downarrow, \uparrow>$ (squares), while solid symbols correspond to dark states $|\Uparrow, \uparrow>$ (circles) and $|\Downarrow, \downarrow>$ (squares). Lines show fitting using Eq. 1 allowing electron and hole g-factors to be determined (see details in text). 57

3.3 Schematic representation of the electron-nuclei hyperfine interaction. Circular polarisation excitation transmit angular momentum to the electron which is then transmitted to the nuclei. Polarised nuclei create and effective Overhauser field B_N acting on the electron, in turn the polarised electrons create and effective Knight field B_e which acts back on the nuclei. 59

3.4 PL emission of all four exciton transitions in presence of positive (open squares) and negligible (solid circles) nuclear polarisation is shown. Zeeman energy splitting of bright states ($|+1>, |-1>$) is enhanced by Overhauser field. 61

3.5 Results of power dependence measurements on InGaAs neutral quantum dot QD2 at $B_Z = 7T$ under σ^+ (open symbols) and σ^- (solid symbols) optical pumping. PL intensities of all bright and dark exciton states are shown at the top of the graph (left scale). Overhauser shift $E_{OHS} = \Delta E_{|\Uparrow\downarrow>,|\Downarrow\uparrow>} - \Delta E^0_{|\Uparrow\downarrow>,|\Downarrow\uparrow>}$ is shown at the bottom of the graph with diamonds (right scale). Additional scale on the right shows effective nuclear field B_N. Vertical dashed line at $P_{exc} \sim 5\mu eV$ shows an approximate boundary between two distinct nuclear spin pumping mechanisms: low power DNP via second order recombination of dark excitons and high-power DNP due to spin transfer from spin polarised excitons/electrons (see explanation in the text). 62

3.6 Energy diagram of exciton states in high magnetic field $B_Z > 5T$. Heavy holes $(\Uparrow, \Downarrow)$ and electrons $(\uparrow, \downarrow)$ with spins parallel (antiparallel) to B_Z form optically allowed "bright" excitons ($|\Uparrow, \downarrow>, |\Downarrow, \uparrow>$) and "dark" excitons ($|\Uparrow, \uparrow>, |\Downarrow, \downarrow>$) with total spin projections $J_Z = |+1>(|-1>)$ and $J_Z = |+2>(|-2>)$ respectively. Zigzag lines show electron-nuclear (e-N) spin flips induced by the hyperfine interaction. 65

3.7 Power dependence measurements on InGaAs neutral quantum dot QD2 under σ^+ optical pumping at $B_Z = 5T$ (top), $B_Z = 7T$ (middle) and $B_Z = 8T$ (bottom). Overhauser shift $E_{OHS} = \Delta E_{|\Uparrow\downarrow>,|\Downarrow\uparrow>} - \Delta E^0_{|\Uparrow\downarrow>,|\Downarrow\uparrow>}$ is shown in the left scale. Additional scale on the right shows effective nuclear field B_N, deduced by $B_N = \frac{E_{OHS}}{\mu_B g_e}$. Horizontal dash lines show B_N values for all three B_Z : $B_N = 1.8T for B_Z = 5T$, $B_N = 3.2T for B_Z = 7T$ and $B_N = 2.7T for B_Z = 8T$. Sketch of the energy separation between bright and dark states for each B_z is presented on the right hand side. 66

3.8 Power dependence measurements on InGaAs neutral quantum dot QD2 under σ^+ optical pumping at B_Z ranging from $0T$ to $8T$. Overhauser shift $E_{OHS} = \Delta E_{|\Uparrow\downarrow>,|\Downarrow\uparrow>} - \Delta E^0_{|\Uparrow\downarrow>,|\Downarrow\uparrow>}$ is represented by color code and shown in the left scale. Horizontal dashed line at $P_{exc} = 1\mu W$ shows an approximate boundary between two distinct nuclear spin pumping mechanism: low-power DNP via second order recombination of dark excitons and high-power DNP due to spin transfer from spin polarised excitons/electrons. 67

4.1 Transmission electron microscope images of InP (a) and InPAs (b) quantum dots. InP QD is larger at the base and shorter in high than InPAs QD. InPAs QD shows a bright capping layer defining a core-shell structure. 78

4.2 PL spectra of InP/GaInP (top) and InPAs/GaInP (bottom) quantum dots sample grown with 16.7 sccm AsH_3 is shown. The top spectrum (black) shows PL emission of InP/GaInP QDs centered around 730 nm, while the bottom spectrum (red) shows sharp peaks corresponding to single quantum dot emission in a broad range of wavelength, from 670 nm up to 940 nm for InPAs/GaInP QDs. 79

4.3 Position dependent PL spectra of InPAs/GaInP QD wafer with 16 sccm. From bottom to top (A-F) indicates the increasing distance to the material source in the chamber, the black arrow indicates the direction of the flow (inset). All PL spectra were taken at optical excitation power of $P_{exc} = 200nW$ and 20 sec of integration time. 80

4.4 Typical PL spectra measured at $B_Z = 0T$ of single InPAs QDs using linearly polarised excitation and σ^+ (black) detection. Top caption shows PL of single quantum dot at low energy $E_{PL} \approx 1.3280eV$ (QD1). Bottom caption shows PL of single quantum dot at high energy $E_{PL} \approx 1.7647eV$ (QD2). Dashed lines show FWHM for both QDs. 81

4.5 PL spectra of InPAs/GaInP single quantum dots at external magnetic field $B_Z = 3T$, and excitation energy $E_{exc} = 1.88eV$. Typical PL spectra of single dot emission at $E_{PL} = 1.830eV$ (a), $E_{PL} = 1.4195eV$ (b) and $E_{PL} = 1.3773eV$ (c) are shown. Energy Zeeman splitting is indicated for each QD with values equal to $\Delta E_{Zemman} = 302\mu eV$ (a), $\Delta E_{Zemman} = 235\mu eV$ (b) and $\Delta E_{Zemman} = 204\mu eV$ (c) respectively. 83

4.6 A typical magnetic field dependence of PL spectra from an InPAs/GaInP quantum dot measured 16.7 sccm sample at 4.2K under non-resonant excitation in σ^+ and σ^- in Faraday geometry and in orthogonal π_1, π_2 linear polarisations in Voigt geometry, where a typical trion behaviour is observed with four peaks. Trion peak energies from spectra in (a) versus external magnetic field. g-factors and exciton diamagnetic shifts are found fitting the curves (solid lines) with equations 1, 2 and 3. 85

4.7 The electron g-factors (g_e) of InPAs/GaInP quantum dots for sample with 16.7sccm of As flux. The g_e increase with energy dot emission following a trend. 87

4.8 PL spectra of InPAs/GaInP quantum dots measured with two circularly polarised optical excitation σ^- (red circles) and σ^+ (gray squares) at $B_Z = 0.5T$. Energy splitting difference between spectra reflects Overhauser shift values according to $\Delta E_{OHS} = \frac{\Delta E_{\sigma^+} - \Delta E_{\sigma^-}}{2}$. Solid curves represent the Gaussian fits to extract ΔE_{σ^+} (gray) and ΔE_{σ^-} (red). For the low energy dot $\Delta E_{OHS} = 29.5\mu eV$ (a) and for high energy dot $\Delta E_{OHS} = 52.5\mu eV$ (b). 89

4.9 Magnetic field dependence of Overhauser shift ΔE_{OHS} for QD5. For each B_Z two spectra representing σ^+ and σ^- are presented. Bottom panel shows summary of the ΔE_{OHS} dependence on B_Z. . 90

4.10 Quantum dot emission energy dependence of Overhauser shift at $B_Z = 3$ T using three different optical excitation energies. $E_{exc} =$ 1.88 eV (solid squares), $E_{exc} = 1.80eV$ (open circles) and $E_{exc} =$ 1.53 eV (solid triangles). 92

4.11 Quantum dot emission energy dependence of Overhauser field B_N. Trend of Overhauser shifts (OHS) at $B_Z = 3$ T see fig. 4.10, is divided by Bohr Magneton μ_B and g_e trend, see fig. 4.7. 93

1 Schematic of quantum dot Schottky diode structures. Sample A used in chapter 2 is presented in top panel (a), and sample B used in the same chapter is presented in bottom panel (b). 106

2 Photograph of fully finished quantum dot Schottky device. Labels indicate the Ohmic contact (bottom), Schottky contact, Large mesas, small mesas. Beneath the Schottky contact and across the mesa a semi-transparent Titanium layer of 8-10nm thick is indicated. 107

3 Nano-apertures for micro-PL characterisation. Top panel shows a optic microscope photograph of the array of apertures with sizes from 400 to 1000nm (a). Bottom panel shows a SEM image of one aperture with dimension of about $1\mu m$ (b). 108

4 Quantum efficiency curves of Spectrum One CCD3000 chips. Top panel shows Q.E. curves for SiTe chips, and bottom panel Q.E. curves for EEV CCD chips. 110

Chapter 1

Introduction

1.1 Background and motivation

Semiconductor QDs are nano-objects with dimensions smaller than the electron de Broglie wavelength. QDs confine carriers in all three directions resulting in quantization of their energy levels resembling electronic levels in atoms. Therefore, semiconductor QDs systems are often referred to as artificial atoms [1, 2]. Their properties can be tailored by using a wide variety of semiconductor materials and several growth methods [3, 4, 5, 6, 7]. Semiconductor QDs have been actively investigated in the last 20 years or so. Most active and successful research directions have been development of QD lasers [8, 9, 10], single photon emitters for quantum cryptography applications and quantum optics [11, 12, 13, 14], and spin and charge qubits for quantum information processing [15, 16, 17, 18]. In this thesis studies of three types of single quantum dots, InP/GaInP, InGaAs/GaAs and InPAs/GaAs, are presented, addressing new physics, materials and QD device development. Work reported in this thesis has been mostly motivated by research into possible future applications of single quantum dots in

quantum computation and generation of non-classical light.

In the last 10 years, significant progress has been made in demonstration of the potential use of QDs for control of spin qubits. First theoretical proposals for a qubit based on the spin of the electron confined in a QD, were made in the late 90's by Loss, DiVincenzo and co-workers [15]. Within several years, electrically and optically addressable QD systems where single electrons could be identified and manipulated were reported [19, 20, 21, 22, 23]. This followed shortly by demonstration of various ways of spin manipulation [24, 25, 26, 27]. Since then, in optical investigations, preference was given to self-assembled InGaAs/GaAs QDs grown by molecular beam epitaxy (MBE) [3]. In this type of dots a reasonably strong confinement (exceeding 100 meV for electrons) can be achieved. In addition, high quality GaAs can be grown, which ensures high stability of the charge environment of the QD [28, 29]. In electron transport measurements, where most advanced spin manipulation has been demonstrated to date, QDs were lithographically defined by metallic gates on the sample surface about a hundred nm above a two dimensional electron gas in a high quality GaAs/AlGaAs quantum well. In such dots, electron charge and spin could be controlled by applying bias to the metallic gates [30, 31, 20].

The spin of the confined electron in a QD made of III-V semiconductor experiences the hyperfine interaction with 10^4-10^6 nuclear spins. This interaction is usually quantified by an effective Overhauser magnetic field, B_N, reaching in some cases up to a few Tesla for highly polarised nuclear spin system, and having a fluctuating part of a few mT [32, 33, 34, 35, 36, 37]. The presence and dynamic properties of the Overhauser field have a significant impact on the behavior of the electron and hole spin, and accordingly have received close attention in the

development of the QD spin qubit [38, 15]. Very high nuclear polarisation degrees now routinely achievable in QDs have also enabled sensitive nuclear magnetic resonance (NMR) to be realised for non-invasive probing of chemical composition and strain in the volume occupied by the confined electron [39, 40].

Optical studies of nuclear spin phenomena have been conducted in a range of QD materials, including self-assembled InGaAs/GaAs and InP/GaInP QDs and so-called interface (and nearly strain-free) GaAs/AlGaAs QDs [28, 36, 41]. Full understanding of the nuclear spin phenomena requires stability and ideally external control of the charge state of the dot. There are two factors underlying this requirement. Firstly, fast nuclear depolarisation occurs as a result of interaction with charges randomly captured in the dot. This, for example complicates nuclear spin dynamics measurements, and also nuclear magnetic resonance (NMR) experiments, in both of which nuclear spin behavior in the 'dark' (without optically excited charges) needs to be investigated [42, 40]. The second factor is that electron-nuclear interaction leads to inhomogeneous Knight field, an effective magnetic field experienced by individual nuclei [43]. Occurrence of this field modifies the nuclear spin energy spectrum and dynamics (e.g. via its effect on the nuclear spin diffusion process). Another useful aspect of QD charge control is that the Knight field of both electron and hole could be studied, and also used for nano-NMR imaging purposes as was proposed by Makhonin et al. [44]. The concept of the hole Knight field has yet to be explored, since until recently interaction of holes with nuclear spins were considered negligible due to the p-symmetry of hole wavefunction [42]. In this respect a relatively simple nuclear spin system should be employed initially, and InP/GaInP QDs present an interesting example since phosphorus nuclei with spin 1/2 are not affected by quadrupole interaction

and have a narrow NMR linewidth (down to 3 kHz), which can potentially be employed for sensitive probing of the Knight field of the hole. So far, however, charge control using bias-tuning in Schottky diodes has been realised reliably in InGaAs QDs only [19]. In this thesis we address this task in detailed studies of InP/GaInP QDs embedded in a Schottky device.

Many recent studies of QDs showed that polarisation of nuclear spins is changed under optical excitation in a wide variety of conditions including resonant and non-resonant cw and pulsed excitation [32, 45, 34, 35, 36, 37]. This indicates the importance of these phenomena for optical manipulation of QD spin qubits, and more generally for understanding the spin physics on the nano-scale. An interesting example here are nuclear spin effects in neutral QDs [46]. Such dots have been used recently in the non-invasive structural studies of QDs using nano-NMR, and also proved to be crucially important in gaining new insights in the hole-nuclear spin interaction [42, 40]. In the latter experiments in particular, dark exciton states played an important role in detection of the Overhauser fields experienced by the holes. The role of dark states in efficient polarisation of nuclear spins via the second order recombination process has recently been demonstrated in InP/GaInP QDs [46]. In this thesis we show that this unusual phenomenon is general for neutral dots and explore these effects in InGaAs/GaAs QDs. We find that extremely high degrees of nuclear polarisation can be achieved at ultra-low powers of non-resonant optical excitation several orders of magnitude below QD saturation. This further emphasizes that nuclear spin effects must be taken into account in III-V nanostructures in the majority of optical experiments.

In the final part of the thesis, results on optical studies of new InPAs/GaInP QDs are presented. Motivation for this work was to explore QDs with enhanced

confinement of carriers, potentially enabling realisation of single photon emitters operating at elevated temperature [47, 48]. So far the majority of non-classical light generation experiments have been carried out on InGaAs/GaAs and InP/GaInP QDs [12, 14, 49]. As an example, the band-gap difference between the QD emission and wetting layer for InGaAs QDs is usually around 150-250 meV, and is around 200-300 meV between the QD PL and GaAs barrier. In the case of InPAs QDs the difference exceeding 0.5 eV should be easily achievable. However, a few studies where high density ensembles of such dots were realised did not exhibit the expected long-wavelength emission [48, 50]. This is now realised in this work. In addition, we demonstrate samples with low dot density suitable for single photon applications. Since no structural information on these dots exists, our initial motivation was to lay foundation for future structural studies, which are now possible in self-assembled dots by using optically detected NMR techniques recently developed in Sheffield [40]. We explore conditions for dynamic nuclear polarisation, which would allow further exploration of material composition and strain distribution in these dots in NMR studies.

1.2 Self-assembled quantum dots - fabrication

Semiconductor quantum dot (QD) structures discussed in this thesis are grown by molecular beam epitaxy (MBE) and metal-organic vapor phase epitaxy (MOVPE).

Self-assembled dots. The self-assembled dots such as InGaAs/GaAs (MBE) and InP/GaInP (MOVPE) are formed when thin layers of materials with higher lattice constant (InGaAs and InP) are deposited on the material with a lower lattice constant (GaAs and GaInP). In that case, the transition from the growth

of 2D layers to the growth of 3D islands occurs after a critical thickness of the material with the higher lattice constant is deposited, the process driven by the increase of the surface energy due to the strain. This way, structures with a low aspect ratio are formed with typical dimensions of 20 to 80 nm in-plane and 2 to 10 nm in height. The shapes are usually described in terms of lenses and pyramids, and also truncated lenses and pyramids (see Fig. 1.1 for example of InAs dot). Significant intermixing of the material usually occurs between the dot and the surrounding barrier as the dots are usually grown at high temperatures in excess of 600^{o}C: in InAs and InP dots, In atoms are usually partially replaced with Ga atoms. This allows to some degree further post-growth modification of the dot properties by high temperature annealing, by which both the composition and shapes of the dots can be altered. The composition of the dot and the barrier plays an important role in determining the confinement energies for electrons and holes. Both InGaAs/GaAs and InP/GaInP are Type I nano-structures, i.e. InGaAs and InP regions have the band gaps smaller than those in GaAs and GaInP, respectively, and present confinement minima for both electrons and holes. Confinement energies in excess of 100 meV for electrons are typical.

In this subsection we review the main process to fabricate self-assembled quantum dots. Tremendous development of growth techniques to obtain QDs had been achieved since the early days, when top-bottom process employing lithography and etching methods were used [51]. These early techniques consist of epitaxial growth of quantum wells, and the desirable pattern definition using lithography masks. Subsequently, plasma etching reveals the quantum wire or dot structures. The main disadvantage of these techniques is the creation of high density of defects due to the abrasive etching process [52, 53].

Major breakthroughs came with the developments of bottom - up quantum dot fabrication. Stranski - Krastanov growth of self-assembled quantum dots and development of interface dots allowed to obtain defect - free quantum dots.

Stranski - Krastanow growth technique relies fundamentally on strained semiconductor layers. These type of QDs are better usually referred as self-assembled dots. Figure 1.1 illustrates this quantum dot formation, for more information on the mechanism of Stranski-Krastanow growth the reader can refer to the recent report by Baskaran [4].

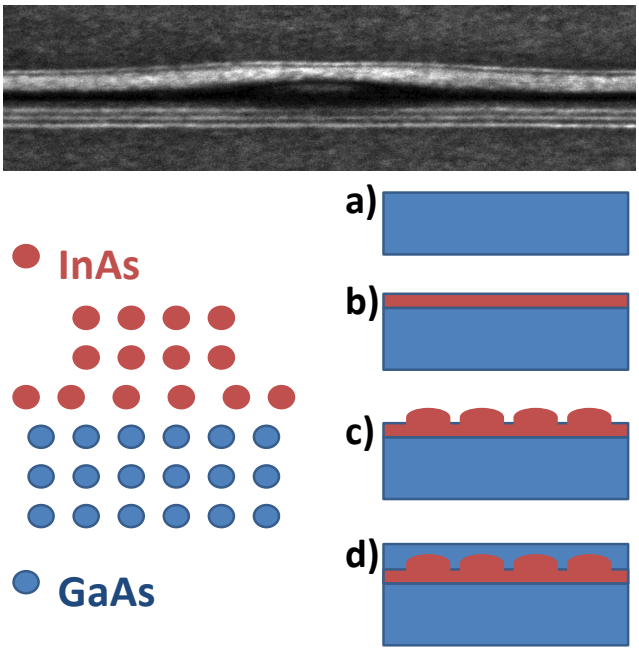

Figure 1.1: Stranski - Krastanov formation of quantum dots. a) GaAs substrate, b) InAs monoatomic layer deposition, c) Formation of InAs nano-islands, d) GaAs capping layer on top of InAs QDs. The inset on the left hand side, shows the strain form by the difference in lattice constants of the two semiconductor materials. In the upper inset typical TEM image of a Stranski-Krastanov QD is shown.

Typically, the dimension of the self-assembled dots are $2-5nm$ high and $20nm$

base, which densities of about $10^{10} - 10^{11}\ cm^{-2}$. The strong confinement obtained at these dimensions is enough to fully quantize the electron and hole states, with quantization energies greater than $k_B T$ which allow important technological implementations. However, homogeneity in size, shape and distribution of QDs represent the major open challenge of self-assembled dots. In order to control the QD position local strain-mediated surface chemical potential [54] and pre-patterned substrates [55] have been employed [56]. In the following subsection we review the main epitaxial methods to fabricate quantum dots.

1.2.1 Epitaxial methods for fabrication of self-assembled quantum dots

In order to obtain high quality semiconductor nanostructures, MBE (Molecular beam epitaxy) and MOCVD (Metal organic chemical vapor deposition) had demonstrated high efficiency and are widely employed [1]. Nevertheless, effective semiconductor nanostructure growth had been demonstrated in less advance epitaxial methods such as LPE (Liquid phase epitaxy) [6]. Here, we will focus on the description of MBE and MOCVD which are the methods utilized to obtain the samples related to the present work.

1.2.1.1 Molecular beam epitaxy

Due to its unique properties such as ultra-slow deposition rate (typically 1μm per hour) conserving low impurities density, MBE is widely used in the semiconductor industry to fabricate high quality devices [3]. First demonstrations of high quality semiconductor nanostructures had taken advantage of this facility [57].

A schematic of an MBE chamber is shown in figure 1.2. It consists of ultra-high vacuum chamber (typically 10^{-8} Pa) with several effusion cells each of them for different elements. In a growth process the cells are heated up to a temperature where the elements start to evaporate. Once the cell shutter of the desirable element is open, an atomic beam leaves the cell targeting a hot substrate (bulk semiconductor). The atomic beams combines the elements at the surface of the substrate and due to the slow deposition rate of about 1μm per hour an epitaxial growth of atomic layer by atomic layer occurs. The substrate holder can be rotated to homogenize the grown layers. Because the shutters can be controlled in a much faster time than the deposition rate, very thin layers with sharp interfaces can be produced.

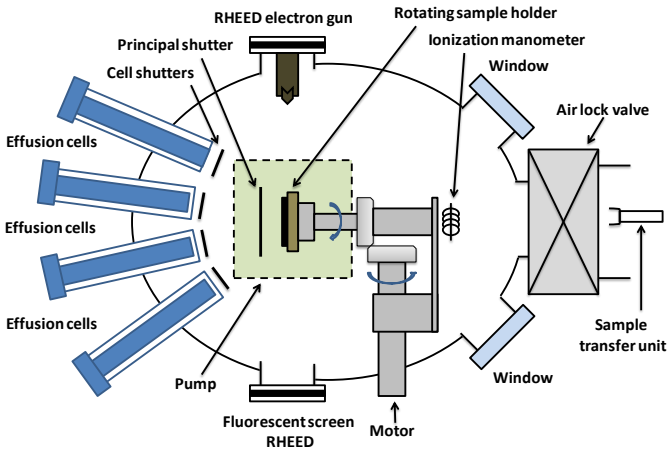

Figure 1.2: Schematic of principal elements of molecular beam epitaxy reactor (MBE).

1.2.1.2 Metal organic chemical vapor deposition

In contrast with the MBE method, MOCVD growth takes place by chemical reactions and not physical deposition. The elements utilized are embedded in gaseous compounds. The elements break down to deposit on the heated substrate with remaining waste gases being removed from the chamber. All the processes described here take place under non-vacuum conditions, and just the gas phases are kept under pressures of 2 - 100 kPa [1, 5]. Figure 1.3 shows a schematic of the main MOCVD components, and the chemical reaction to obtain GaAs. Valves in the gas lines allow to control an appropriate sequence to grow the desirable semiconductor structure. In general, the growth rate of MOCVD process is faster than MBE, which is more suitable for industrial applications.

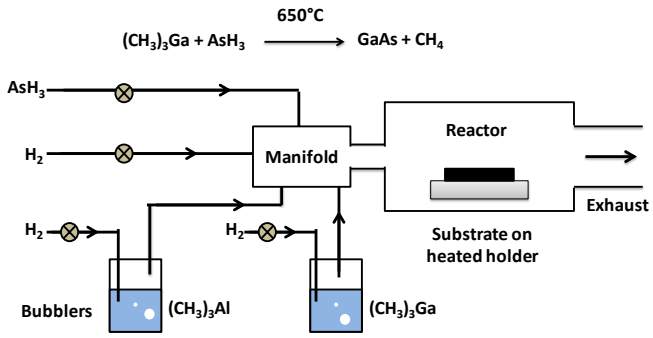

Figure 1.3: Schematic of principal elements of metal organic chemical vapor deposition system (MOCVD)

1.3 Optical techniques for studies of QDs

Quantum dots have been extensively studied for applications in diverse fields like physics, chemistry and biology. In particular, for quantum physics, optical techniques allow studies of confined carrier and spin systems within the QD. Several research groups have reported experimental evidence and detail description of diverse phenomena in quantum dots, such as Coulomb interaction [23], Pauli blocking effect [58], spin polarisation [59] and charge control [21, 19], just to mention few.

Here we review the main optical techniques for studies of QDs. In the first subsection we will refer to non-resonant excitation method. In this method, a light source typically a laser beam with energy greater than the relevant excitonic transition in the QD is used. The optical excitation generates exciton population in either a higher exciton QD transition or in the bulk semiconductor of the host matrix. The created higher energy carriers non-radiatively relax, releasing energy through carrier scattering and phonons, and finally populate the lowest available QD energy state. The second subsection we will refer to resonant excitation method. Here, we use a laser with energy equal to the relevant excitonic transition, which creates an electron-hole pair populating the QD energy state. Figure 1.4 shows schematics of non-resonant excitation which creates carriers in the barriers (top panel), and resonant excitation which generates e-h pairs in the dot transitions (bottom panel).

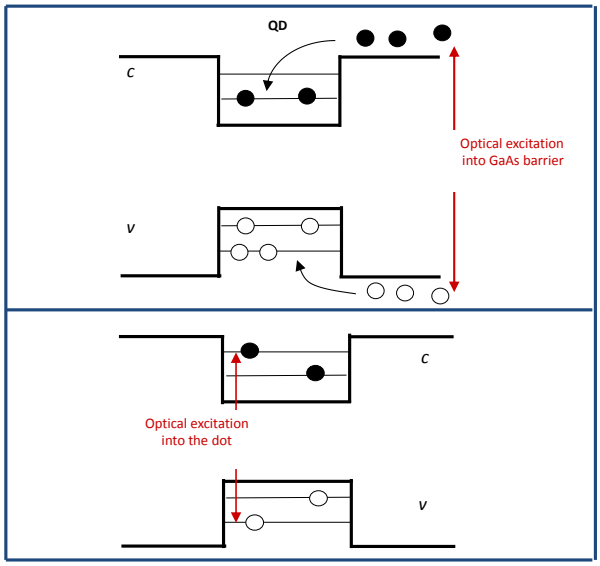

Figure 1.4: Optical excitation techniques. Top panel shows non-resonant optical excitation which creates carriers in the barriers. Bottom panel shows resonant optical excitation which generates e-h pairs in the dot transitions.

1.3.1 Non-resonant optical excitation

Non-resonant excitation optically excites electron-hole pairs at energies higher than the QD excitonic transitions (e.g. wetting layer). Some of the carriers relax into quantum dot levels before they recombine and emit a photon with information about, relaxation times (typically picoseconds), QD energy levels, spin polarisation etc. However, conventional photoluminescence techniques use a laser beam with typical diameter of $\sim 100\mu m$ which for QD densities of $10^{10}-10^{11}cm^{-2}$ simultaneously excites $10^6 - 10^7$ dots. Despite the fact that a typical quantum dot contains discrete energy levels, the fluctuations in sizes, shapes, and composition of the dots is reflected as inhomogeneous broad spectra with linewidths $100meV$ [2]. These inhomogeneously broadened spectra restrict studies of individual dot behaviour. Hence, micro-photoluminescence $\mu - PL$ under which a

laser spot size of $\sim 2\mu m$ can be achieved have been essential for single quantum dot studies [60]. Additional to smaller laser spot size, QD samples analyzed by $\mu - PL$ technique could also use further metal shadow mask with nano-apertures for optical access with sizes from $200nm - 1\mu$ to further reduce the excitation area.

Figure 1.5 shows PL spectra of a QD ensemble under optical excitation with a laser beam diameter of $\sim 100\mu m$ (gray spectrum), which reflects the inhomogeneous broadening, and $\mu - PL$ spectra of a QD ensemble (black spectrum) under optical excitation with a laser beam diameter of $\sim 2\mu m$ and nano-apertures for optical access $\sim 400nm$ (inset), which shows individual QD emission peaks.

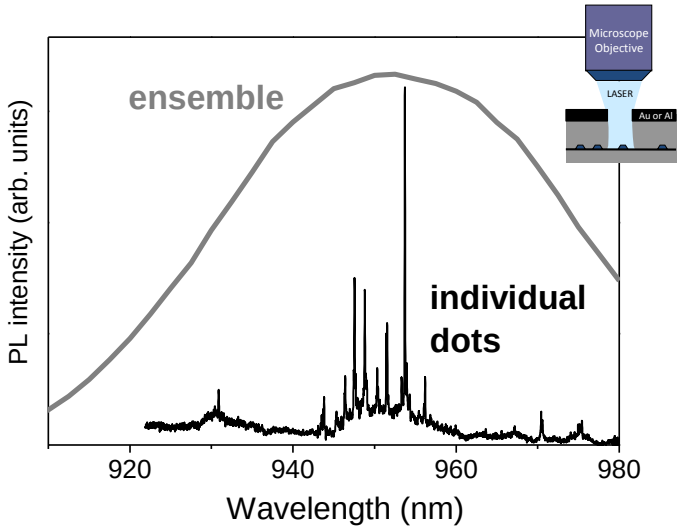

Figure 1.5: Comparison of a PL spectra of a QD ensemble under optical excitation with a laser beam diameter of $\sim 100\mu m$ (gray spectrum), and $\mu - PL$ spectra of a QD ensemble (black spectrum) under optical excitation with a laser beam diameter of $\sim 2\mu m$ and nano-apertures for optical access $\sim 400nm$ (inset).

Figure 1.6 shows s typical μPL set-up including the sample attached to a three-

dimensional piezo-positioner with electrical connections for electrical charging control, which is placed in the bore of a superconductive magnet for magneto-spectroscopy experiments. The laser beam is focused in a $\sim 2\mu m$ spot on the sample by the lens with a short focal length.

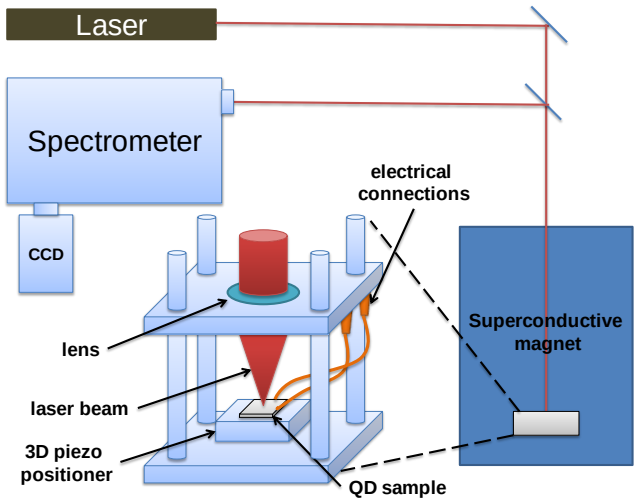

Figure 1.6: A typical micro-photoluminescence (micro-PL) set-up including the sample attached to a three-dimensional piezo-positioner with electrical connections, which is immersed into a superconducting magnet. The laser beam is focused in a $\approx 2\mu$m spot on the sample by the lens with a short focal length.

1.3.2 Resonant optical excitation

When non-resonant excitation is used and creates carriers in higher exciton transitions or semiconductor host material we establish an incoherent pumping of the dot. This incoherent pumping mainly due to non-radiative relaxation paths before emission reduce the usefulness of this optical technique for linear optics quantum computing algorithms [60]. Resonant excitation optically generates co-

herent e-h pairs into the QD transition of interest. Additional, resonant optical excitation allows spectrally access to individual QD electronic transitions [24].

An example of resonant technique used in this thesis is photocurrent. Photocurrent (PC) techniques rely on resonant excitation and quantum dot diode structures, where an electric field can be applied to control the tunneling time of carriers [61]. PC techniques applied to single QDs is a powerful spectroscopy method which gives information about the interband optoelectronic properties in QDs [62]. PC has been widely employed for coherent control studies, as was first demonstrated by Zrenner et al. [63], and has been extensively exploited since then [24]. Using this technique, QD spectra are obtained by moving the optical transition in and out of resonance with the excitation laser using the confined Stark effect [64]. Hence, additional to the specialise experimental set up (similar to that for micro-PL studies), we require the dots to be grown within a structure which allows the application of an electric field.

Figure 1.7, shows the mechanism for photocurrent detection. A resonant excitation creates an electron-hole pair in the dot. Under the applied electric field the carrier tunnel out of the dot and are detected as a change in photocurrent of up to 1nA in cw measurements.

1.4 Electron-hole complexes in quantum dots

The types of QDs described above provide strong confinement for electrons and holes, and usually can accommodate many charge carriers. Of particular interest for the present thesis are neutral (empty or uncharged) and singly-charged QDs. The latter include positively and negatively charged dots containing a hole or

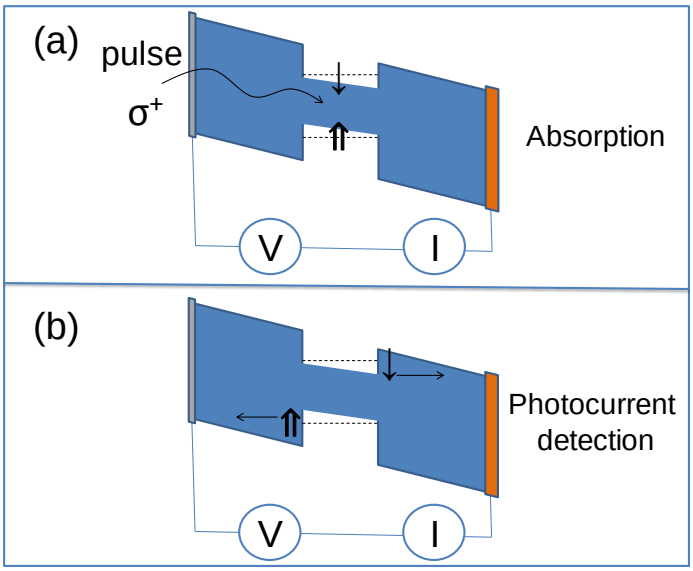

Figure 1.7: Principle of photocurrent detection. QD embedded in a Schottky diode structure. (a) Resonant excitation with an optical transition creates an electron-hole pair. (b) When applied electric field the carriers scape from the dot and are detected as a change in photocurrent.

electron in the ground state, respectively. Recently, these two types of charged dots have been extensively studied owing to the promise of developing solid state spin-qubits based on single hole or electron [25, 63, 30]. The control of the charge state was thus an essential first step and will be briefly described here.

Confinement of carrier in QDs leads to quantization of energy states for conduction and valence band in semiconductor materials. Normally just the heavy holes states with its twofold degeneracy $S_Z = \pm 3/2$ and the conduction band with $S_Z = \pm 1/2$ are necessary for accurate description of optical transitions in semiconductor QDs [65].

Charges can be introduced in the dot by using modulation doped structures, where a delta-layer of dopants of a very low density is deposited during the structure growth a few nm below or above the dot layer [66, 67]. Structures where

on average one electron per dot was created in this way were routinely obtained. An important characteristic of the dot charging created in this way is that it is relatively stable, and events such as co-tunneling observed in charge-tunable devices (discussed in chapter 1) do not occur. Usually, it is more difficult to create modulation doped samples of p-type, especially if doping is achieved with Be, which is a very mobile atom. An alternative solution, which has been used in several reported cases is doping with carbon [36]. Charging of QDs also occurs naturally due to the residual doping. Dots charged both with single holes and electrons have routinely been observed in MOVPE grown InP/GaInP system [37]. Charging may also occur under the non-resonant optical excitation due to different efficiencies of the hole and electron capture into the dots. Although such charging usually does not provide stable charge configurations on the dot as charges of both signs can be randomly created in this way.

Interaction among these excited carriers confined in a semiconductor QD lead to well known effects, such as electron-hole exchange interaction, Pauli-blocking of states, energy renormalization due to Coulomb interaction and other interactions resulting in dephasing [19, 23, 21].

Electron-hole pair within a QD can form an exciton, which is bonded by electrostatic Coulomb force, and is better known as neutral exciton (X^0). Additional to this, other exciton complexes can be formed within a quantum dot. A resident carrier could already exist in the QD due to the possibility of doping the semiconductor material with n-type or p-type impurities as just mentioned above. Then, if an electron-hole pair is photon-generated, a negatively charge exciton is formed (X^{-1}) by the presence of the additional electron. Under the same principle, if a resident hole exist in the QD and an electron-hole pair is photon-generated, a

positively charge exciton is created (X^{+1}). A so-called biexciton can form if an electron-hole pair exist in the quantum dot when another electron-hole pair is photon-generated [19, 68, 69, 21]. Representation of these exciton complexes can be seen in figure 1.8.

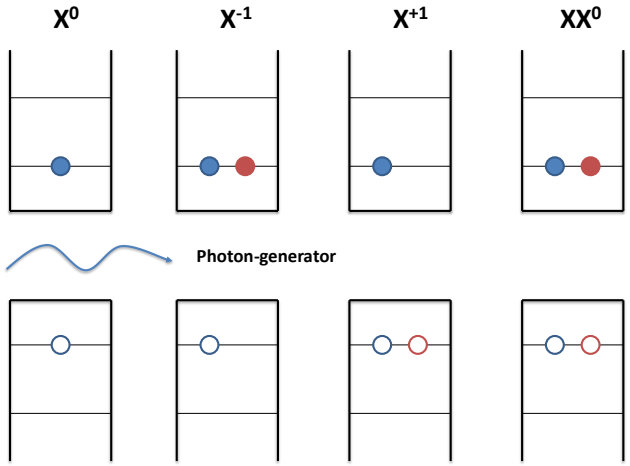

Figure 1.8: Exciton complexes in semiconductor quantum dots. Photon-generated carriers are represented by blue solid (electron) and open (hole) circles, while resident carrier are red solid (electron) and open (hole) circles. From left to right hand we have neutral exciton (X^0), negative exciton (X^{-1}), positive exciton (X^{+1}) and biexciton (XX^0).

An alternative solution enabling precise control of the charge state of the dot is the use of so-called charge-tunable devices. A schematic of such a device is shown in Fig. 1.9. The charge state of the dot is controlled by the voltage applied between the back contact usually located 25-80 nm below the QD layer and the Schottky contact formed by a metal gate on the top surface of the device. By biasing the diode the electron energies of the quantized states in the quantum dot can be moved in resonance with the edge of the Fermi sea, E_F, thus enabling

tunneling of electrons from the contact into the dot. The precise control of the charge state is achieved at low temperature (a few tens of Kelvin or lower), where the maximum energy of electrons in the contact is rather well defined [68, 21]. When a single electron is loaded in the dot, the Coulomb blockade prohibits charging by the second electron, unless the bias is changed so that the energies of the dot states are lowered with respect to that of the contact. The electron captured in the dot can still tunnel out of the dot, and additional processes known as co-tunneling may occur [70]. However, stable charging with a single electron may be achieved at voltages where the energy of one electron on the dot is sufficiently lower than E_F, but the energy of two electrons on the dot is sufficiently higher than E_F. Similarly, charging with holes can be achieved by using p-type Schottky devices, preferably with carbon doping [22, 71, 25]. Alternatively, charging with holes is achieved in n-type Schottky devices under optical excitation at high bias: photo-generated electrons quickly tunnel out of the dot, while heavier holes may remain for few microseconds. Figure 1.9 demonstrate the charging process of a QD embedded in a Schottky diode structure. Top panel shows the charging control of a single hole under forward bias. The bottom panel shows a typical PL spectra of a InGaAs neutral and singly positive charge exciton (left), and ratio of X^+/X^0 under applied bias.

1.5 Conclusions

We presented the main growth techniques and generic optical properties of self-assembled semiconductor quantum dots.

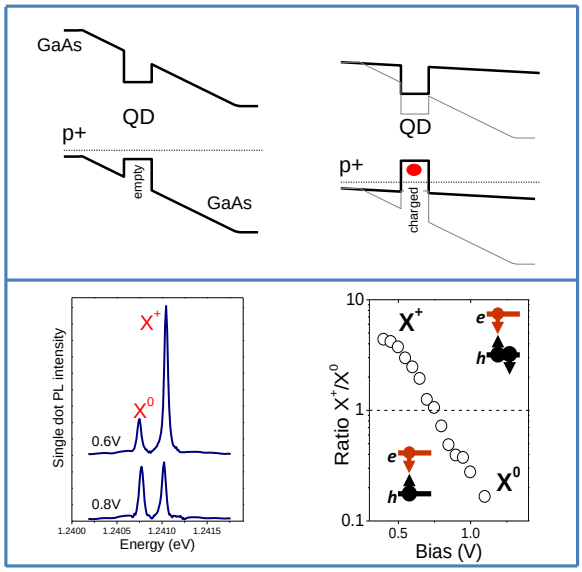

Figure 1.9: Charging of a quantum dot embedded in a Schottky diode structure. Top panel shows the charging control of a single hole under forward bias. The bottom panel shows a typical PL spectra of a InGaAs neutral and singly positive charge exciton (left), and ratio of X^+/X^0 under applied bias.

References

[1] Dieter Bimberg. *Quantum dot heterostructures*. Berlin: John Wiley and Sons, 1999 (cit. on pp. 1, 8, 10).

[2] Maurice Skolnick and David Mowbray. "Self-Assembled Semiconductor Quantum Dots: Fundamental Physics and Device Applications". In: *Annual Review of Materials Research* 34 (2004), pp. 181–281 (cit. on pp. 1, 12).

[3] Eric Tourni. "MBE growth and interface formation of compound semiconductor heterostructures for optoelectronics". In: *Physica Status Solidi* 244 (2007), pp. 2683–2696 (cit. on pp. 1, 2, 8).

[4] Arvind Baskaran. “Mechanisms of Stranski-Krastanov growth”. In: *Journal of Applied Physics* 111 (2012), p. 044321 (cit. on pp. 1, 7).

[5] Aixtron. *How MOCVD works. Deposition Technology for Beginners*. Herzogenrath: Aixtron SE, 2011 (cit. on pp. 1, 10).

[6] F.E. Ortiz Vzquez. “GaIn As Quantum Dots (QD) grown by Liquid Phase Epitaxy (LPE)”. In: *Journal of Physics: Conference Series* 167 (2009), p. 012002 (cit. on pp. 1, 8).

[7] E. I. Ivchenko and G. E. Pikus. *Superlattices and Other Heterostructures, Symmetry and Optical Phenomena*. Berlin: Springer - Verlag, 1995 (cit. on p. 1).

[8] D. Bimberg and N. Kirstaedter. “InGaAs-GaAs quantum-dot lasers”. In: *Selected Topics in Quantum Electronics, IEEE* 3 (1997), pp. 196 –205 (cit. on p. 1).

[9] H. Schmeckebier. “Complete pulse characterization of quantum dot modelocked lasers suitable for optical communication up to 160 Gbit/s”. In: *Optics Express* 18 (2010), pp. 3415–3425 (cit. on p. 1).

[10] N. N. Ledentsov. “Quantum dot heterostructures: fabrication, propreties, lasers”. In: *Semiconductors* 32 (1998), pp. 343–366 (cit. on p. 1).

[11] V. Zwiller. “Single quantum dots emit single photons at a time: Antibunching experiments”. In: *Appl. Phys. Lett.* 78 (2001), pp. 2476–2478 (cit. on p. 1).

[12] R. M. Stevenson. “A semiconductor source of triggered entangled photon pairs”. In: *Nature* 439 (2006), pp. 179–182 (cit. on pp. 1, 5).

[13] A. K. Nowak. "Thermal effects in InP/(Ga,In)P quantum-dot single-photon emitters". In: *Phys. Rev. B* 80 (2009), p. 161305 (cit. on p. 1).

[14] Zhiliang Yuan. "Electrically Driven Single-Photon Source". In: *Science* 295 (2002), pp. 102–105 (cit. on pp. 1, 5).

[15] D. Loss. "Quantum computation with quantum dots". In: *Physical Review A* 57 (1998), 120126 (cit. on pp. 1–3).

[16] A. Marent. "Hole-based memory operation in an InAs/GaAs quantum dot heterostructure". In: *Applied Physics Letters* 95 (2009), p. 242114 (cit. on p. 1).

[17] Peter Michler. *Single Semiconductor Quantum Dots*. Berlin: Springer, 2009 (cit. on p. 1).

[18] Alexander Tartakovskii. *Quantum Dots: Optics, Electron Transport and Future Applications*. Cambridge: Cambridge, 2012 (cit. on p. 1).

[19] R. J. Warburton. "Optical emission from a charge-tunable quantum ring". In: *Nature* 405 (2000), pp. 926–929 (cit. on pp. 2, 4, 11, 17, 18).

[20] L. P. Kouwenhoven. "Excitation Spectra of Circular, Few-Electron Quantum Dots". In: *Science* 278 (1997), pp. 1788–1792 (cit. on p. 2).

[21] ODD Couto Jr and J Puebla. "Charge control in InP/(Ga, In) P single quantum dots embedded in Schottky diodes". In: *Physical Review B* 84 (2011), p. 125301 (cit. on pp. 2, 11, 17–19).

[22] J. J. Finley. "Quantum-confined Stark shifts of charged exciton complexes in quantum dots". In: *Phys. Rev. B* 70 (2004), p. 201308 (cit. on pp. 2, 19).

[23] R. J. Warburton. "Coulomb interactions in small charge-tunable quantum dots: A simple model". In: *Phys. Rev. B* 58 (1998), p. 16221 (cit. on pp. 2, 11, 17).

[24] A J Ramsay. "A review of the coherent optical control of the exciton and spin states of semiconductor quantum dots". In: *Semicond. Sci. Technol.* 25 (2010), p. 103001 (cit. on pp. 2, 15).

[25] T. M. Godden. "Coherent Optical Control of the Spin of a Single Hole in an InAs/GaAs Quantum Dot". In: *Physical Review Letters* 108 (2012), p. 017402 (cit. on pp. 2, 16, 19).

[26] R. J. Epstein. "Voltage control of nuclear spin in ferromagnetic Schottky diodes". In: *Phys. Rev. B* 68 (2003), p. 041305 (cit. on p. 2).

[27] Sandra Foletti. "Universal quantum control of two-electron spin quantum bits using dynamic nuclear polarization". In: *Nature Physics* 5 (2009), pp. 903–908 (cit. on p. 2).

[28] D. Gammon. "Electron and Nuclear Spin Interactions in the Optical Spectra of Single GaAs Quantum Dots". In: *Phys. Rev. Lett.* 86 (2001), pp. 5176–5179 (cit. on pp. 2, 3).

[29] J. G. Tischler. "Fine Structure of Trious and Excitons in Single GaAs Quantum Dots". In: *Phys. Rev. B* 66 (2002), p. 081310 (cit. on p. 2).

[30] J. R. Petta. "Coherent Manipulation of Coupled Electron Spins in Semiconductor Quantum Dots". In: *Science* 309 (2005), pp. 2180–2184 (cit. on pp. 2, 16).

[31] W. G. van der Wiel. “Electron transport through double quantum dots”. In: *Rev. Mod. Phys.* 75 (2002), pp. 1–22 (cit. on p. 2).

[32] Urbaszek Bernhard and Marie Xavier. “Nuclear spin physics in quantum dots: an optical investigation”. In: *arXiv:1202.4637* 84 (2012), p. 195305 (cit. on pp. 2, 4).

[33] I.A. Merkulov. “Electron spin relaxation by nuclei in semiconductor quantum dots”. In: *Phys. Rev. B* 65 (2002), p. 205309 (cit. on p. 2).

[34] P. Maletinski. “Dynamics of quantum dot nuclear spin polarization controlled by a single electron”. In: *Phys. Rev. Lett.* 99 (2007), p. 056804 (cit. on pp. 2, 4).

[35] A. I. Tartakovskii. “Nuclear Spin Switch in Semiconductor Quantum Dots”. In: *Phys. Rev. Lett.* 98 (2007), p. 026806 (cit. on pp. 2, 4).

[36] B. Eble. “Dynamic nuclear polarization of a single charge-tunable InAs GaAs quantum dot”. In: *Phys. Rev. B* 74 (2006), p. 081306 (cit. on pp. 2–4, 17).

[37] E. A. Chekhovich. “Pumping of Nuclear Spins by Optical Excitation of Spin-Forbidden Transitions in a Quantum Dot”. In: *Phys. Rev. Lett.* 104 (2010), p. 066804 (cit. on pp. 2, 4, 17).

[38] Alexander V. Khaetskii. “Electron Spin Decoherence in Quantum Dots due to Interaction with Nuclei”. In: *Phys. Rev. Lett.* 88 (2002), p. 186802 (cit. on p. 3).

[39] D. Gammon. "Nuclear spectroscopy in single quantum dots: nanoscopic Raman scattering and nuclear magnetic resonance". In: *Science* 277 (1997), pp. 85–88 (cit. on p. 3).

[40] E. A. Chekhovich, K. V. Kavokin, and J. Puebla. "Structural analysis of strained quantum dots using nuclear magnetic resonance". In: *Nat. Nanotechnology* 7 (2012), 646650 (cit. on pp. 3–5).

[41] J. Skiba-Szymanska. "Overhauser effect in individual InP/Ga_xIn_{1x}P dots". In: *Phys. Rev. B* 77 (2008), p. 165338 (cit. on p. 3).

[42] E. A. Chekhovich. "Direct Measurement of the Hole-Nuclear Spin Interaction in Single InP/GaInP Quantum Dots Using Photoluminescence Spectroscopy". In: *Phys. Rev. Lett.* 106 (2011), p. 027402 (cit. on pp. 3, 4).

[43] C.W. Lai. "Knight-field-enabled nuclear spin polarization in single quantum dots". In: *Phys. Rev. Lett.* 96 (2006), p. 167403 (cit. on p. 3).

[44] M.N. Makhonin. "Fast control of nuclear spin polarization in an optically pumped single quantum dot". In: *Nature Mat.* 10 (2011), pp. 844–848 (cit. on p. 3).

[45] C. Latta. "Confluence of resonant laser excitation and bidirectional quantum-dot nuclear-spin polarization". In: *Nature Phys.* 5 (2009), p. 758 (cit. on p. 4).

[46] E. A. Chekhovich. "Light-polarization-independent nuclear spin alignment in a quantum dot". In: *Phys. Rev. B* 83 (2011), p. 125318 (cit. on p. 4).

[47] H. Kosaka and A.A. Kiselev. "Electron g factor engineering in III-V semiconductors for quantum communications". In: *Electronics Letters* 37 (2001), p. 464 (cit. on p. 5).

[48] E. Ribeiro and R.L. Maltez. "Optical and structural properties of InAsP ternary self-assembled quantum dots embedded in GaAs". In: *Applied Physics Letters* 81 (2002), pp. 2953–2955 (cit. on p. 5).

[49] I. Luxmoore. "III-V quantum light source and cavity-QED on Silicon". In: *arXiv:1211.5254 [cond-mat.mes-hall]* (2012), online (cit. on p. 5).

[50] D.A. Vinokurov and V.A. Kapitonov. "Self-organized nanosize InP and InAsP clusters obtained by metalorganic compound hydride epitaxy". In: *Technical Physics Letters* 24 (1998), pp. 623–625 (cit. on p. 5).

[51] Mark A. Reed. "Quantum dots". In: *Scientific american* 268 (1993), pp. 118–123 (cit. on p. 6).

[52] L. Birotheau. "Optical investigation of the onedimensional confinement effects in narrow GaAs/GaAlAs quantum wires". In: *Applied physics letters* 61 (1992), pp. 3023–3025 (cit. on p. 6).

[53] P.M. Petroff. "Toward quantum well wires: Fabrication and optical properties". In: *Applied physics letters* 41 (1982), pp. 635–638 (cit. on p. 6).

[54] Bin Yang. "Local Strain-Mediated Chemical Potential Control of Quantum Dot Self-Organization in Heteroepitaxy". In: *Physical review letters* 92 (2004), p. 025502 (cit. on p. 8).

[55] M.H. Baier. "High uniformity of site-controlled pyramidal quantum dots grown on prepatterned substrates". In: *Applied physics letters* 84 (2004), pp. 1943–1945 (cit. on p. 8).

[56] O.G. Schmidt. *Lateral Alignment of Epitaxial Quantum Dots (Nanoscience and Technology)*. Springer: Heidelberg, 2007 (cit. on p. 8).

[57] John H. Davies. *The Physics of low dimensional semiconductors*. Cambridge: Cambridge University Press, 1998 (cit. on p. 8).

[58] V. K. Kalevich. "Spin redistribution due to Pauli blocking in quantum dots". In: *Phys. Rev. B* 64 (2001), p. 045309 (cit. on p. 11).

[59] A.S. Bracker. "Optical Pumping of the Electronic and Nuclear Spin of Single Charge-Tunable Quantum Dots". In: *Phys. Rev. Lett.* 94 (2005), p. 047402 (cit. on p. 11).

[60] A.N. Vamivakas and M. Atature. "Photons and (artificial) atoms: an overview of optical spectroscopy techniques on quantum dots". In: *Contemporary Physics* 51 (2010), pp. 17–36 (cit. on pp. 13, 14).

[61] F. Findeis and M. Baier. "Photocurrent and photoluminescence of a single self-assembled quantum dot in electric fields". In: *Applied Physics Letters* 78 (2001), pp. 2958–2960 (cit. on p. 15).

[62] P.W. Fry. "Photocurrent spectroscopy of InAs/GaAs self-assembled quantum dots". In: *Physical Rev. B* 62 (2000), 1678416791 (cit. on p. 15).

[63] A. Zrenner. "Coherent properties of a two-level system based on a quantum-dot photodiode". In: *Nature* 418 (2002), 612614 (cit. on pp. 15, 16).

[64] S. A. Empedocles and M. G. Bawendi. "Quantum-Confined Stark Effect in Single CdSe Nanocrystallite Quantum Dots". In: *Science* 278 (1997), pp. 2114–2117 (cit. on p. 15).

[65] Mikhail I. Dyakonov. *Spin Physics in Semiconductors*. Berlin: Springer Series in Solid-State Sciences, 2008 (cit. on p. 16).

[66] A. Greilich. "Mode Locking of Electron Spin Coherences in Singly Charged Quantum Dots". In: *Science* 313 (2006), p. 341 (cit. on p. 16).

[67] S. Laurent. "Negative circular polarization as a general property of n-doped self-assembled InAsGaAs quantum dots under nonresonant optical excitation". In: *Phys. Rev. B* 73 (2006), p. 235302 (cit. on p. 16).

[68] R. J. Warburton. "Charged Excitons in Self-Assembled Semiconductor Quantum Dots". In: *Phys. Rev. Lett.* 79 (1997), 52825285 (cit. on pp. 18, 19).

[69] M. Bayer. "Fine structure of neutral and charged excitons in self-assembled In(Ga)As/(Al)GaAs quantum dots". In: *Phys. Rev. B* 65 (2002), p. 195315 (cit. on p. 18).

[70] J. M. Smith. "Voltage Control of the Spin Dynamics of an Exciton in a Semiconductor Quantum Dot". In: *Phys. Rev. Lett.* 94 (2005), p. 197402 (cit. on p. 19).

[71] A. J. Ramsay. "Fast Optical Preparation, Control, and Readout of a Single Quantum Dot Spin". In: *Physical Review Letters* 100 (2008), p. 197401 (cit. on p. 19).

Chapter 2

Charge control in InP/GaInP single quantum dots embedded in Schottky diodes

2.1 Introduction

Control and understanding of charge states in a quantum dot is important for spintronic applications [1]. For this propose, semiconductor QDs have been embedded into diodes [2, 3, 4]. Pioneering work of Warburton on InAs charge tunable quantum rings revealed optical emission of diverse quantum charge states as electrons are added one-by-one to the artificial atom, this revealing its shell structure [2]. This breakthrough permitted further development of QD research and applications. By tilting the band structure of a semiconductor QD, it is possible to control the tunneling times of charges, as consequence a single electron or hole can be isolated for single spin coherent control [5, 6] and diverse applications

ranging from single-photon emitters [7, 8] to spin qubits for quantum information processing [7, 9, 10] have emerged. The majority of results have been achieved using InGaAs/GaAs QD structures [11], which emit at long wavelength $\geq$ 900nm where Si detectors are inefficient. Another class of QDs made of InP/GaInP received less attention mainly due to less mature technology. On the other hand, recent studies have also shown intriguing nuclear spin phenomena in InP/GaInP QDs grown by MOVPE. In optically pumped QDs, record high degrees of nuclear spin polarisation $\approx 65\%$ [12] and ultra-long nuclear depolarisation times up to 5000s have been observed [13]. A direct measurement of the hole hyperfine interaction in semiconductors has also been demonstrated [14], placing these dots in the context of the intensively pursued research into QD-based spin qubits [7].

Nevertheless, the use of InP dots for spin studies encounters the following major challenge: InP/GaInP samples commonly contain multi-modal distributions of QD sizes, consisting of short wavelength ($660 - 730$nm at 10 K) small QDs and longer wavelength ($730 - 770$nm at 10 K) large QDs [15, 16]. Although these reproducibly grown samples allow access to individual QDs in the short wavelength range, their properties are uncontrollably influenced by interactions with high density large QDs. These large QDs have been shown to accumulate high numbers of charges at low temperatures [17], leading to charge instability and additional spin relaxation pathways in the neighboring small QDs. The presence of large dots is the most likely reason for a certain time delay, in comparison to InGaAs/GaAs structures, for the achievement of effective charge control in InP single QDs placed in Schottky diodes. This is now realised in our work, after the growth of QDs with a single-mode size distribution has been achieved. This essential step enabled realisation of charge-tunable InP QDs for future studies of

charge-controlled few spin nano-systems.

Here, control by electric field of exciton charge states in individual InP dots by placing them in the intrinsic region of n-i-Schottky diode structures is presented. The optimized growth using low-pressure metalorganic vapor phase epitaxy (MOVPE) enabled us to avoid formation of high densities of large highly charged QDs, leading to optimized samples containing only small QDs with densities below $10^9 \mathrm{cm}^{-2}$. From bias and polarisation-dependent analysis of the photoluminescence (PL), multi-particle excitonic complexes could be observed and identified as the neutral (X_0), singly (X^{-1}), doubly (X^{-2}) and even triply (X^{-3}) negatively charged excitons. Binding energies for the X^{-1} are demonstrated to range from 4 to 7 meV. We probe the PL bias dependence of a relatively high number of individual dots, which allows for a general characterization of the electron-hole permanent dipole moment and polarisability of this system. From the dipole moment analysis, we demonstrate that for InP/GaInP QDs the electron-hole alignment along the growth direction is generally opposite to what is usually observed for InGaAs/GaAs QDs. From the polarisability study, we characterize the lateral extent of the exciton wavefunction in the QD plane and the hole wavefunction extension along the growth direction. Complementary to PL measurements, we carry out resonant excitation experiments, where photon absorption by the dot is measured using photocurrent (PC) technique, opening perspectives to manipulate the electron and hole lifetimes for application in resonant coherent spin control measurements.

The chapter is organised as follows. We start in Sec. 2.2 with a description of the samples structure and the experiments. The experimental results are presented in Sec. 2.3, where in subsection 2.3.1 we discuss the QD growth opti-

mization procedure necessary to obtain a uniform distribution of QD sizes. Subsections 2.3.2 and 2.3.3 are devoted to single QD characterization and statistical analysis of QD properties performed in a large ensemble of QDs, respectively. In subsection 2.3.4 we present single QD characterization by resonant photocurrent spectroscopy. Section 2.4 summarizes the main conclusions of this chapter.

2.2 Experimental

The sample growth was performed in a horizontal flow quartz reactor using low-pressure MOVPE on (100) n-type GaAs substrates misorientated by 3° towards $\langle 111 \rangle$. The growth temperature of the GaAs buffer and bottom $Ga_{0.5}In_{0.5}P$ layer was 700°C. Before proceeding to the deposition of InP and the $Ga_{0.5}In_{0.5}P$ capping layer, the wafer was cooled to 650°C. The grown GaInP layers were nominally lattice matched to GaAs. A low InP growth rate of 1.1Å/s and deposition time of 3 seconds was chosen. Two different Schottky diode structures were analyzed. Sample A consisted of a QD layer grown on top of a 40 nm thick i-GaInP layer above the n-doped GaInP region. Capping was performed with a 160 nm-thickness i-GaInP layer only. Sample B consisted of a QD layer also grown 40 nm above the n-doped GaInP region, but capped by a sequence of undoped GaInP/AlGaInP/GaInP layers with thicknesses of 85, 25, and 50 nm, respectively, in order to create a blocking barrier for holes.

The optical measurements were carried out using a micro-photoluminescence (μPL) set-up with 2 μm spatial resolution for a bare wafer or $\approx 1\mu$m resolution defined by apertures in the opaque mask deposited on the sample surfaces. PL was analyzed using a 1 m double spectrometer with a charge coupled device

(CCD). Photocurrent (PC) measurements were performed via resonant excitation with commercial current/temperature tunable laser-diodes and electrical detection with a picoammeter added to the μPL set-up circuit. All measurements were carried out at 10 K.

2.3 Results

2.3.1 Ensemble characterization

Figure 2.1 presents μPL spectra of unmasked samples obtained in the growth optimization procedure. Figure 2.1(a) demonstrates that by varying the InP deposition thickness (d_{InP}) it is possible to control the size distribution of the InP QDs. As we observe, by changing d_{InP} from 1.65 to 4.4 Å, the center of the QD emission band can be shifted from 665 to 710 nm (the peak around 650nm corresponds to the GaInP barrier emission). This transition is markedly more gradual with deposition thickness than the one observed in the molecular beam epitaxy (MBE) growth of widely studied InGaAs/GaAs QDs[18, 7]. Importantly, this procedure also allows the formation of high densities of large QDs to be avoided. The large dots are formed for higher values of d_{InP}, which is illustrated in Fig. 2.1(c), where, for d_{InP} = 11Å, where we observe a pronounced multimodal size distribution which is characterized by two broad PL peaks: a weak peak at 705 nm and a pronounced band at 750 nm, which correspond to small and large QD size distributions [15, 16, 17], respectively.

The low excitation power spectra shown in Fig. 2.1(b) demonstrate that the optimum conditions for the growth of low densities of small QDs are obtained for

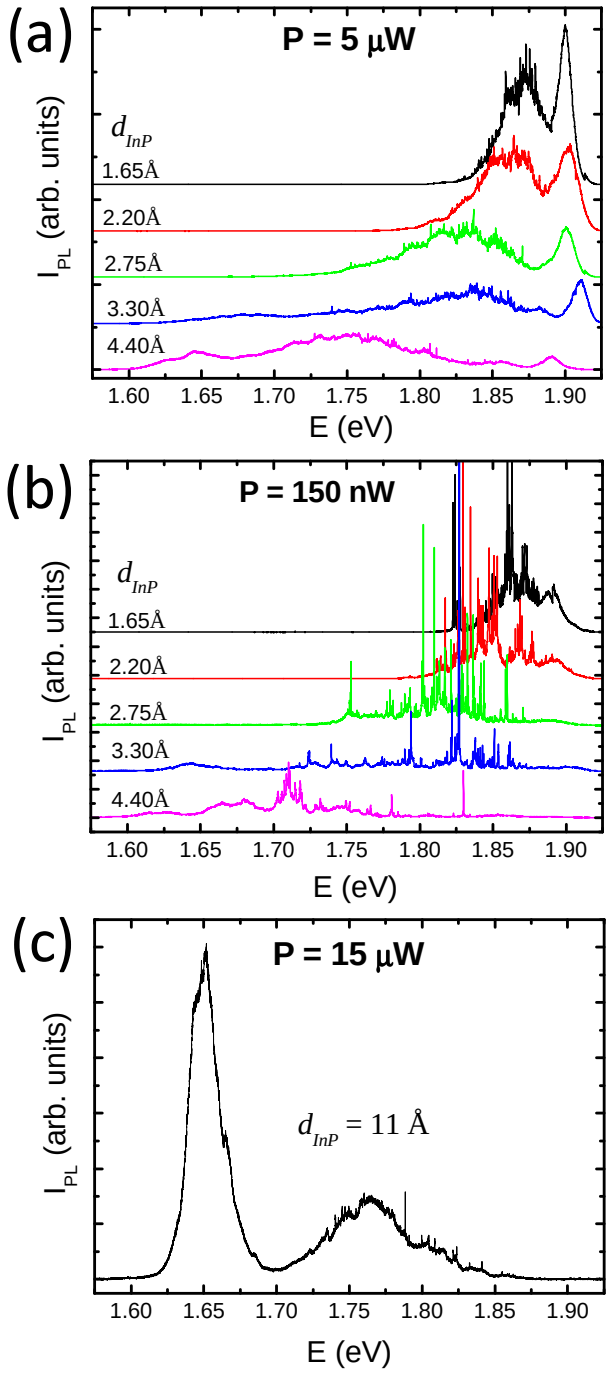

Figure 2.1: μPL spectra of InP/GaInP QD ensembles measured with HeNe laser (λ=632 nm). Spectra for samples with d_{InP} varying from 1.65Å to 4.4 Å are shown for laser excitation powers: (a) $P = 5\mu$W and (b) $P = 0.15\mu$W. (c) Spectrum of a QD ensemble grown with d_{InP}=11Å measured at $P = 15\mu$W.

d_{InP} values in the range of 2.75 Å and 3.3 Å. For these two values, we observe a relatively small number of individual QD PL emission lines, corresponding to QDs densities of 1x10^{9}cm^{-2} and 8x10^{8}cm^{-2}, respectively, which are similar to the ones obtained by MBE growth [19]. We note that the observed range of d_{InP} (from 2.7 Å to 3.3 Å), which leads to growth of suitable samples at our InP deposition rate of 1.1Å/s, is equivalent to 0.2 atomic monolayers (ML). This range is large in comparison to the mechanical growth-control time, thus resulting in very reproducible growth confirmed in our further growth experiments. The variation of the dot density by a factor 1.25 in this range of d_{InP} is up to a factor of 2 smaller than in MBE growth of InP/GaInP (InGaAs/GaAs) QDs for a similar range of deposition thicknesses and dot density around 10^9cm^{-2} [18, 19]. In this way, the MOVPE method discussed here offers a robust and well controlled method for fabrication of QD structures with ideal densities for individual QD studies, thus providing a suitable alternative to InGaAs structures.

2.3.2 Single dot properties

After growth optimization, which led to identification of the optimum d_{InP} ≈3Å, samples A and B were grown as described in Sec. 2.2. The samples were processed in diodes with the top surfaces covered with opaque Au-film contacts, and 1 μm apertures were open for optical access to dots [see Appendix]. Figure 2.2(a) shows an example of a bias dependence of the μPL spectrum of a single QD in sample B measured at excitation wavelength and power of 650 nm and 40 μW, respectively. For high negative bias (reverse bias) occupancy of the dot is low due to the high electron-hole tunneling rates. At V ≈ -2.8 V a single emission

line appears (marked as X_0). As the reverse bias is decreased, a second line appears on the low-energy side of X_0 separated by 6.32 meV. We attribute these two lines to the neutral (X_0) and singly-charged (X^{-1}) exciton states of the QD. This is confirmed by the cross-polarised linear PL detection measurements shown in Fig. 2.2(b). As expected, X_0 shows a fine-structure energy splitting (Δ_{FS}=55 μeV), while X^{-1} is insensitive to polarisation of the detection because the electron-hole exchange interaction is zero due to the presence of a second electron in the QD [20].

Figure 2.2(c) presents the X^{-1} binding energies obtained for a large number of single QDs measured in samples A (dots) and B (empty squares) as a function of E_0, the X_0 energy at zero electric field (obtained from the fit of the QD Stark shift, as explained below). The binding energy is found not to depend on the confinement energy. The distribution presented in Fig. 2.2(d) shows that most of the QDs have binding energies between 4 and 7 meV, similar to what has been reported for InGaAs/GaAs based QDs [2, 21, 22]. This can be attributed to the similarity of effective masses and dielectric constant of both systems, which also should lead to similar values for biexciton binding energies [23].

Note also in Fig. 2.2(a) that, as reverse bias continues to be decreased, electrons tunnel from the back n-type contact into the QD, thus leading to the observation of more negatively charged exciton complexes, namely the X^{-2} and X^{-3} [2, 21]. In general, besides the X_0 emission, the μPL lines observed in the bias dependence measurements on samples A and B were predominantly due to negatively charged multi-exciton complexes. In sample B, even with the presence of the hole blocking barrier, in a very small number of QDs biexciton (XX) emission lines could be identified by cross-polarised linear PL measurements. Precise

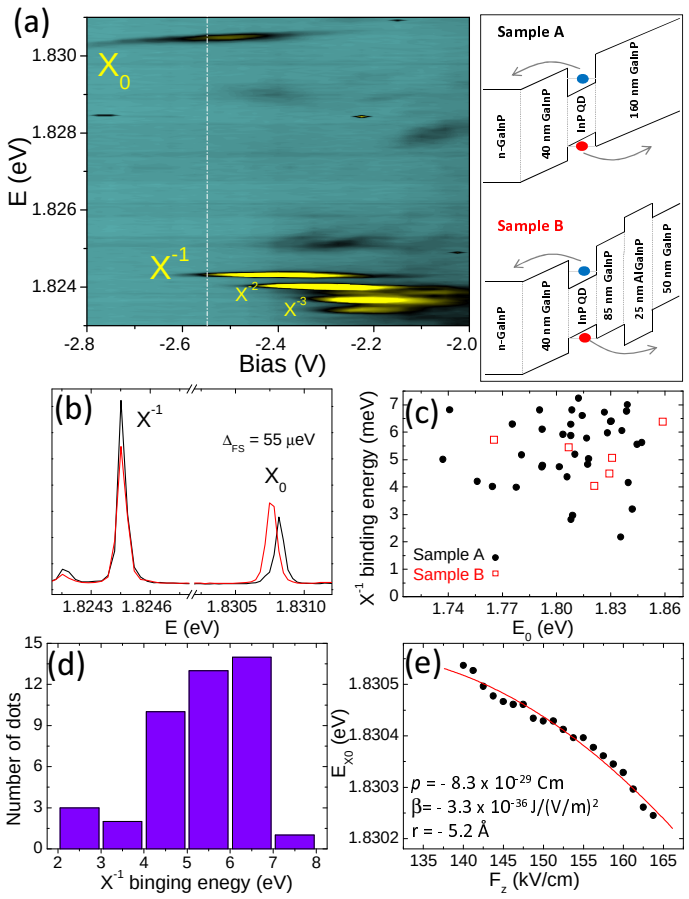

Figure 2.2: (a) Single QD μPL as a function of the bias applied between the n and Schottky contacts. (b) Linear polarisation resolved PL measured at -2.55 V for the X_0 and X^{-1} lines shown on (a). The black and red lines represent polarisation parallel to the [110] and [1$\bar{1}$0] crystallographic directions, respectively. (c) Negatively charged exciton (X^{-1}) binding energy for samples A (black dots) and B (empty squares) against E_0, the energy of the neutral exciton at zero field. (d) Distribution of the X^{-1} binding energy. (e) Neutral-exciton energy E_{X0} as a function of the applied electric field F_z. Inset shows the values of p and β obtained from the fit to the data (solid curve).

determination of the biexciton binding energies was however difficult because of the high spectral density of QD peaks at the low reverse bias where such lines start to be observed. Emission of the positively charged exciton (X^+) was not identified in any of the samples, possibly due to the very low confinement potential for holes expected for InP/$Ga_{0.5}In_{0.5}P$ structures [23].

Figure 2.2(e) shows the emission energy (E_{X0}) of X_0, presented in Fig 2.2(a), as a function of the applied electric field (F_z). The solid line is a fit with the equation $E_{X0} = E_0 - pF_z + \beta F_z^2$, where E_0 is the energy at F_z=0, p is the QD permanent dipole moment, and β is the exciton polarisability [22, 24]. The values obtained for p and β are shown in the inset. From p we extract an electron-hole separation $r = p/e$ = -5.2 Å. The negative sign obtained for r reflects the permanent dipole orientation at zero field for this particular QD: the electron is more localized in the direction of the apex and the hole in the direction of the base of the QD. The hole wavefunction located below that of the electron has previously been inferred from PL bias dependence measurements in InP QD ensembles [17]. However, this is not always true at the single QD level because the electron-hole wavefunction alignment along **z**-direction is sensitive to the specific confinement characteristics of each individual dot. This property is discussed in detail in the following subsection.

2.3.3 Exciton wavefunction

The dependence of the permanent dipole moment p on E_0 for a large number of QDs in samples A (dots) and B (empty squares) is shown in Fig. 2.3(a). We find that p, which is normally sensitive to the QD height and In concentration [22, 25],

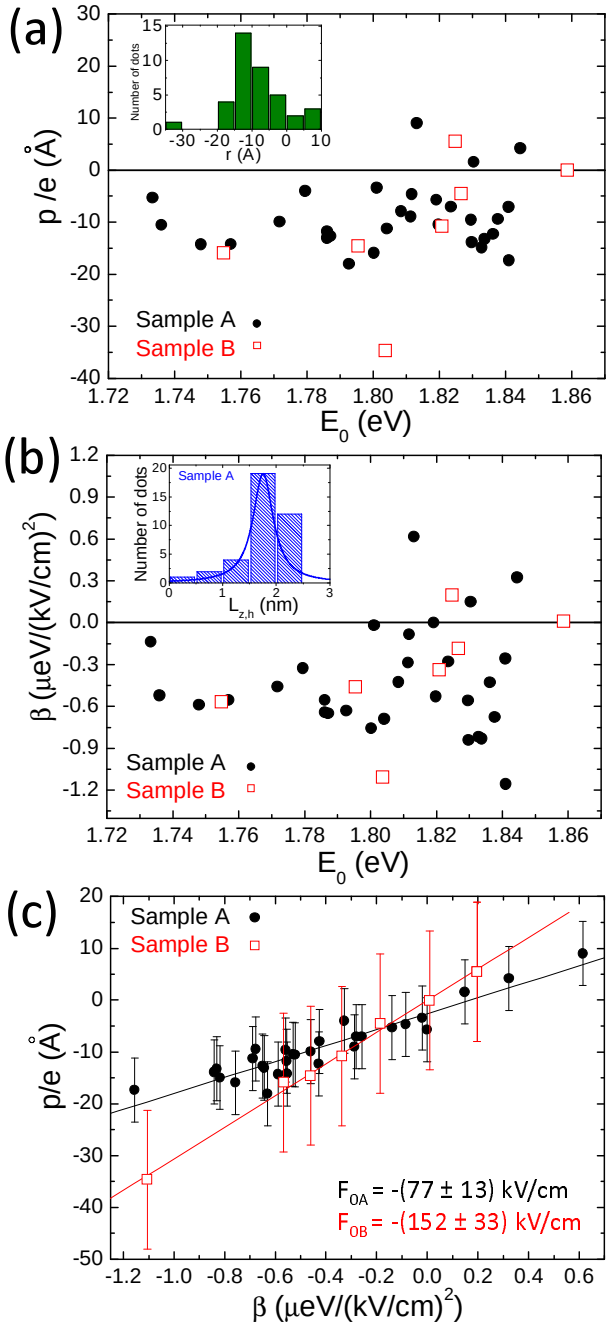

Figure 2.3: (a) Permanent dipole moment p and (b) polarisability β plotted against the neutral exciton energy E_0 for samples A (dots) and B (empty squares). In (a), the inset shows the distribution of the electron-hole separation r. In (b), the inset shows the extent of the hole wavefunction along **z** direction ($L_{h,z}$) for sample A. (c) Permanent dipole moment p against polarisability β for samples A and B. Solid lines are linear fits to the data.

does not depend on the confinement energy in a range of approximately 150 meV. Besides this, the distribution of electron-hole separation r presented on the inset shows that for the majority of the QDs the hole wavefunction is localized below that of the electron. Such a result is consistent with what is expected for strained QDs with a weak gradient of In distribution, for which a minimum of energy for holes is created at the QD base due to the higher strain at the interface with the barrier [26, 27].

However, as also observed in Fig. 2.3(a), some QDs ($\approx$ 13%) show positive values for the permanent dipole moment p. As in the case of InGaAs/GaAs based systems, the occurrence of positive values for p is possibly related to the presence of a positive In gradient from base to apex of the QDs [24, 28, 25]. This gradient, caused by the presence of more Ga atoms close to the interface with the barrier, ensures a smaller strain at the base with respect to the apex, thus inverting the natural dipole moment orientation of the system. The low occurrence of QDs with positive dipole (and the smaller magnitudes of such dipoles) is probably associated with the low mobility of Ga during growth since the QDs were grown at a lower temperature than the bottom GaInP barrier. In addition, NMR measurements by Chekhovich. *et. al* (*unpublished*) indicate an occurrence between 10 and 15% of Ga in such QDs, which can make some dots subject to composition inhomogeneities.

Figure 2.3(b) presents the QD polarisability β plotted as a function of E_0 for samples A (dots) and B (empty squares). Comparing distribution of p and β with E_0 in Figs. 2.3(a) and (b), we can observe that there is a correspondence between the values of the QD permanent dipole moment and its polarisability. Such relationship provides information about the exciton wavefunction extension

in the QD plane. This is clearly illustrated in Fig. 2.3(c), where the values of the permanent dipole moments are displayed as function of the polarisability for both samples. In the harmonic confinement potential approximation, the presence of a permanent dipole moment can be associated with a built-in electric field F_0 along the growth direction. It can be easily shown that the ratio between dipole moment and polarisability characterizes this field $p/\beta = -2F_0$ [22]. By fitting the experimental data with this equation, we obtain the fields $F_{0A} = -(77 \pm 13)$ kV/cm for sample A and $F_{0B} = -(152 \pm 33)$ kV/cm for sample B. The presence of an approximately constant built-in field for the two ensembles of QDs allows for a classical interpretation of the electron and hole wavefunctions as representing the two plates of a circular capacitor [22]. In that case, F_0 depends only on the area (A) of the capacitor $F_0 = e/A\varepsilon_0\varepsilon_r$, not on the distance between the plates. Here, $\varepsilon_r = 12.6$ is the InP dielectric constant [29]. This relationship allows us to estimate, independent of the size of the permanent dipole moment, the lateral extension of the excitonic wavefunction by assuming it to be determined by the area A. From F_{0A} and F_{0B} we obtain $a_A = 7.7$ nm and $a_B = 5.5$ nm for the average excitonic radius encountered in samples A and B, respectively. By comparing with the calculations of Wimmer *et.al* [23], the excitonic radius obtained experimentally from us should correspond to QDs with diameters around 20 and 30 nm.

Furthermore, for InP/$Ga_{0.5}In_{0.5}P$ QDs, the statistics on QD polarisability provides information specifically about the hole wavefunction. Assuming a parabolic confinement in the vertical direction **z** for electrons and holes, the Stark shift of the states is given by $\Delta E = -(e^2/2\hbar^2)(m_h L_{h,z}^4 - m_e L_{e,z}^4)F_z^2$, so that the polarisability depends on the electron (hole) effective mass m_e (m_h) and spatial extent

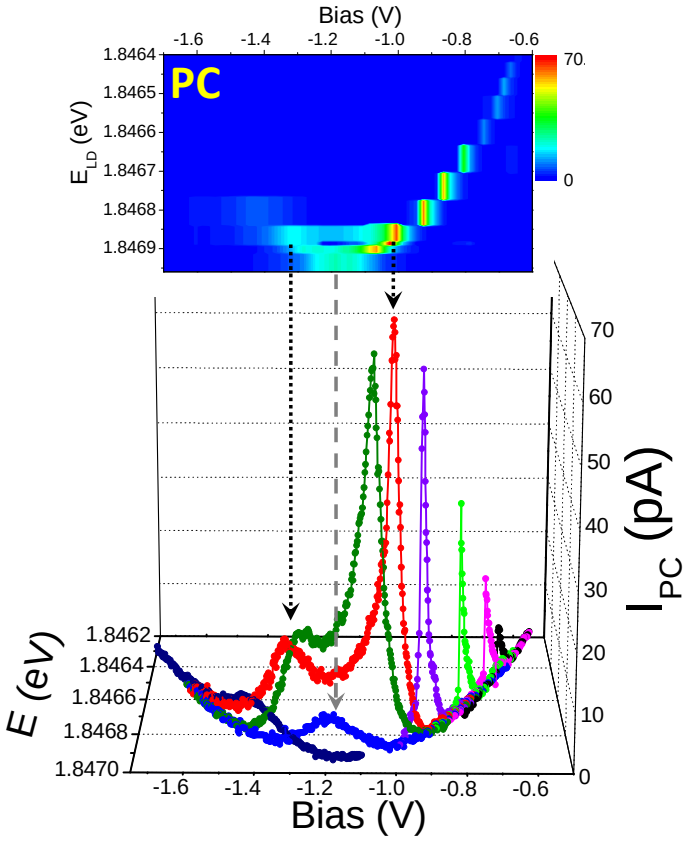

Figure 2.4: Photocurrent a neutral exciton state X_0 measured in a single InP QD for different excitation-laser energies. The 2D-plot inset shows, for comparison, the μPL bias dependence of X_0 for the same single QD. The upper inset illustrates the measurement procedure, where the laser is fixed at different excitation energies E_{LD}, and the QD energy is tuned by the applied bias and brought in resonance with the laser, as described in the text.

of the wavefunction along confinement direction $L_{e,z}$ ($L_{h,z}$) [28, 22]. However, besides the fact that $m_h > m_e$, for InP/$Ga_{0.5}In_{0.5}P$ structures the confinement energy for holes along the vertical direction is expected to be much smaller than the one for electrons [23]. This implies that the hole wavefunction is expected to be more delocalized than the electron one ($L_{h,z} > L_{e,z}$), in contrast to the case of InGaAs/GaAs system [30]. The polarisability measured in our QDs is, therefore, basically characterized by the contribution of holes and can be written as $\beta \approx (e^2/2\hbar^2)m_h L_{h,z}^4$. Using the values obtained from the statistics performed for β and assuming hole effective masses values for InP/$Ga_{0.5}In_{0.5}P$ given by Wimmer [23], we plot on the inset of Fig. 2.3(b) the distribution for the extent of the hole wavefunction along the confinement direction $L_{h,z}$ for the dots probed in sample A. As we observe, the hole wavefunction extension is on average around 2 nm, which, comparing to Fig. 2.3(a), corresponds to QDs with permanent dipoles $p \approx -10$ $\mathring{A}$.

This analysis allows to make more specific conclusions about the nature of the electron-hole alignment in the studied dots. Since electron is under a higher confinement regime the sign of the dipole for InP/$Ga_{0.5}In_{0.5}P$ QDs is mainly determined by the position of center of the hole wavefunction, which is more sensitive to the type of confinement added by the strain. As we observe experimentally, the majority of the QDs are characterized by an electron-above-hole alignment which occurs as a consequence of a high strain at the QD base but also indicates a more homogeneous distribution of In along its height. On the other hand, the presence of a higher concentration of Ga at the base of a small number of QDs relieves the strain at the interface and enhances the In gradient along the QD height, thus contributing to the appearance of smaller positive dipole moments. The height

and strain distribution in the QDs, however, do not affect the in-plane extent of the exciton wavefunction, as demonstrated by the linear relationship between p and β shown in Fig. 2.3(c).

2.3.4 Photocurrent of single dots

As previously mentioned in Chapter 1 photocurrent technique gives information of the carrier absorption in the QD. If a laser is in resonant with a optical transition, absorption creates and electro-hole pair in the dot. The carriers can tunnel from the dot if an electric field is applied and finally the carriers are detected as a change in photocurrent. A photocurrent spectrum is obtained scanning the energy of the laser and monitoring the photocurrent variations. Ideally 100% detection efficiency of photocurrent could be achieved if the device acts like an optically triggered single-electron source. However, this is mainly limited by the competition between radiative recombination and charge tunneling rates.

Figure 2.4 presents resonant-excitation experiments performed on single InP QDs by photocurrent technique (PC). It shows a 3D-plot of X_0 neutral exciton PC performed for one of the QDs in sample A. The corresponding PL bias dependence is shown in the 2D-plot on the inset. Each PC curve is obtained by fixing the energy (E_{LD}) of a single-mode laser-diode and tuning the QD neutral exciton energy through the resonance with E_{LD} by changing the applied bias. The upper inset in Fig. 2.4 illustrates the projection of the 3D-plot into the *E-Bias* plane. By setting E_{LD} = 1.8470 eV (blue horizontal line), approximately equal to the maximum energy of the X_0 Stark-shift parabola, a PC curve with one maximum at this energy is measured (blue-doted PC curve). As E_{LD} is de-

creased to 1.8467 eV (red horizontal line on the inset) two PC peaks are observed (red-doted PC curve) at different bias, corresponding to the resonances achieved at the two sides of the Stark-shift parabola. The linewidth of the PC peak measured at higher reverse bias is broader due to shortening of the carrier lifetime in the dot [31]. In this way, as the laser-diode energy is tuned in small steps across the energy range of the X_0 Stark-shift parabola, the PC bias dependence can be characterized, as demonstrated by plotting the PC curves obtained for different values of E_{LD} in Fig. 2.4. Note that the bias regime where PC is measured coincides with that of PL (see inset). This PC characteristics, observed in all QDs measured in samples A and B, are possibly related to fast hole tunneling which occurs as a consequence of the weak confinement regime that holes are subject. Most important, Fig. 2.4 demonstrates clearly that the single InP QD states can be directly addressed by resonant excitation and detected electrically [as previously reported for In(Ga)As dots only], thus opening the way for more sophisticated experiments involving resonant manipulation of electron, hole and nuclear spins in single dots employing bias control [32, 33].

2.4 Conclusions

In summary, by realising MOVPE growth of low density InP/GaInP QDs, we have overcome the major hurdle of the presence of high densities of large QDs in this system. We achieve a reproducible and smooth transition in QD size distribution and density by varying nominal InP deposition thickness. Such an achievement has allowed the detection and manipulation of neutral (X_0) and negatively charged (X^{-1}) exciton energy levels in individual QDs by application

of vertical electric fields using Schottky devices. X^{-1} binding energies are shown to range from 4 to 7 meV, similar to InGaAs/GaAs QDs. Systematic studies of QD permanent dipole moment and polarisability in a large ensemble of QDs allows for the characterization of the exciton wavefunction in such system. We argue that due to a relatively higher confinement regime imposed to electrons, the sign of QD permanent dipole moments are mainly determined by the position of the hole wavefunction along the growth direction, which provides insight into the QD composition and strain distribution. Moreover, from the relationship between dipole moment and polarisability, we show that the lateral extent of the exciton wavefunction varies very little from dot to dot. We obtain an average in-plane exciton radius of 7.7 and 5.5 nm for two QD ensembles probed in different samples. Photocurrent technique has been demonstrated, allowing for resonant manipulation and electrical detection of excitons in single InP/GaInP QDs.

References

[1] David D. Awschalom and Michael E. Flatte. "Challenges for semiconductor spintronics". In: *Nature Physics* 3 (2007), pp. 153–159 (cit. on p. 29).

[2] R. J. Warburton. "Optical emission from a charge-tunable quantum ring". In: *Nature* 405 (2000), pp. 926–929 (cit. on pp. 29, 36).

[3] F. Findeis and M. Baier. "Photocurrent and photoluminescence of a single self-assembled quantum dot in electric fields". In: *Applied Physics Letters* 78 (2001), pp. 2958–2960 (cit. on p. 29).

[4] Miro Kroutvar. "Optically programmable electron spin memory using semiconductor quantum dots". In: *Nature* 432 (2004), pp. 81–84 (cit. on p. 29).

[5] T. M. Godden. "Coherent Optical Control of the Spin of a Single Hole in an InAs/GaAs Quantum Dot". In: *Physical Review Letters* 108 (2012), p. 017402 (cit. on p. 29).

[6] A J Ramsay. "A review of the coherent optical control of the exciton and spin states of semiconductor quantum dots". In: *Semicond. Sci. Technol.* 25 (2010), p. 103001 (cit. on p. 29).

[7] F Henneberger and O Benson. *Collection of reviews on QDs: 2009*. Singapore: Pan Stanford Publishing, 2009 (cit. on pp. 30, 33).

[8] P. Michler. "A Quantum Dot Single-Photon Turnstile Device". In: *Science* 290 (2000), pp. 2282–2285 (cit. on p. 30).

[9] M. Atature. "Quantum-Dot Spin-State Preparation with Near-Unity Fidelity". In: *Science* 312 (2006), pp. 551–553 (cit. on p. 30).

[10] A. J. Ramsay. "Fast Optical Preparation, Control, and Readout of a Single Quantum Dot Spin". In: *Physical Review Letters* 100 (2008), p. 197401 (cit. on p. 30).

[11] R.J. Warburton. "Optical emission from a charge-tunable quantum ring". In: *Nature* 405 (2000), pp. 926–929 (cit. on p. 30).

[12] E. A. Chekhovich. "Pumping of Nuclear Spins by Optical Excitation of Spin-Forbidden Transitions in a Quantum Dot". In: *Phys. Rev. Lett.* 104 (2010), p. 066804 (cit. on p. 30).

[13] J. Skiba-Szymanska. "Overhauser effect in individual InP/Ga_xIn_{1x}P dots". In: *Phys. Rev. B* 77 (2008), p. 165338 (cit. on p. 30).

[14] E. A. Chekhovich. "Direct Measurement of the Hole-Nuclear Spin Interaction in Single InP/GaInP Quantum Dots Using Photoluminescence Spectroscopy". In: *Phys. Rev. Lett.* 106 (2011), p. 027402 (cit. on p. 30).

[15] W. M. Schulz. "Optical and structural properties of InP quantum dots embedded in $(Al_xGa_{1x})_{0.51}In_{0.49}$P". In: *Phys. Rev. B* 79 (2009), p. 035329 (cit. on pp. 30, 33).

[16] J. Persson. "Optical and theoretical investigations of small InP quantum dots in Ga_xIn_{1-x}P". In: *Phys. Rev. B* 67 (2003), p. 035320 (cit. on pp. 30, 33).

[17] D. Hessman. "Electron accumulation in single InP quantum dots observed by photoluminescence". In: *Phys. Rev. B* 64 (2001), p. 233308 (cit. on pp. 30, 33, 38).

[18] Q. Xie. "Strained coherent InAs quantum box islands on GaAs(100): Size equalization, vertical selforganization, and optical properties". In: *J. Vac. Sci. Technol. B* 14 (1996), pp. 2203–2207 (cit. on pp. 33, 35).

[19] A. Ugur. "Single-dot optical emission from ultralow density well-isolated InP quantum dots". In: *Appl. Phys. Lett.* 93 (2008), p. 143111 (cit. on p. 35).

[20] A. K. Nowak. "Thermal effects in InP/(Ga,In)P quantum-dot single-photon emitters". In: *Phys. Rev. B* 80 (2009), p. 161305 (cit. on p. 36).

[21] J. J. Finley. "Charged and neutral exciton complexes in individual self-assembled In(Ga)As quantum dots". In: *Phys. Rev. B* 63 (2001), p. 073307 (cit. on p. 36).

[22] R. J. Warburton. "Giant permanent dipole moments of excitons in semiconductor nanostructures". In: *Phys. Rev. B* 65 (2002), p. 113303 (cit. on pp. 36, 38, 41, 43).

[23] M. Wimmer. "Biexciton recombination rates in self-assembled quantum dots". In: *Phys. Rev. B* 73 (2006), p. 165305 (cit. on pp. 36, 38, 41, 43).

[24] P.W. Fry. "Inverted Electron-Hole Alignment in InAs-GaAs Self-Assembled Quantum Dots". In: *Phys. Rev. Lett.* 84 (2000), p. 733 (cit. on pp. 38, 40).

[25] J. J. Finley. "Quantum-confined Stark shifts of charged exciton complexes in quantum dots". In: *Phys. Rev. B* 70 (2004), p. 201308 (cit. on pp. 38, 40).

[26] C. Pryor. "Electronic structure of strained InP/$Ga_{0.51}In_{0.49}$P quantum dots". In: *Phys. Rev. B* 56 (1997), p. 10404 (cit. on p. 40).

[27] M. Grundmann. "InAs/GaAs pyramidal quantum dots: Strain distribution, optical phonons, and electronic structure". In: *Phys. Rev. B* 52 (1995), p. 11969 (cit. on p. 40).

[28] J. A. Barker. "Theoretical analysis of electron-hole alignment in InAs-GaAs quantum dots". In: *Phys. Rev. B* 61 (2000), p. 13840 (cit. on pp. 40, 43).

[29] *Landolt-Börnstein. Numerical Data and Function Relationships in Science and Technology, Group III.* Berlin: Springer-Verlag, 1982 (cit. on p. 41).

[30] R. J. Warburton. "Coulomb interactions in small charge-tunable quantum dots: A simple model". In: *Phys. Rev. B* 58 (1998), p. 16221 (cit. on p. 43).

[31] R. Oulton. "Subsecond Spin Relaxation Times in Quantum Dots at Zero Applied Magnetic Field Due to a Strong Electron-Nuclear Interaction". In: *Phys. Rev. Lett.* 98 (2007), p. 107401 (cit. on p. 45).

[32] M. N. Makhonin. "Nuclear spin pumping under resonant optical excitation in a quantum dot". In: *Appl. Phys. Lett.* 93 (2008), p. 073113 (cit. on p. 45).

[33] C. Kloeffel. "Controlling the Interaction of Electron and Nuclear Spins in a Tunnel-Coupled Quantum Dot". In: *Phys. Rev. Lett.* 106 (2011), p. 046802 (cit. on p. 45).

Chapter 3

Dynamic nuclear polarization in InGaAs/GaAs quantum dots under non-resonant ultra-low power optical excitation

3.1 Introduction

Hyperfine interaction within semiconductor quantum dots is one of the main mechanisms which prevents long lived electron spin memory and coherence. Materials with well-isolated nuclear spins such as Si nuclei, ^{31}P impurities in silicon and ^{13}C in diamond have called attention as an option to overcome this problem isolating the electron spin from magnetic environments [1, 2, 3]. Nevertheless, despite all atoms in III-V semiconductors carry nonzero nuclear spin, these material systems are favored for fabrication of advanced quantum dot nanostructures

suitable for both electrical and optical control of single electron and hole spin states [4, 5, 6]. Even more, semiconductor quantum dots have been recently reported as an efficient source of entangled photons when driven electrically, which is desirable for quantum information processing [7, 8]; However, here as well hyperfine interactions play a major role limiting fidelity [9]. Therefore, it is desirable to pump high nuclear polarisation in a semiconductor quantum dot. It has been predicted that if a 100% polarisation of the nuclei is obtained, the electron spin decoherence due to nuclear spin fluctuations will be suppressed [10]

Previously, highly efficient nuclear spin pumping has been demonstrated using both resonant optical excitation of optical transitions within a chosen dot and non-resonant optical pumping creating non-equilibrium populations of electron spins causing dynamic nuclear polarisation [11, 12, 13, 14, 15, 16]. The majority of nuclear spin pumping methods (especially in resonant excitation configurations) employ relatively high excitation powers to create sizable nuclear polarisation. In contrast, in a recent report by Chekhovich et al [17], effective nuclear spin pumping has been achieved in InP/GaInP quantum dots under low power excitation, in the regime where both bright and dark excitons are readily observed. Control of the nuclear spin environment in such a low power regime may be favourable for spin physics studies in QD diode structures, where perturbations to the charge state of the dot (controlled by the electric field) may be minimised by using the low excitation power.

Here we report measurements of DNP at ultra-low excitation power (4 orders of magnitude lower than QD saturation) in individual neutral InGaAs/GaAs self-assembled dots. We show that the main mechanism of DNP at ultra-low excitation powers is electron - nuclear spin flip-flop caused by second order re-

combination of dark states similar to the mechanism reported for InP/GaInP dots [17]. Very large Overhauser shifts (OHS) up to 80μeV were found at ultra-low excitation power, this representing an Overhauser field B_N=-3.2T. Here, the effect observed in InGaAs QDs is significatively more pronounced than InP/GaInP, mainly due to higher electron spin polarisation achievable in InGaAs.

3.2 Techniques and samples

The experiments were performed on neutral quantum dots in a nominally undoped InGaAs/GaAs sample. The structure was grown by molecular beam epitaxy (MBE), for more details on the growth technique see growth techniques subsection in Introduction. Self-assembled InGaAs/GaAs dots were grown in a low Q-factor (Q = 250) cavity that enhances the quantum dot luminescence signal [18, 19, 20]. All experiments were carried out in a μ-PL set up with a helium gas-exchange cryostat at T=4.2 K. The sample was excited by the laser light focused by an aspheric lens into a spot of 1 μm in diameter. The same lens was used to collect the PL signal which was then analyzed by a double spectrometer, equipped with a back-illuminated deep-depletion charge-coupled device (CCD) camera. Excitation energy was chosen to match the wetting layer for InGaAs dots (E_{exc}=1.46 eV). Magnetic field B_Z up to 8 T was applied normal to the sample surface and parallel to the direction of PL excitation and collection. Pump-probe measurements are employed to extract behaviour at optical saturation powers, and to deduce $B_N = 0$ keeping the sample in dark for sufficiently long time to allow the nuclear spins to relax (>200s).

3.3 Photoluminescence spectroscopy of dark and bright exciton states in neutral quantum dots

In a neutral QD, electrons ($\uparrow, \downarrow$) and heavy holes ($\Uparrow, \Downarrow$) spins can form either optically forbidden dark excitons $|\Uparrow, \uparrow>$ ($|\Downarrow, \downarrow>$) with spin projections $J_Z = +2$(-2) or bright excitons $|\Uparrow, \downarrow>$ ($|\Downarrow, \uparrow>$) with $J_Z = +1$(-1) [21]. The structure of the exciton eigenstates in the dot is determined by the electron-hole ($e-h$) exchange interaction [11, 22]. In QDs with low symmetry exchange interaction mixes bright and dark states [22, 15]. As a result dark excitons gain dipole oscillator strength and become visible in PL.

Typical PL spectrum of single InGaAs/GaAs neutral QD measured in magnetic field $B_Z = 8T$ along the sample growth axis is shown in figure 3.1. Two spectra are shown: at ultra-low optical excitation power $P_{exc} = 11nW$ (bottom spectrum) and at high power $P_{exc} = 3\mu W$ (top spectrum). Saturation power of X_0 for this dot is $100\mu W$.

We start with discussion of the spectra measured at ultra-low powers. At these powers QD is in the linear regime, i.e. PL intensity of all exciton lines depend linearly on excitation power P_{exc}. Such regime is realised when the total probability to find the dot occupied by an exciton (in any spin state) is much less then unity ($\ll 1$). Under these conditions PL intensity of each exciton state will be determined by two factors (i) the probability for this state to be populated by the laser excitation and (ii) non-radiative escape rate (spin-flips, or non-radiative recombination). If the rate of non-radiative processes is negligibly small the relative PL intensity of each exciton state will be proportional to its initial population probability after the optical excitation. This is because each

exciton (dark or bright) will have sufficient time to emit a photon before the dot captures another e-h pair. As a result at ultra-low power all four possible excitons have comparable intensities in PL spectrum (Fig. 3.1). We note that observation of dark excitons in InGaAs/GaAs QDs at ultra-low optical powers complement the previous report for InP/GaInP quantum dots [17], demonstrating that this phenomenon is not specific to a certain QD material system.

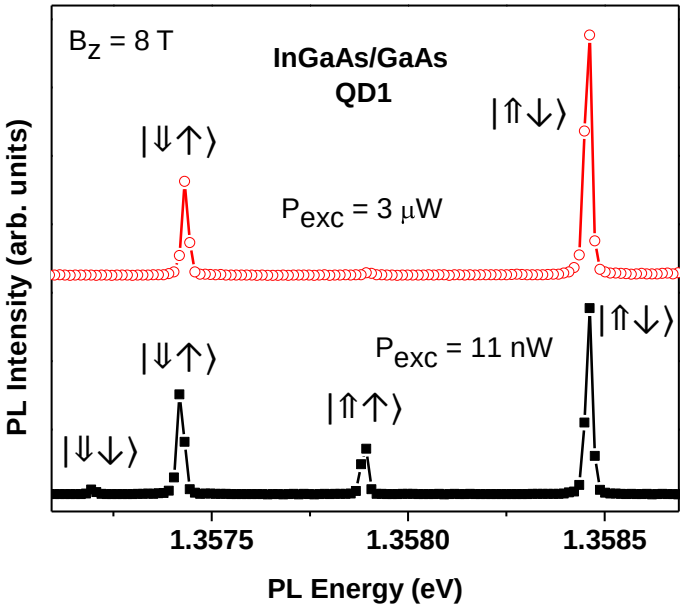

Figure 3.1: PL spectrum of neutral InGaAs QD1, measured in external magnetic field applied along the sample growth axis $B_Z = 8T$. Two spectra are shown: at ultra-low optical excitation power $P_{exc} = 11nW$ (bottom spectrum) and at high power $P_{exc} = 3\mu W$ (top spectrum). In a neutral quantum dot heavy holes $(\Uparrow, \Downarrow)$ and electrons $(\uparrow, \downarrow)$ with spins parallel (antiparallel) can form optically allowed "bright" states $(|\Uparrow, \downarrow>, |\Downarrow, \uparrow>)$ and forbidden "dark" states $(|\Uparrow, \uparrow>, |\Downarrow, \downarrow>)$ with total spin projections $J_Z = |+1>(|-1>)$ and $J_Z = |+2>(|-2>)$ respectively. At ultra low excitation power all four (bright and dark) excitons are observed in PL spectrum. At high power, PL of dark states is saturated and only bright states are observed.

When optical excitation power is increased the PL of dark excitons saturates

due to their small optical recombination rate as shown in the top spectrum of fig. 3.1. This saturation takes place when QD is no longer in the linear regime, and dark excitons can be effectively depopulated via capture of a second exciton and formation of a biexciton state. As a result dark excitons have relatively small intensity compared to bright sates at increased optical power (Fig. 3.1).

The dependence of PL energies of dark (E_d) and bright (E_b) exciton states on external field B_Z is shown with symbols in Fig. 3.2 for InGaAs/GaAs QD2. We use the following model equations for exciton energies [22, 17]:

for bright states with J_Z=$\pm$1

$$E_b(B_Z) = E_0 + \kappa B_Z^2 + \delta_0/2 \pm \sqrt{\delta_b^2 + \mu_B^2 (g_{h,z} - g_{e,z})^2 B_Z^2}/2 \tag{3.1}$$

while for dark states with J_Z=$\pm$2 we have

$$E_d(B_Z) = E_0 + \kappa B_Z^2 - \delta_0/2 \pm \sqrt{\delta_d^2 + \mu_B^2 (g_{h,z} + g_{e,z})^2 B_Z^2}/2 \tag{3.2}$$

where μ_B is Bohr magneton, E_0 QD band-gap energy, κ diamagnetic constant, $g_e(g_h)$ electron (hole) g-factor, δ_0 is the splitting between dark and bright exciton doublets and $\delta_d(\delta_b)$ is the dark (bright) doublet fine structure splitting.

Optical excitation creates bright states in the first instance, and spin relaxation of bright states before optical recombination fills up dark states.

Since the Zeeman splitting of bright (dark) excitons is determined by the difference (sum) of g_e and g_h electron and hole g-factors can be determined independently from the experiment. The results of fitting using Eq. 3.1 and 3.2 are shown in Fig. 3.2 with lines. We find the following fitting parameters: $\kappa \approx 7.5$ μeV, $\delta_0 \approx 365$ μeV, $\delta_b \approx 35$ μeV, g_e = - 0.42 and g_h = 1.82 for InGaAs/GaAs

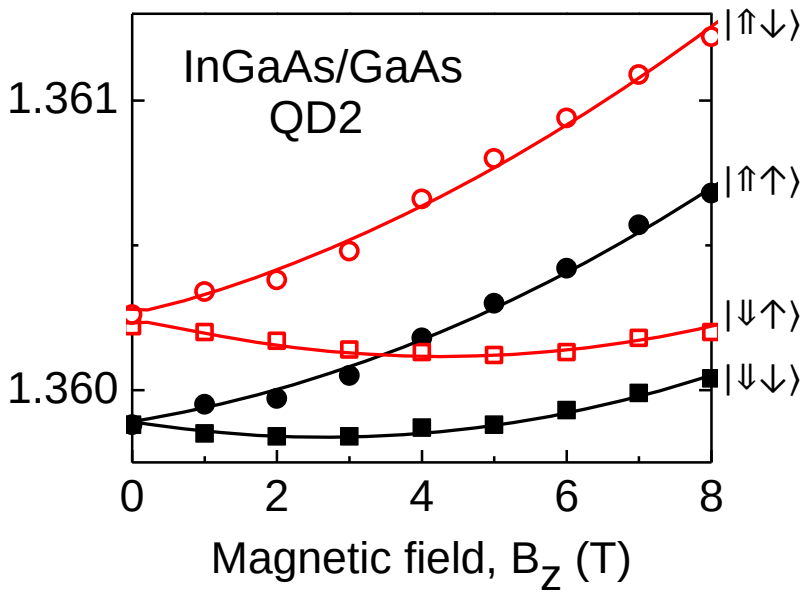

Figure 3.2: Magnetic - field dependence of exciton PL energies in InGaAs QD2. Open symbols represent bright states $|\Uparrow,\downarrow>$ (circles) and $|\Downarrow,\uparrow>$ (squares), while solid symbols correspond to dark states $|\Uparrow,\uparrow>$ (circles) and $|\Downarrow,\downarrow>$ (squares). Lines show fitting using Eq. 1 allowing electron and hole g-factors to be determined (see details in text).

QD2 at $B = 0$ T and optical power $P_{exc} = 50nW$. The splitting δ_d could not be resolved and was fixed at zero during the fitting. From the measurements on several other dots from the same samples we find very similar values of κ, δ_0, g_e, g_h while fine structure splitting δ_b changes considerably from dot to dot.

3.4 Dynamic nuclear polarisation in neutral quantum dots at ultra-low excitation power

3.4.1 Detection of nuclear spin polarisation in quantum dots

Optical detection of the nuclear spin polarisation in single dots may be achieved as follows [23]. When an external field B_Z is applied along the sample growth direction, the exciton Zeeman splitting is observed in PL (see Fig. 3.4): the four visible PL lines correspond to recombination of two bright excitons with spin projections $\mid -1 >, \mid +1 >$ and two dark excitons with projections $\mid +2 >, \mid -2 >$. Circularly polarised optical excitation transfer angular momentum to the electron which is then transmitted to the nuclei due to hyperfine interaction. Polarisation of nuclear spins (to be considered in the following subsections) will lead to occurrence of the Overhauser field B_N, a collective result of the hyperfine interaction of 10^5 nuclei in the dot with the spin of the confined electron [24]. In turn polarised electrons act like an effective magnetic field known as Knight Field B_e which is in the millitesla range, significant smaller than the maximum Overhauser field which can reach several tesla [14]. The electron-nuclei hyperfine interaction and created Overhauser and Knight fields are illustrated in Fig. 3.3.

Here, for simplicity we will neglect the hyperfine interaction of the hole [25, 26]. When nuclear spins are polarised either along or opposite the external field [12, 27], the bright exciton Zeeman splitting change corresponding to the Overhauser shift will be as follows: $E_{OHS} = g_e \mu_B B_N$ (where g_e electron g-factor, μ_B- Bohr magneton). Note, that E_{OHS} is directly proportional to the degree of nuclear

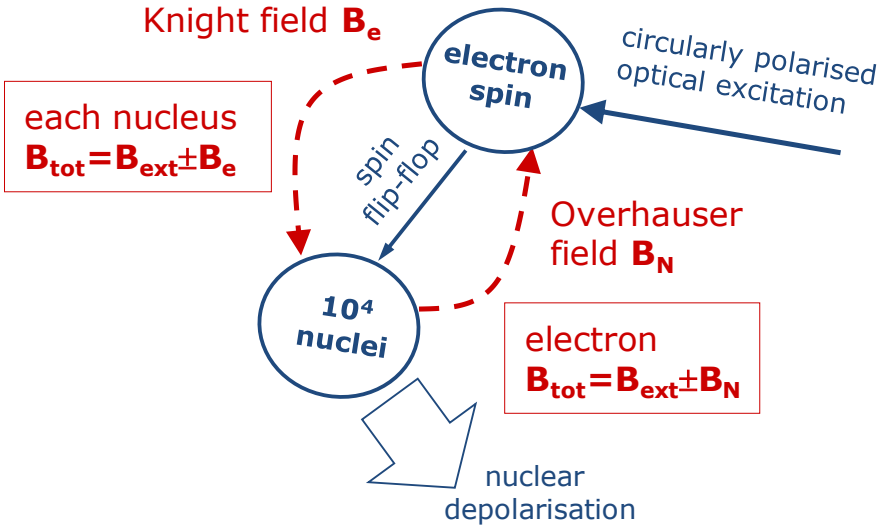

Figure 3.3: Schematic representation of the electron-nuclei hyperfine interaction. Circular polarisation excitation transmit angular momentum to the electron which is then transmitted to the nuclei. Polarised nuclei create and effective Overhauser field B_N acting on the electron, in turn the polarised electrons create and effective Knight field B_e which acts back on the nuclei.

polarisation S_N : $B_N \propto S_N$. In PL, where the typical linewidths are in the range of 30-80 μeV, using lineshape fitting, E_{OHS} can be measured with an accuracy of $\approx 1\mu eV$, potentially providing a very high accuracy in the measurements of S_N [26]. In practice, QDs with complex compositions are used, where polarisation degrees for different isotopes may be different. In that case $E_{OHS} = \Sigma\rho_i A_i I_i S_{N,i}$, where ρ_i is the relative concentration of the ith isotope, A_i, I_i and $S_{N,i}$ - its hyperfine constant, spin and polarisation degree, respectively [12]. Thus, in most cases the determination of the absolute degree of nuclear polarisation is a difficult task, and it is more practical to operate in terms of the Overhauser shifts, which in some cases, when g_e is known, can also be converted in to the Overhauser

fields, B_N.

Similarly to PL, in other types of optical measurements on single dots, such as differential transmission (DT) [16] or resonance fluorescence (RF) [25], the Overhauser shifts can usually be measured. The advantage of the non-resonant measurement such as PL on a single dot is that the energies of all states are detected in a single PL spectrum measurement, enabling precise determination of the Overhauser shift [12, 27, 26]. This can be achieved using resonant techniques only when two or more resonant lasers are used [25]. In the measurements on ensembles of QDs the degree of nuclear polarisation can be either extracted from the detailed measurements of the PL polarisation [28] or from the ultra-fast optical measurements of the Larmor precession of electrons [29].

Figure 3.4 shows PL emission at $B_Z = 5.35T$ and $P_{exc} = 13nW$ of all four exciton transitions in presence of positive (open squares) and negligible (solid circles) nuclear polarisation. Zeeman energy splitting of bright states ($|+1>$,$|-1>$) is enhanced by Overhauser field.

3.4.2 Dynamic nuclear polarisation at ultra-low optical powers in InGaAs quantum dots

We now turn to the analysis of the mechanisms of the optically induced dynamic nuclear polarisation in the studied quantum dots. For that we perform a series of power-dependent measurements on a set of different quantum dots at different magnetic fields B_Z. In each measurement optical excitation power P_{exc} is varied in a wide range of more than six orders of magnitude and PL intensities of excitons as well as the Overhauser shift E_{OHS} are deduced as a function of P_{exc}

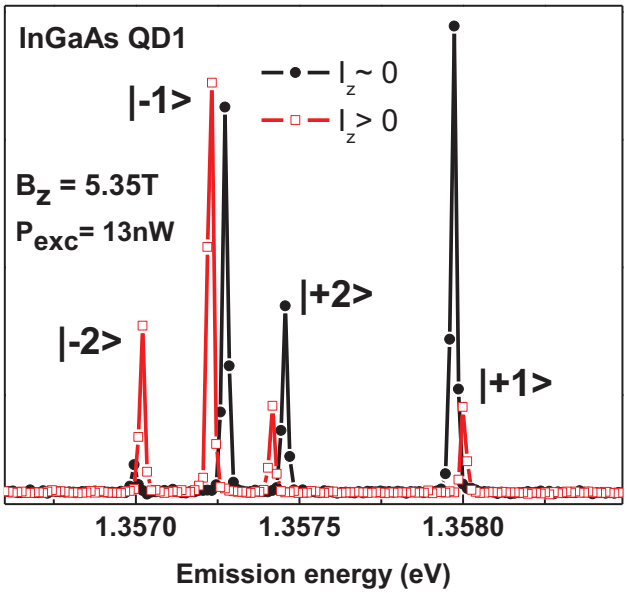

Figure 3.4: PL emission of all four exciton transitions in presence of positive (open squares) and negligible (solid circles) nuclear polarisation is shown. Zeeman energy splitting of bright states ($|+1>, |-1>$) is enhanced by Overhauser field.

with the expression: $E_{OHS} = \Delta E_{|\Uparrow\downarrow>,|\Downarrow\uparrow>} - \Delta E^{0}_{|\Uparrow\downarrow>,|\Downarrow\uparrow>}$; where $\Delta E_{|\Uparrow\downarrow>,|\Downarrow\uparrow>}$ corresponds to energy splitting between the bright states ($|\Uparrow\downarrow>, |\Downarrow\uparrow>$) for $B_N \neq 0$, and $\Delta E^{0}_{|\Uparrow\downarrow>,|\Downarrow\uparrow>}$ corresponds to the energy splitting of bright states ($|\Uparrow\downarrow>, |\Downarrow\uparrow>$) for $B_N = 0$. This can be measured accurately only when the conditions with $B_N = 0$ are known. In order to obtain an accurate measurements of the OHS we extract the ΔE for bright excitons at $B_Z = 8T$, using pump-probe measurements. We keep the sample sufficiently long time to allow the nuclear spins to relax (>200s), and we obtain a $\Delta E = 1050\mu eV$. The results of such an experiment done on InGaAs QD2 at $B_Z = 7T$ are presented in Fig. 3.5 for σ^+ polarised optical pumping (open symbols) and σ^- pumping (solid symbols). Additional scale on the far right shows effective nuclear field B_N, deduced by $B_N = \frac{E_{OHS}}{\mu_B g_e}$.

PL intensities of all four exciton transitions are shown in the top part of

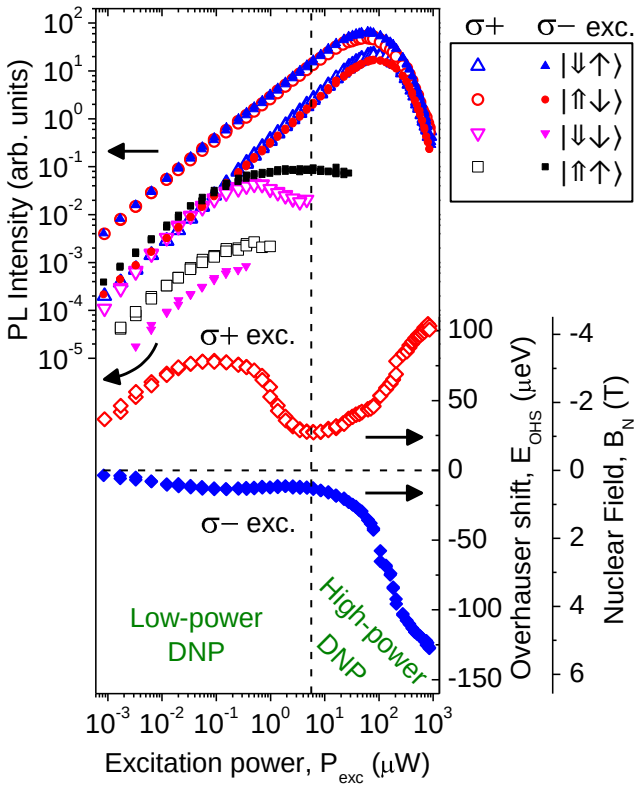

Figure 3.5: Results of power dependence measurements on InGaAs neutral quantum dot QD2 at $B_Z = 7T$ under σ^+ (open symbols) and σ^- (solid symbols) optical pumping. PL intensities of all bright and dark exciton states are shown at the top of the graph (left scale). Overhauser shift $E_{OHS} = \Delta E_{|\Uparrow\downarrow>,|\Downarrow\uparrow>} - \Delta E^0_{|\Uparrow\downarrow>,|\Downarrow\uparrow>}$ is shown at the bottom of the graph with diamonds (right scale). Additional scale on the right shows effective nuclear field B_N. Vertical dashed line at $P_{exc} \sim 5\mu eV$ shows an approximate boundary between two distinct nuclear spin pumping mechanisms: low power DNP via second order recombination of dark excitons and high-power DNP due to spin transfer from spin polarised excitons/electrons (see explanation in the text).

Fig. 3.5 (left scale). The intensities of bright excitons saturate at a power of $\sim 80\mu W$, while dark excitons saturate at much lower power $< 5\mu W$ due to their significantly smaller oscillator strengths.

The power dependence of nuclear polarisation is shown in the bottom part

of Fig. 3.5 (right scale). Two distinct regimes can be observed. High-power DNP ($P_{exc} \geq 5\mu W$) is characterized by monotonic power dependence and direct correspondence between the helicity of light and the direction of the resulting nuclear field. Such pattern in DNP power dependence is well studied [13, 30, 17]. In this regime σ^+ (σ^-) optical pumping results in positive (negative) Overhauser shift E_{OHS} which exceeds +100 μeV (-120 μeV), corresponding to effective nuclear field in excess of +4 T (-5 T). However these large values of E_{OHS} are achieved only at very large pumping powers $P_{exc} \sim 1000\mu W$ for which exciton luminescence is saturated and suppressed, for which pump-probe measurements are needed (Fig. 3.5). Thus high-power DNP can not be ascribed to ground state excitons and is likely to be a result of nuclear spin transfer from spin polarised electrons in the wetting layer or highly excited QD states [17].

A significantly different nontrivial pattern is observed in the low-power DNP regime ($P_{exc} \leq 5\mu W$). At σ^+ pumping Overhauser shift depends non-monotonically on the excitation power with maximum $E_{OHS} \approx 80\mu eV$ observed at a very low power of $P_{exc} \approx 100nW$. We note that with the high-power DNP the same magnitude of E_{OHS} can only be achieved for excitation powers at least 3000 times higher. For σ^- pumping, less pronounced monotonic behavior is observed at ultra-low powers, while at high power similar behavior is detected although with opposite signs.

The underlying mechanisms of DNP observed in the low power regime has been described for InP/GaInP QDs [17]. Schematic representation of the two bright and two dark states involved in the process of DNP at ultra-low excitation powers for InGaAs QD at $B_{ext} > 5$ is presented in figure 3.6. In this mechanism, DNP occurs via second-order process which involves virtual transitions between

bright and dark excitons [22]. For instance, if the dot contains a $|-2>$ dark exciton it can increase the total nuclear spin by -1 by making a virtual flip into the $|-1>$ bright state (zigzag line Fig. 3.6). Such process which changes nuclear spin polarisation by +1(-1) can start from $|+2>$($|-2>$) or $|-1>$($|+1>$ states (see Fig. 3.6). Here the difference arise from the longer lifetimes of dark states ($|\pm 2>$) which therefore dominate the DNP at ultra-low power excitations. In the present InGaAs QD system, the rate of virtual flip - flops of the $|-2>$ exciton exceeds that of the $|+2>$. This imbalance arises from the asymmetry of the exciton configuration of the dot (see figures 3.2 and 3.4). Here the energy splitting between $|-2>$ and $|-1>$ is significantly smaller than $|+2>$ and $|+1>$. This results in a considerably more effective nuclear spin pumping for σ^+ excitation, which populates the $|-2>$ dark state. Here, the nuclear spin pumping efficiency scales roughly as $1/\Delta E_{DB}^2$, where ΔE_{DB} is the energy splitting between dark and bright states.

Figure 3.7 shows power dependence measurements on InGaAs neutral quantum dot QD2 under σ^+ optical pumping at $B_Z = 5T$ (top), $B_Z = 7T$ (middle) and $B_Z = 8T$ (bottom). Overhauser shift $E_{OHS} = \Delta E_{|\Uparrow\downarrow>,|\Downarrow\uparrow>} - \Delta E^0_{|\Uparrow\downarrow>,|\Downarrow\uparrow>}$ is shown in the left scale. Additional scale on the right shows effective nuclear field B_N, deduced by $B_N = \frac{E_{OHS}}{\mu_B g_e}$. Horizontal dash lines show maximum B_N values for all three B_Z : for $B_Z = 5T a B_N = 1.8T$, for $B_Z = 7T a B_N = 3.2T$ and for $B_Z = 8T a B_N = 2.7T$. A non-monotonic dependence of the maximum B_N in the low power regime on B_Z is apparent in these figures(shown with horizontal line).

Energy splitting between $|-2>$ and $|-1>$ decreases as B_Z increases (see Fig. 3.2), which leads to increase of OHS due to more efficient interaction between relevant dark and bright states, this effect can be clearly identify by increasing B_N

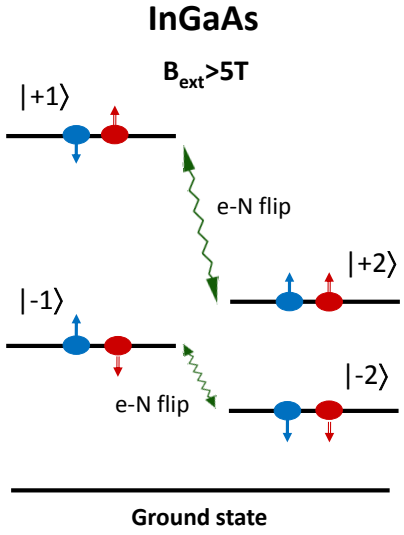

Figure 3.6: Energy diagram of exciton states in high magnetic field $B_Z > 5T$. Heavy holes $(\Uparrow, \Downarrow)$ and electrons $(\uparrow, \downarrow)$ with spins parallel (antiparallel) to B_Z form optically allowed "bright" excitons $(|\Uparrow, \downarrow>, |\Downarrow, \uparrow>)$ and "dark" excitons $(|\Uparrow, \uparrow>, |\Downarrow, \downarrow>)$ with total spin projections $J_Z = |+1>(|-1>)$ and $J_Z = |+2>(|-2>)$ respectively. Zigzag lines show electron-nuclear (e-N) spin flips induced by the hyperfine interaction.

when we move from $B_Z = 5T$ ($B_N = 1.8T$) to $B_Z = 7T$ ($B_N = 3.2T$). However, when we increase B_Z from $7T$ to $8T$ we detect a decrease of B_N ($3.2T \rightarrow 2.7T$). At $B_Z = 8T$ small energy splitting between $|-2>$ and $|-1>$ excitons causes strong mixing of the states which in fact decrease the lifetime of the $|-2>$ dark state, hence reducing the nuclear spin pumping efficiency.

In figure 3.8 we present power dependence measurements on InGaAs neutral quantum dot QD2 under σ^+ optical pumping at B_Z ranging from $0T$ to $8T$. Overhauser shift E_{OHS} is represented by color code and shown in the left scale of Fig. 3.8. Horizontal dashed line at $P_{exc} = 1\mu W$ shows an approximate boundary between two distinct nuclear spin pumping mechanism: low-power DNP via second order recombination of dark excitons and high-power DNP due to spin

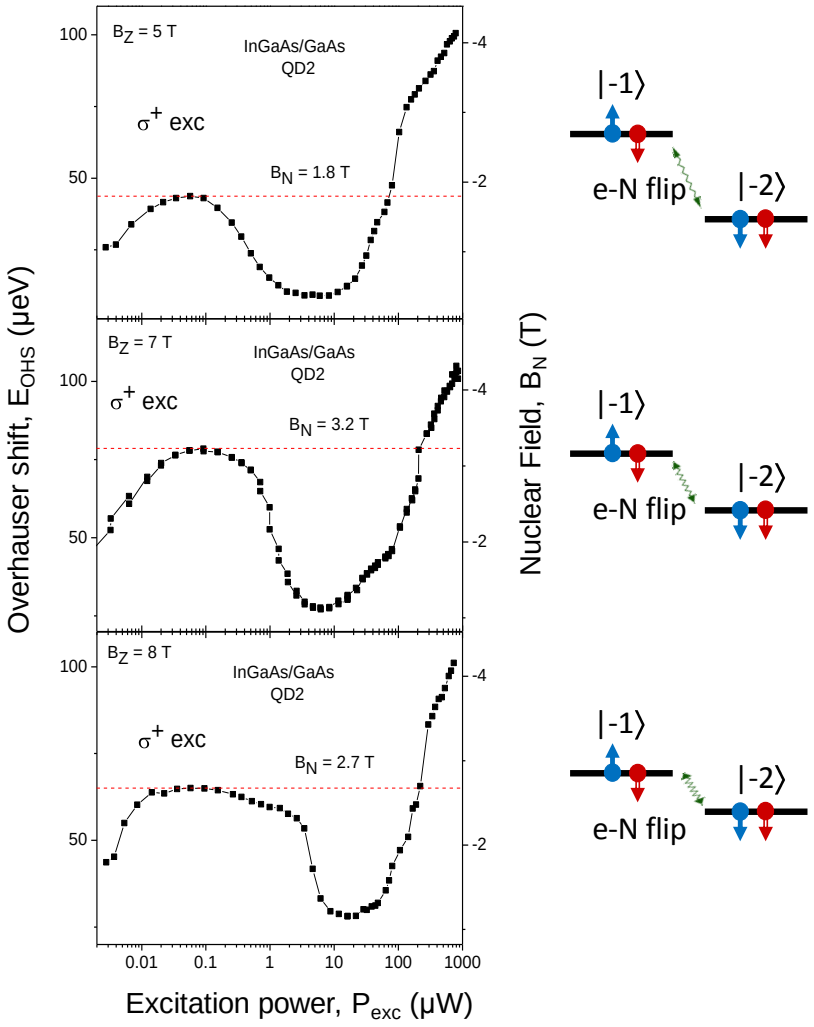

Figure 3.7: Power dependence measurements on InGaAs neutral quantum dot QD2 under σ^+ optical pumping at $B_Z = 5T$ (top), $B_Z = 7T$ (middle) and $B_Z = 8T$ (bottom). Overhauser shift $E_{OHS} = \Delta E_{|\Uparrow\downarrow>,|\Downarrow\uparrow>} - \Delta E^0_{|\Uparrow\downarrow>,|\Downarrow\uparrow>}$ is shown in the left scale. Additional scale on the right shows effective nuclear field B_N, deduced by $B_N = \frac{E_{OHS}}{\mu_B g_e}$. Horizontal dash lines show B_N values for all three B_Z : $B_N = 1.8T for B_Z = 5T$, $B_N = 3.2T for B_Z = 7T$ and $B_N = 2.7T for B_Z = 8T$. Sketch of the energy separation between bright and dark states for each B_z is presented on the right hand side.

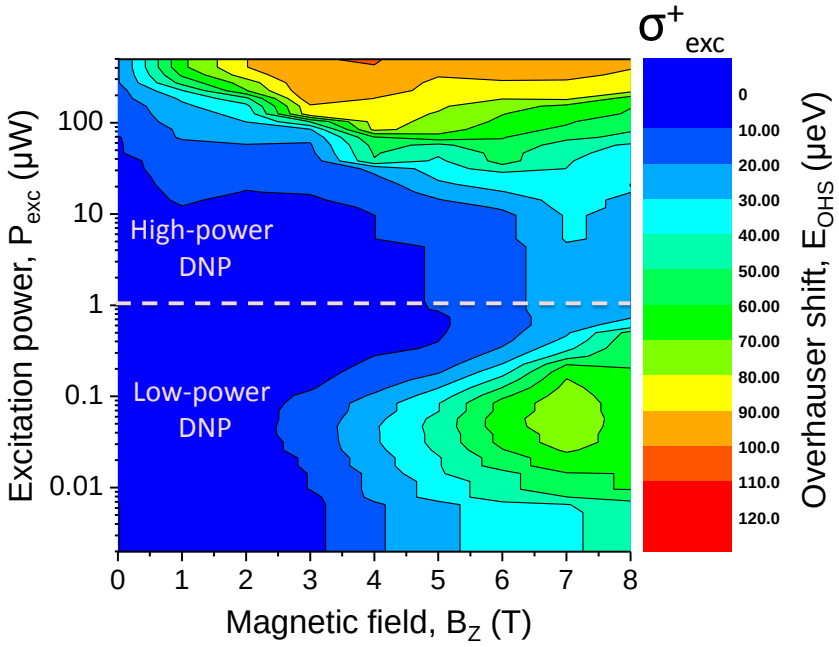

Figure 3.8: Power dependence measurements on InGaAs neutral quantum dot QD2 under σ^+ optical pumping at B_Z ranging from $0T$ to $8T$. Overhauser shift $E_{OHS} = \Delta E_{|\Uparrow\downarrow>,|\Downarrow\uparrow>} - \Delta E^0_{|\Uparrow\downarrow>,|\Downarrow\uparrow>}$ is represented by color code and shown in the left scale. Horizontal dashed line at $P_{exc} = 1\mu W$ shows an approximate boundary between two distinct nuclear spin pumping mechanism: low-power DNP via second order recombination of dark excitons and high-power DNP due to spin transfer from spin polarised excitons/electrons.

transfer from spin polarised excitons/electrons. In the low-power regime increase of B_Z reduces energy splitting between dark ($|\ -2\ >$) and bright ($|\ -1\ >$) states, which dominate nuclear spin pumping in our QD system (see Fig. 3.2). Hence, decrease of the energy splitting is reflected as a systematic increment of OHS with B_Z from 0 T to 7 T. Nevertheless, when we increase B_Z from 7 T ($\Delta E_{|\Downarrow\uparrow>-|\Downarrow\downarrow>} = 188\mu eV$) to 8 T ($\Delta E_{|\Downarrow\uparrow>-|\Downarrow\downarrow>} = 159\mu eV$), OHS is reduced. This is observed since the small energy splitting at $B_Z = 8T$ ($\Delta E_{|\Downarrow\uparrow>-|\Downarrow\downarrow>} = 159\mu eV$) causes strong bright-dark mixing reducing non-radiative lifetime of dark excitons

and nuclear spin pumping efficiency.

3.5 Conclusions

We studied experimentally the dependence of dynamic nuclear spin polarisation on the power of non-resonant optical excitation in neutral InGaAs/GaAs quantum dots. We showed that the recently reported mechanism of nuclear spin pumping in InP/GaInP QDs via second order recombination of optically forbidden ("dark") exciton states in InP/GaInP quantum dots is relevant to the material system considered in this work [17]. In the studied InGaAs/GaAs dots this nuclear spin polarisation mechanism is particularly pronounced due to long non-radiative lifetime of "dark" excitons, resulting in nuclear spin polarisation degree up to $\sim 45\%$ and $B_N = 3.2T$ achieved at optical excitation powers ~ 1000 times smaller than the power required to saturate ground state excitons. Polarisation degrees reported in this work under ultra - low power optical pumping are comparable to those achieved by more demanding techniques such as resonant excitation or optical pumping with high power circular polarised light [11, 12, 13, 14, 15, 16]. Dynamic nuclear polarisation via second - order recombination of "dark" excitons may become a useful tool in single quantum dot applications, where manipulation of the nuclear spin environment is required.

References

[1] John J L Morton. "Solid-state quantum memory using the ^{31}P nuclear spin". In: *Nature* 455 (2008), p. 1085 (cit. on p. 51).

[2] J. R. Maze. "Electron spin decoherence of single nitrogen-vacancy defects in diamond". In: *Physical Rev B* 78 (2008), p. 094303 (cit. on p. 51).

[3] Gopalakrishnan Balasubramanian. "Ultralong spin coherence time in isotopically engineered diamond". In: *Nature Materials* 8 (2009), p. 383 (cit. on p. 51).

[4] Alexander Tartakovskii. *Quantum Dots: Optics, Electron Transport and Future Applications*. Cambridge: Cambridge, 2012 (cit. on p. 52).

[5] Peter Michler. *Single Semiconductor Quantum Dots*. Berlin: Springer, 2009 (cit. on p. 52).

[6] A J Ramsay. "A review of the coherent optical control of the exciton and spin states of semiconductor quantum dots". In: *Semicond. Sci. Technol.* 25 (2010), p. 103001 (cit. on p. 52).

[7] C. L. Salter. "An entangled-light-emitting diode". In: *Nature* 465 (2010), 594597 (cit. on p. 52).

[8] R. M. Stevenson. "A semiconductor source of triggered entangled photon pairs". In: *Nature* 439 (2006), pp. 179–182 (cit. on p. 52).

[9] R. M. Stevenson. "Coherent entangled light generated by quantum dots in the presence of nuclear magnetic fields". In: *arXiv:1103.2969* online (2011), non (cit. on p. 52).

[10] Alexander V. Khaetskii. "Electron Spin Decoherence in Quantum Dots due to Interaction with Nuclei". In: *Phys. Rev. Lett.* 88 (2002), p. 186802 (cit. on p. 52).

[11] D. Gammon. "Electron and Nuclear Spin Interactions in the Optical Spectra of Single GaAs Quantum Dots". In: *Phys. Rev. Lett.* 86 (2001), pp. 5176–5179 (cit. on pp. 52, 54, 68).

[12] B. Eble. "Dynamic nuclear polarization of a single charge-tunable InAs GaAs quantum dot". In: *Phys. Rev. B* 74 (2006), p. 081306 (cit. on pp. 52, 58–60, 68).

[13] J. Skiba-Szymanska. "Overhauser effect in individual InP/Ga_xIn_{1x}P dots". In: *Phys. Rev. B* 77 (2008), p. 165338 (cit. on pp. 52, 63, 68).

[14] C.W. Lai. "Knight-field-enabled nuclear spin polarization in single quantum dots". In: *Phys. Rev. Lett.* 96 (2006), p. 167403 (cit. on pp. 52, 58, 68).

[15] E. A. Chekhovich. "Pumping of Nuclear Spins by Optical Excitation of Spin-Forbidden Transitions in a Quantum Dot". In: *Phys. Rev. Lett.* 104 (2010), p. 066804 (cit. on pp. 52, 54, 68).

[16] C. Latta. "Confluence of resonant laser excitation and bidirectional quantum-dot nuclear-spin polarization". In: *Nature Phys.* 5 (2009), p. 758 (cit. on pp. 52, 60, 68).

[17] E. A. Chekhovich. "Light-polarization-independent nuclear spin alignment in a quantum dot". In: *Phys. Rev. B* 83 (2011), p. 125318 (cit. on pp. 52, 53, 55, 56, 63, 68).

[18] D. M. Whittaker. "High Q modes in elliptical microcavity pillars". In: *Appl. Phys. Lett.* 90 (2007), p. 161105 (cit. on p. 53).

[19] A. Daraei. "Control of polarized single quantum dot emission in high-quality-factor microcavity pillars". In: *Appl. Phys. Lett.* 88 (2006), p. 051113 (cit. on p. 53).

[20] D. Sanvitto. "Observation of ultrahigh quality factor in a semiconductor microcavity". In: *Appl. Phys. Lett.* 86 (2005), p. 191109 (cit. on p. 53).

[21] E. I. Ivchenko and G. E. Pikus. *Superlattices and Other Heterostructures, Symmetry and Optical Phenomena*. Berlin: Springer - Verlag, 1995 (cit. on p. 54).

[22] M. Bayer. "Observation of ultrahigh quality factor in a semiconductor microcavity". In: *Phys. Rev. B* 65 (2002), p. 195315 (cit. on pp. 54, 56, 64).

[23] S W Brown. "Spectrally resolved Overhauser shifts in single GaAs/Al". In: *Phys. Rev. B* 54 (1996), pp. 339–342 (cit. on p. 58).

[24] A. Abragam. *The principles of Nuclear Magnetism*. London: Oxford University Press, 1961 (cit. on p. 58).

[25] P. Fallahi. "Measurement of a heavy-hole hyperfine interaction in InGaAs quantum dots using resonance fluorescence". In: *Phys. Rev. Lett.* 105 (2010), p. 257402 (cit. on pp. 58, 60).

[26] E. A. Chekhovich. "Direct Measurement of the Hole-Nuclear Spin Interaction in Single InP/GaInP Quantum Dots Using Photoluminescence Spectroscopy". In: *Phys. Rev. Lett.* 106 (2011), p. 027402 (cit. on pp. 58–60).

[27] A. I. Tartakovskii. "Nuclear Spin Switch in Semiconductor Quantum Dots". In: *Phys. Rev. Lett.* 98 (2007), p. 026806 (cit. on pp. 58, 60).

[28] R. Oulton. "Subsecond Spin Relaxation Times in Quantum Dots at Zero Applied Magnetic Field Due to a Strong Electron-Nuclear Interaction". In: *Phys. Rev. Lett.* 98 (2007), p. 107401 (cit. on p. 60).

[29] A. Greilich. "Nuclei-Induced Frequency Focusing of Electron Spin Coherence". In: *Science* 307 (2007), pp. 1896–1899 (cit. on p. 60).

[30] A. E. Nikolaenko. "Suppression of nuclear spin diffusion at a GaAs/$Al_xGa_{1x}As$ interface measured with a single quantum-dot nanoprobe". In: *Phys. Rev. B* 79 (2009), p. 081303 (cit. on p. 63).

Chapter 4

Magneto - spectroscopy and dynamic nuclear polarisation of InPAs/GaInP quantum dots

4.1 Introduction

Semiconductor quantum dots are atom-like systems. Their electronic properties can be tailored by modifying their size and composition. For example electronic properties of QDs can be engineered using ternary alloys. For instance, variation of the content of the chemical elements of the alloy results in modification of the optical energy emission, shape, size and strain distribution of the dot. In this context, $III_xIII_{1-x}V$ QD systems have received most of the attention. Here, self-assembled Stranski-Krastanow $In_xGa_{1-x}As$/GaAs is the most studied quantum dot system, in which the alloy composition can be modified to obtain a broad range of emission energies [1, 2, 3]. An important crystal growth method for QD

fabrication is so-called self-assembly relies fundamentally on strained semiconductor layers. If we grow a semiconductor epitaxial layer on top of a substrate or host material with a different lattice constant, for a small deposition thickness the lattice constant in the layer will remain similar to the substrate thus accumulating energy due to the strain. This energy will build up, and eventually a more energetically preferential 3D growth mode occurs leading to formation of QDs. Ternary $IIIV_xV_{1-x}$ Stranskii - Krastanov QDs have not been studied in detail. InPAs QDs grown by self-assembly on GaInP is the system to be considered in this chapter. In this type of QDs an extremely large confinement energies can be achieved, which potentially may lead to robust performance of single dot devices such as single photon emitters at high T. Such deep confinement is achieved by combining small band gap of InAs with a large band gap for the GaInP barrier. Composition, strain distribution and other characteristics of InPAs quantum dots on GaInP matrix are largely unknown. Here, in order to lay foundations for investigation of such a structures in optically detected nuclear magnetic resonance (ODNMR) we study the dynamic nuclear polarisation (DNP) of single InPAs/GaInP QDs.

The first successful attempt to grow InPAs QDs on GaInP matrix was reported by Vinokurov in 1998, demonstrating highly efficient radiative recombination [4]. However, this first report did not show dramatic differences of optical energy emission with the well-known InP QD system. Later on, Ribeiro and collaborators reported on studies of InAsP/GaAs quantum dots [5, 6]. In Ref. [5] it was found that InPAs/GaAs dots emit at about 1.25 eV at 77 K. In Ref. [6], it was shown that it is possible to tailor the electronic properties of InAsP/GaAs QDs by controlling the PH_3 flux during the growth of InAs QDs. As they increase

the PH_3 flux, the energy emission increases towards InP QD energy. However, no systematic studies on InPAs/GaInP QDs exist, and no single dot emission was reported. Here, we report on magneto-optical studies of single InPAs/GaInP quantum dots. The chapter starts with description of the sample growth process and experimental set up. In the next section photoluminescence results at B = 0 are presented. Then, the following section shows magneto-spectroscopy measurements revealing a g-factor dependence on energy emission and dynamic nuclear polarisation which allows for further investigation of strain distribution and chemical composition of these QDs by NMR [7]. Finally, conclusions, future work and prospectives are discussed.

4.2 Techniques and samples

The samples of ternary InPAs QDs embedded in GaInP studied in this work were grown by low pressure (150 Torr) metalorganic vapour phase epitaxy in a horizontal flow reactor on (100) GaAs substrates with a miscut angle of 3° towards $(1\bar{1}0)$. Trimethylgallium and trimethylindium (TMIn) were used as precursors for group III elements and arsine (AsH_3) and phosphine (PH_3) were used as group V precursors. (Dimethylzinc and disilane were used for p-type and n-type doping, respectively.) Hydrogen was used as a carrier gas. The growth rates were maintained at 7.6 $\mathring{A}$/s for the GaAs buffer layers and GaInP matrix material. QDs were deposited at a lower nominal growth rate of 1.1 $\mathring{A}$/s. The GaAs buffer and the subsequent/following GaInP barrier material were grown at 690°C. The growth of the QD layer included several steps. Before the deposition of the QDs, the growth was halted under PH_3 flow, and the susceptor temperature was

lowered to 650°C. Then, TMIn was introduced to the reactor for 1-2 s followed by adding AsH_3 for 3-5 s. The final step was deposition of nominally binary InP material for 1 s or PH_3 purge for 1-10 s followed by GaInP growth. The compositions of InPAs were controlled by the flow rate of AsH_3 while keeping the flow of PH_3 constant. In order to assess the nominal arsenic fractions a thick layer of InPAs was grown and examined by means of X-ray difractometry. According to the X-ray diffraction measurements, the AsH_3 flow of 10.5 sccm (standard cubic centimeters per minute) results into the As fraction in solid of 35%. Based on this data, the calculated nominal As fractions in solid are 7%, 13%, 24%, 38%, 46%, 53% and 72% for the arsine flows of 1.5 sccm, 3 sccm, 6 sccm, 13.2 sccm, 16.7 sccm, 22.1 sccm and 50 sccm, respectively. However the corresponding long wavelength shift of the QD emission in PL spectra appeared to be smaller than one could expect, i.e. the actual fractions of As in the dot material is smaller than measured/calculated for bulk InPAs.

For the data presented in this chapter we chose the sample grown with 16.7 sccm (46%) of AsH_3 flux. This particular sample (referred to below as 16.7 sccm sample) shows relatively high intensity optical emission in the range from 670nm to 940nm, which allows for PL studies in a broad wavelength range. Photoluminescence was measured at T = 4.2 K in external magnetic field B_Z up to 10 T normal (Faraday geometry) and parallel (Voigt geometry) to the sample surface. For sample positioning and high stability of the experiment, Attocube piezo-stages were used. To optically excite QDs for most of the data in this chapter a diode laser with photon energy E_{exc} = 1.88eV was employed, which corresponds to the low-energy tail of the InPAs wetting layer (below the GaInP barrier band-gap excitation). Additional to this, other two diode lasers with pho-

ton energies $E_{exc} = 1.80eV$ and $E_{exc} = 1.53eV$ were used to study efficiency of dynamic nuclear polarisation. Quantum dot PL in the range from 1.38 eV to 1.85 eV was excited and collected with an aspheric lens, which gives a micro-PL laser spot of 1-2 μm diameter. The collected PL was analyzed using a 1-m double spectrometer and a charge-coupled device. We used linearly and circularly polarised excitation, which was achieved with appropriate linear polarisers and half and quarter-wave plates.

4.2.1 Transmission electron microscopy characterization

Figure 4.1 shows typical transmission electron microscopy (TEM) images of InP (top) and InPAs (bottom) quantum dots. Typical in-plane dimensions of InP dots observed in TEM are $\sim$ 50nm. This is somewhat larger than typical in-plane sizes of QDs in InPAs samples, where dimensions of $\sim$ 30nm were observed.

4.3 Photoluminescence spectroscopy of InPAs/GaInP quantum dots

We start by discussing PL of InPAs/GaInP quantum dots. Photoluminescence of InPAs/GaInP quantum dots was detected in a broad range of wavelengths when using E_{exc} = 1.88 eV. Fig. 4.2 shows a comparison between InPAs 16.7 sccm sample and nominally InP dots grown without As.

Both spectra were taken under the same excitation power $P_{exc} = 200nW$ and exposition time of 20 sec. The PL intensity for InPAs/GaInP QDs (bottom) shows noticeable decrease compared with that for pure InP/GaInP QDs (top).

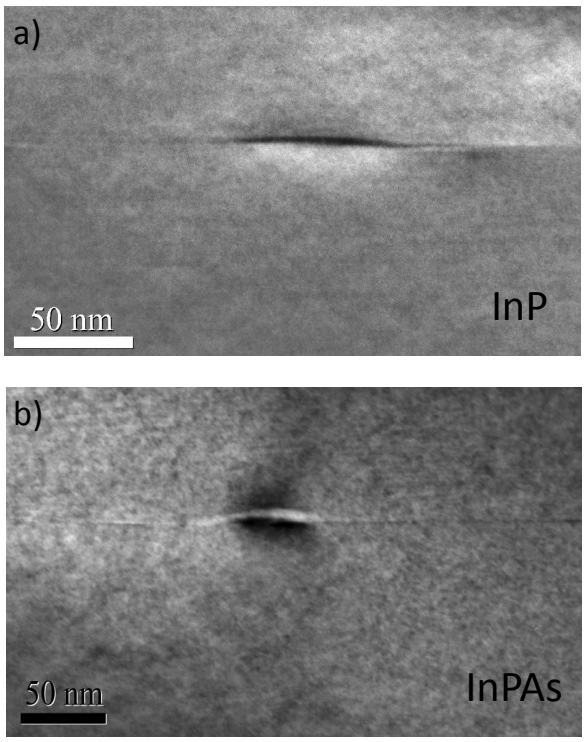

Figure 4.1: Transmission electron microscope images of InP (a) and InPAs (b) quantum dots. InP QD is larger at the base and shorter in high than InPAs QD. InPAs QD shows a bright capping layer defining a core-shell structure.

In addition a notably broader spectral distribution of PL intensity is observed: nominally InP sample emits in the range 680-780nm, whereas InPAs QD emission is observed from 680 to 920nm. We will now discuss the homogeneity of the quantum dot formation across the InPAs/GaInP wafer. Figure 4.3 shows PL spectra of six places across the InPAs/GaInP wafer taken from the line parallel to the chamber flow. All six spectra were measured under the same conditions, optical excitation power $P_{exc} = 200nW$ and 20 sec of integration time.

As can be seen, QD-like emission is detected across the whole wafer. The bottom two spectra (A-B) show considerably higher QD density compared with

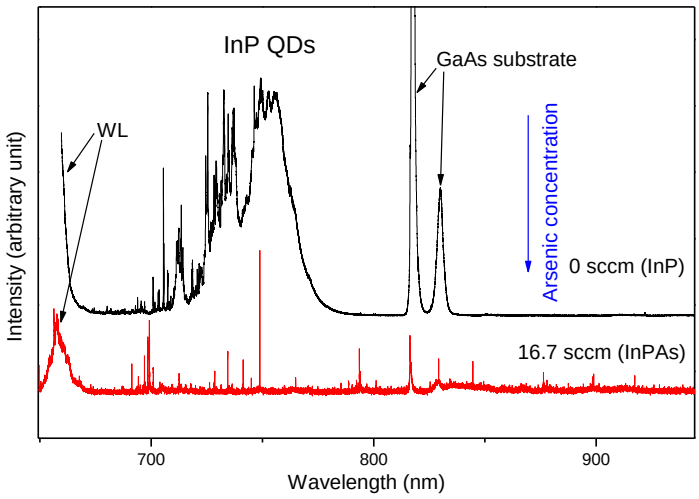

Figure 4.2: PL spectra of InP/GaInP (top) and InPAs/GaInP (bottom) quantum dots sample grown with 16.7 sccm AsH_3 is shown. The top spectrum (black) shows PL emission of InP/GaInP QDs centered around 730 nm, while the bottom spectrum (red) shows sharp peaks corresponding to single quantum dot emission in a broad range of wavelength, from 670 nm up to 940 nm for InPAs/GaInP QDs.

the rest of the wafer. Then starting from C-F positions, the QD density gradually decreases as it gets further from the material source in the chamber. Similar spread of PL wavelength 680-950 nm can be clearly observed for all positions across the wafer. QD PL intensity drops down after $800nm$ mainly due to reduction of the sensitivity of the charge coupled device (CCD) used for PL detection. CCD quantum efficiency plot against wavelength for the model Spectrum One CCD 3000 can be seen in Appendix.

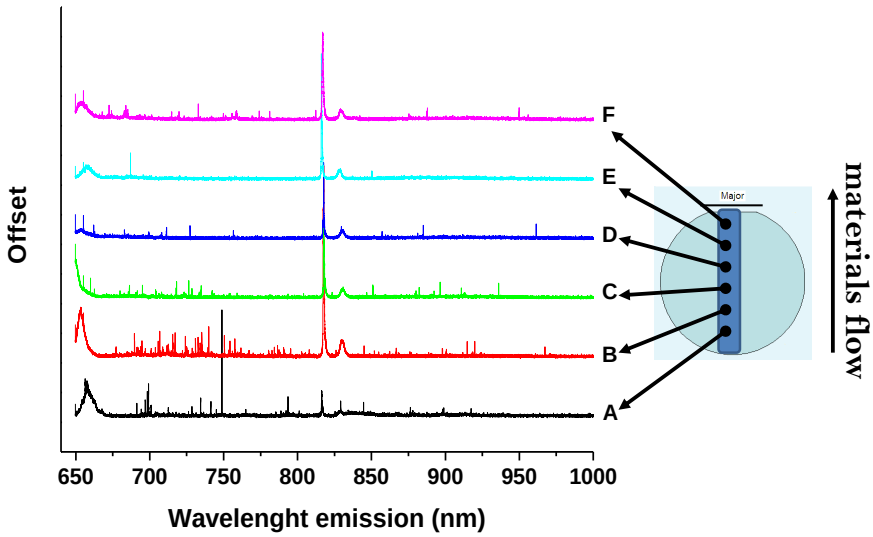

Figure 4.3: Position dependent PL spectra of InPAs/GaInP QD wafer with 16 sccm. From bottom to top (A-F) indicates the increasing distance to the material source in the chamber, the black arrow indicates the direction of the flow (inset). All PL spectra were taken at optical excitation power of $P_{exc} = 200nW$ and 20 sec of integration time.

4.3.1 Photoluminescence detection of single InPAs/GaInP quantum dots

In order to study magnetic phenomena, such as g-factors and dynamic nuclear polarisation, we need to be able to detect small energy shifts (typically few tens of μeV) [8, 9, 10, 11, 12, 13]. Hence, detection of single quantum dot emission is desirable.

Figure 4.4 shows typical PL spectra measured at $B_Z = 0T$ of single InPAs QDs using linearly polarised excitation and σ^+ detection. Top panel shows PL of a single quantum dot at a low energy $E_{PL} \approx 1.3280eV$ (QD1). Bottom panel

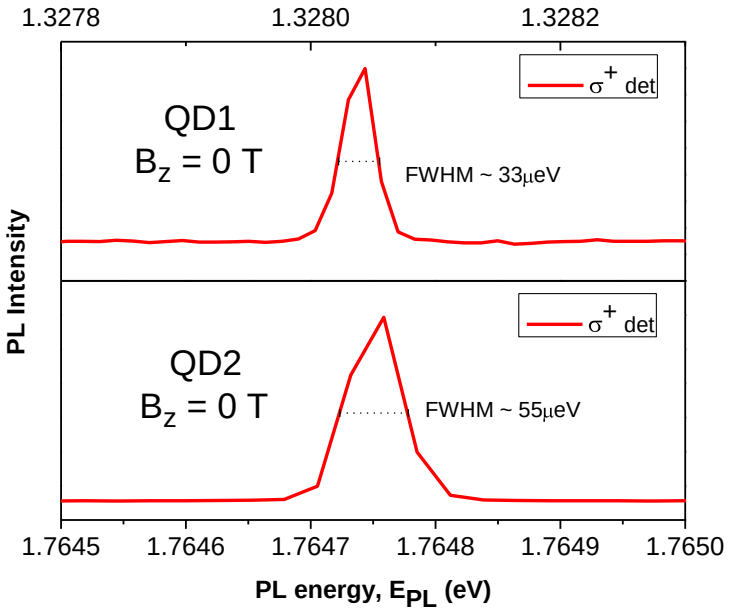

Figure 4.4: Typical PL spectra measured at $B_Z = 0T$ of single InPAs QDs using linearly polarised excitation and σ^+ (black) detection. Top caption shows PL of single quantum dot at low energy $E_{PL} \approx 1.3280eV$ (QD1). Bottom caption shows PL of single quantum dot at high energy $E_{PL} \approx 1.7647eV$ (QD2). Dashed lines show FWHM for both QDs.

shows PL of a single quantum dot at a high energy $E_{PL} \approx 1.7647eV$ (QD2). We find that typically QD PL exhibit no fine structure splitting, a signature of dot charging [14, 15, 16]. Charging of QDs was further confirmed by magneto-spectroscopy in Voigt geometry. Dashed lines in fig. 4.4 show FWHM for QD1 $\approx 33\mu eV$ and QD2 $\approx 55\mu eV$, which are close to the instrument spectra resolution $\sim 30\mu eV$ and are comparable to the best linewidths of high quality GaAs and InGaAs QDs [17, 18].

4.4 Magneto - spectroscopy of individual InPAs/GaInP quantum dots

We carry out magneto - spectroscopy measurements of about 75 InPAs/GaInP QDs in order to explore the dependence of g-factors and nuclear polarisation effects on the QD emission energy, which gives valuable information about the intrinsic QD magnetic environment and will lay foundations for future studies of composition and strain distribution by novel techniques like NMR spectroscopy [7]. InPAs/GaInP QDs were measured in two different magnetic field configurations: (i) Magnetic field normal to the sample surface (Faraday geometry) and (ii) Magnetic field parallel to the sample surface (Voigt Geometry).

Firstly, we present typical PL spectra of single QDs at $B_Z = 3T$ for dots emitting about $E_{PL} = 1.830eV$ (a), $E_{PL} = 1.419eV$ (b) and $E_{PL} = 1.377eV$ (c) in figure 4.5. PL was excited with linearly polarised light with excitation energy $E_{exc} = 1.88eV$ for all three QDs. Zeeman splittings are indicated for each QD with values equal to $\Delta E_{Zeeman} = 302\mu eV$ (a), $\Delta E_{Zeeman} = 235\mu eV$ (b) and $\Delta E_{Zeeman} = 204\mu eV$ (c) respectively. An observed trend in ΔE_{Zeeman} reflects the gradual variation of QD composition across the QD ensemble. The observed trend is presented in the following subsections.

In the first subsection we will show g-factors measured at several QD emission energies. In the following subsection, external magnetic field in Faraday geometry is used to determine experimental conditions for effective creation of DNP in InPAs/GaInP single quantum dots at different energies.

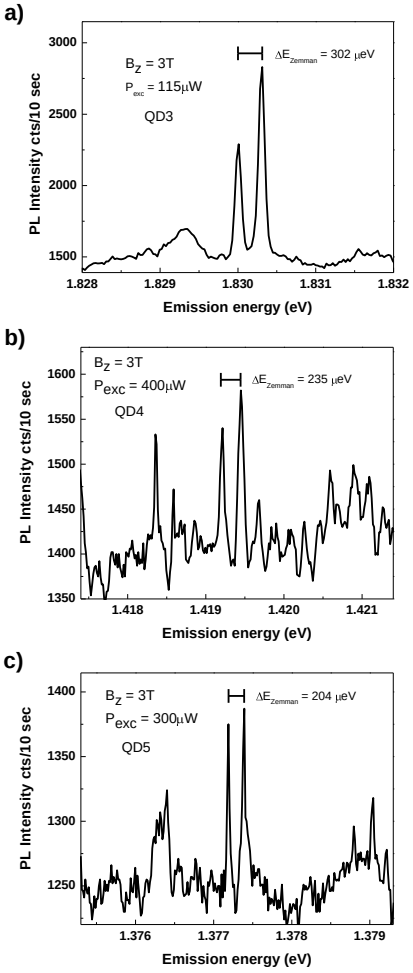

Figure 4.5: PL spectra of InPAs/GaInP single quantum dots at external magnetic field $B_Z = 3T$, and excitation energy $E_{exc} = 1.88eV$. Typical PL spectra of single dot emission at $E_{PL} = 1.830eV$ (a), $E_{PL} = 1.4195eV$ (b) and $E_{PL} = 1.3773eV$ (c) are shown. Energy Zeeman splitting is indicated for each QD with values equal to $\Delta E_{Zemman} = 302\mu eV$ (a), $\Delta E_{Zemman} = 235\mu eV$ (b) and $\Delta E_{Zemman} = 204\mu eV$ (c) respectively.

4.4.1 Using magneto-optics for determination of the QD charging

Measurements of magneto-photoluminescence in Faraday and Voigt geometries allows to determine in and out of plane g-factors and corresponding diamagnetic shifts. Typical magnetic field dependence of the position of the peaks for InPAs QDs can be seen in figure 4.6 for both magnetic field configurations (Faraday and Voigt) exhibiting Zeeman splitting. In Faraday geometry the emission line splits in two circularly polarised peaks (σ^+ and σ^-), in Voigt geometry it splits in four linearly polarised peaks (π_1 and π_2). This behaviour presented in Fig. 4.6 has been previously found for singly charged InGaAs and InP dots [19, 20]. In order to obtain the g-factors and diamagnetic shifts, the energy lines as a function of magnetic field $E(B)$ are plotted using the equation:

$$E(B_Z) = E_0 + \kappa_F B_Z^2 \pm \frac{1}{2} g_x \mu_B B_Z \tag{4.1}$$

for Faraday geometry and the equations:

$$E(B_X) = E_0 + \kappa_V B_Z^2 \pm \frac{1}{2} \mu_B B_X (\pm g_{h,\perp} \pm g_e) \tag{4.2}$$

$$E(B_X) = E_0 + \kappa_V B_X^2 \pm \frac{1}{2} \mu_B B_X (\pm g_{h,\perp} \mp g_e) \tag{4.3}$$

for Voigt geometry. In these three equations E_0 is the emission energy at zero field, $B_{Z(X)}$ is the magnetic field in Faraday (Voigt) geometry, μ_B the Bohr magneton, g_X, $g_{h,\perp}$, g_e are the exciton, in-plane hole and electron g-factor respectively, κ_F the diamagnetic shift in Faraday geometry and κ_V in Voigt geometry.

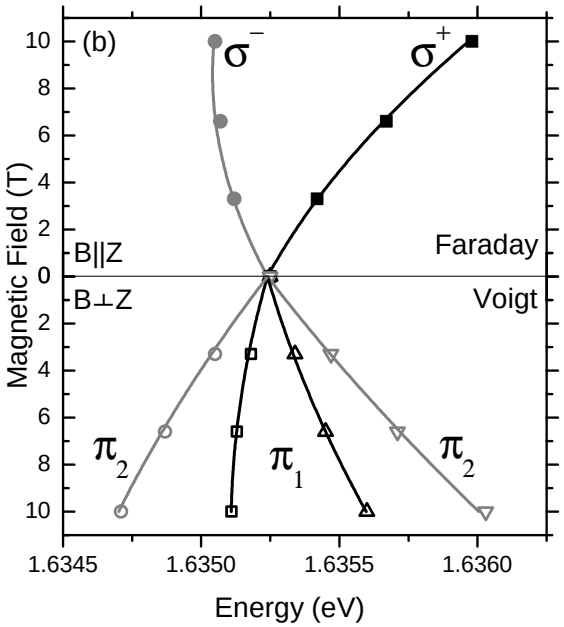

Figure 4.6: A typical magnetic field dependence of PL spectra from an InPAs/GaInP quantum dot measured 16.7 sccm sample at 4.2K under non-resonant excitation in σ^+ and σ^- in Faraday geometry and in orthogonal π_1, π_2 linear polarisations in Voigt geometry, where a typical trion behaviour is observed with four peaks. Trion peak energies from spectra in (a) versus external magnetic field. g-factors and exciton diamagnetic shifts are found fitting the curves (solid lines) with equations 1, 2 and 3.

For this particular dot $g_X = 1.592$, $g_e = 1.58$, $g_{h,\perp} = 0.737$, $\kappa_F = 2.67\mu eV/T^2$ and $\kappa_V = 1.12\mu eV/T^2$. Here we assume isotropic g-factor for electrons. Using these parameters we can also deduce hole g-factor along Z $g_{h,\parallel} = 3.175$.

Figure 4.7 shows a summary of electron g-factor g_e values at several emission energies, ranging from 1.3 eV to 1.8 eV. To study the dynamic nuclear polarisation which is the main interest of this work just g_e is relevant as hole-nuclear

spin interaction is about 10 times weaker [10]. More detailed analysis of all g-factors (g_e, $g_{h,\perp}$, $g_{h,\parallel}$, g_X) is in progress and will be published elsewhere. Clear dependence of QD g_e on energy emission can be seen. Electron g-factors increase with the energy of the dot emission. In earlier work was found that for InP QDs which emit around 1.8 eV the electron g-factor $g_e \approx 1.5$ [21]. This is close to the g-factor value at $1.8eV$ in figure 4.7. This suggest a $P-rich$ QD behaviour for dots emitting at these energies. Even for dots emitting at 1.3eV strong contribution of P in the composition of the volume occupied by electron is evident, as large $g_e \approx +1$ are measured. This is in contrast with InAs/GaAs QD emitting at this energy, where negative $g_e \approx -0.5$ are usually measured. This observation either indicates that InPAs dots at 1.3eV are still rich in P, or that the electron wavefunction leaks into the $P-rich$ around the more $As-rich$ core of the dot.

4.4.2 Dynamic nuclear polarisation in InPAs/GaInP quantum dots

In this section we will discuss dynamic nuclear polarisation in single InPAs/GaInP quantum dots emitting in a wide range of PL energies. DNP is essential for further studies of material composition and strain distribution in the dots by NMR spectroscopy [7]. The measurements were performed under external magnetic field parallel to the sample growth direction (Faraday geometry). Main difference to previous experiments is that the optical excitation was circularly polarised using a quarter-wave plate, which typically facilitates dynamic nuclear polarisation [11, 22, 23, 17]. We measure the InPAs/GaInP QD sample grown with 16 sccm As flux. Single quantum dot emission was obtained using a micro-PL set up. The

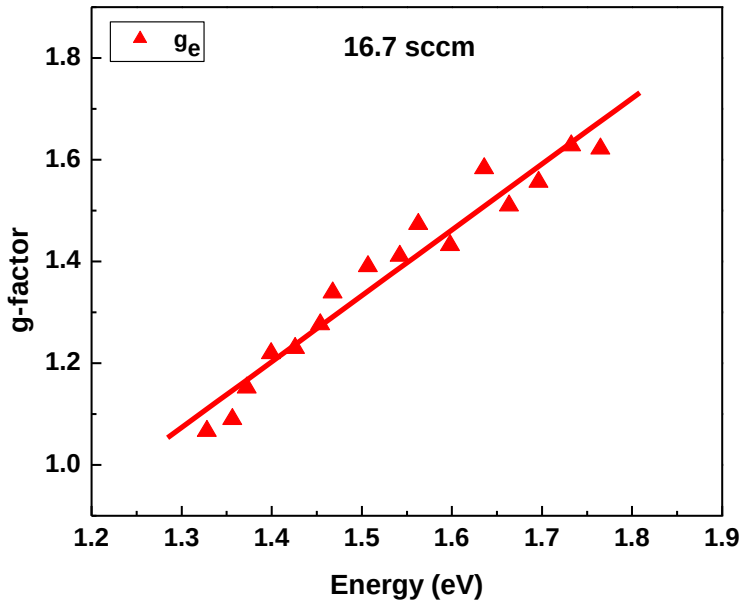

Figure 4.7: The electron g-factors (g_e) of InPAs/GaInP quantum dots for sample with 16.7sccm of As flux. The g_e increase with energy dot emission following a trend.

sequence used for the DNP measurements was as follows: First we excite with negative circular polarisation for more than 5 sec and then measure PL using linearly polarised detection (red spectrum) with an integration time of 20 sec; then we set opposite circular polarisation and detect again with linear polarisation (gray spectrum in fig. 4.8) under the same time scales. These time scales allow nuclear polarisation to build up according to the sign of circular polarisation.

Polarisation of nuclear spins lead to occurrence of the Overhauser field B_N, a collective result of the hyperfine interaction of 10^5 nuclei in the dot with the spin of the confined electron [24]. Here, for simplicity we will neglect the hyperfine interaction of the hole, since its contribution is at least 10 times smaller than that of the electron [25, 10]. In practice, QDs with complex compositions are

used, where polarisation degrees for different isotopes may be different. In that case $\Delta E_{OHS} = \sum \rho_i A_i I_i S_{N,i}$, where ρ_i is the relative concentration of the ith isotope, A_i, I_i and $S_{N,i}$ - its hyperfine constant, spin and polarisation degree, respectively [26]. Thus, in most cases the determination of the absolute degree of nuclear polarisation is a difficult task, and it is more practical to operate in terms of the Overhauser shifts (OHS), which in some cases, when g_e is known, can also be converted in the Overhauser fields, B_N.

In figure 4.8, the Overhauser shift (OHS) induced by optical pumping of nuclear spins can be observed for both QDs, measured in external magnetic field $B_Z = 0.5T$. ΔE_{σ^+} (ΔE_{σ^-}) stands for the energy splitting of bright excitons under σ^+ (σ^-) excitation. For σ^- excitation it was not possible to resolve the energy splitting at $B_Z = 0.5T$. When the Zeeman splitting at $B_N = 0$ is known, it is possible to accurately extract the Overhauser shift. This is very important when strong non-linearities of the DNP are present, as shown for ultra-low excitation powers in Chapter 3 and reported for InP before [12]. However, since we do not observe strong non-linearities of DNP in our dots, we assume similar values of nuclear polarisation with opposite signs for σ^+ and σ^- excitation. Therefore, ΔE_{OHS} values were obtained comparing the energy splitting for the spectrum excited with σ^- circular polarisation (red circles) and the spectrum excited with σ^+ (gray squares) circular polarisation according to $\Delta E_{OHS} = \frac{\Delta E_{\sigma^+} - \Delta E_{\sigma^-}}{2}$ [22]. Solid curves in fig. 4.8 represent the Gaussian fits to extract ΔE_{σ^-} (red) and ΔE_{σ^+} (gray). ΔE_{σ^-} can be roughly estimated from the linewidth if the red spectrum, this will be the high boundary of ΔE_{σ^-}, which means ΔE_{OHS} will be the low boundary. For the low energy dot $\Delta E_{OHS} = 29.5\mu eV$ and for high energy dot $\Delta E_{OHS} = 52.5\mu eV$.

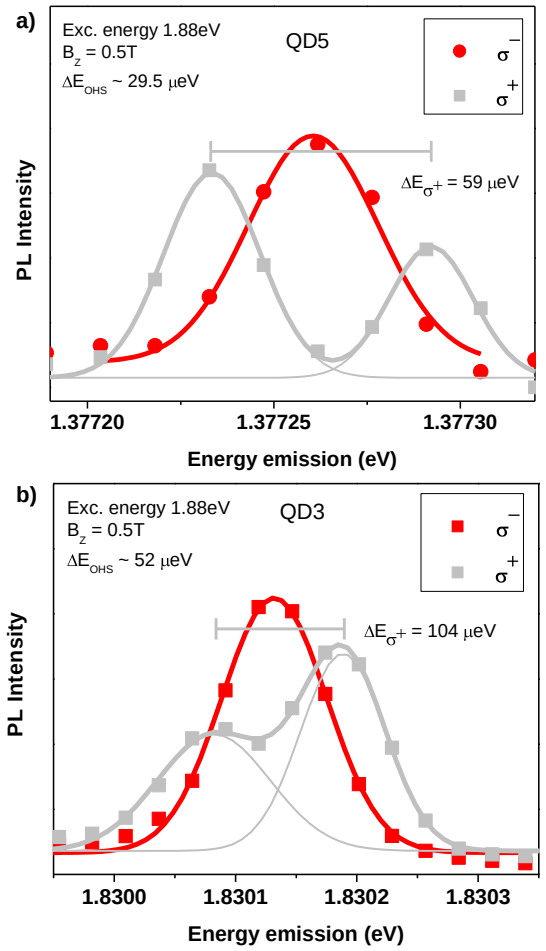

Figure 4.8: PL spectra of InPAs/GaInP quantum dots measured with two circularly polarised optical excitation σ^- (red circles) and σ^+ (gray squares) at $B_Z = 0.5T$. Energy splitting difference between spectra reflects Overhauser shift values according to $\Delta E_{OHS} = \frac{\Delta E_{\sigma^+} - \Delta E_{\sigma^-}}{2}$. Solid curves represent the Gaussian fits to extract ΔE_{σ^+} (gray) and ΔE_{σ^-} (red). For the low energy dot $\Delta E_{OHS} = 29.5 \mu eV$ (a) and for high energy dot $\Delta E_{OHS} = 52.5 \mu eV$ (b).

Now, we present full magnetic field dependence of Overhauser shift ΔE_{OHS} for QD5 (figure 4.9). For each B_Z two spectra representing σ^+ (solid symbols) and σ^- (open symbols) are presented. Right panel shows summary of the ΔE_{OHS} dependence on B_Z. As can be observed, ΔE_{OHS} decreases linearly as B_Z is

increased.

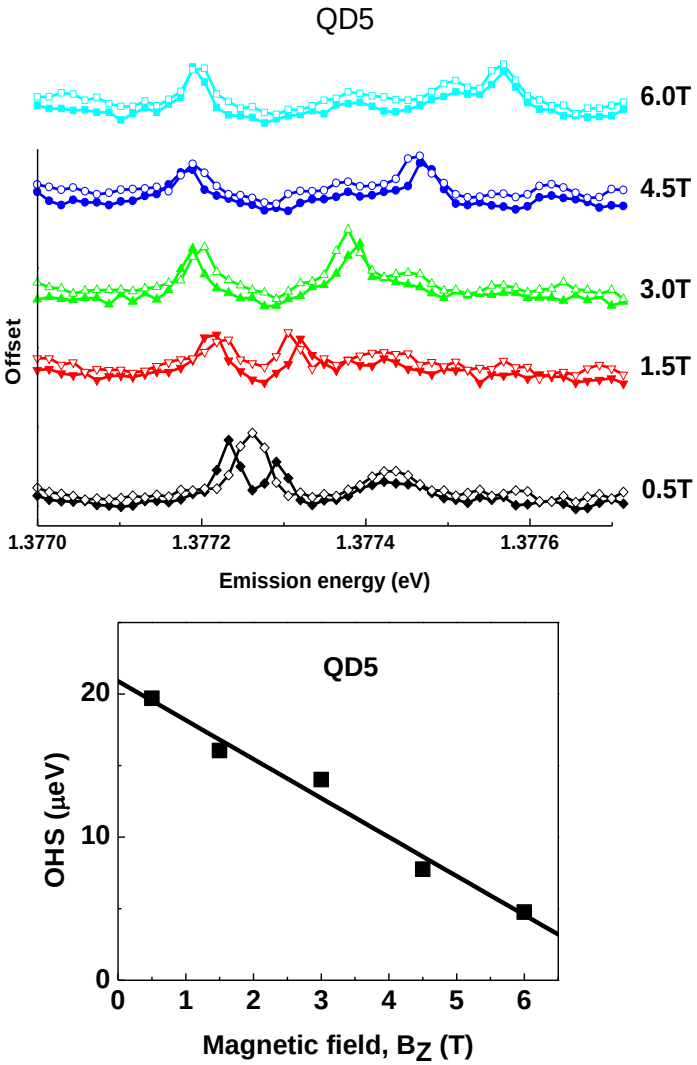

Figure 4.9: Magnetic field dependence of Overhauser shift ΔE_{OHS} for QD5. For each B_Z two spectra representing σ^+ and σ^- are presented. Bottom panel shows summary of the ΔE_{OHS} dependence on B_Z.

Nuclear polarisation builds up as a result of the electron spin flip-flop which simultaneously changes the spin of one nuclear spin. This process is repeated many times for different re-pumped electrons. The efficiency of the spin transfer

depends on the energy splitting between the initial and final electron (exciton) states involved in the electron spin-flip. For X_0 this is the splitting between the dark and bright states, E_{DB} as presented in Chapter 3, and for charged dots it is the electron Zeeman splitting E_{eZ}, i.e. the splitting between $\Uparrow\Downarrow\uparrow$ and $\Uparrow\Downarrow\downarrow$ for X^+, and between $\uparrow$ and $\downarrow$ for a negatively charged dot [26]. Owing to the requirement of the energy conservation, in most cases the spin flip-flop occurs as a second order process: at the first stage, as a result of the hyperfine interaction, the electron is virtually transferred to the state with the opposite spin while at the same time flopping a single nuclear spin (changing its spin state by ± 1); the electron then escapes from the dot (or a trion is formed in a charged dot), the process accomplished by emission (absorption) of a photon [10, 26, 23, 27] or electron tunneling from the dot [8, 28, 29]. Thus, the process efficiency scales roughly as $1/\Delta E^2_{\uparrow\downarrow}$, where $\Delta E_{\uparrow\downarrow}$ equals to E_{DB} or E_{eZ} depending on the type of the dot. For charged dots like in our case here, $E_e = \mid g_e \mid \mu_B(B_Z \pm B_N)$. Hence, the origin of the gradual decrement of OHS with increasing B_Z in the bottom panel of figure 4.9, arises due to gradually increasing separation of exciton states with opposite electron spin states.

In figure 4.10, we present QD energy emission dependence of OHS for several dots measured at $B_Z = 3T$, where PL line splitting can be clearly measured (figure 4.10). Most of the QDs were measured with excitation energy $E_{exc} = 1.88$ eV (solid squares) which is in resonance with the low-energy tail of the wetting layer and usually employed to induce DNP in InP/GaInP QDs [9, 12]. Two additional optical excitation energies $E_{exc} = 1.80eV$ (open circles) and $E_{exc} = 1.53$ eV (solid triangles) were used to explore the effect of optical excitation in resonance with the QD ensemble.

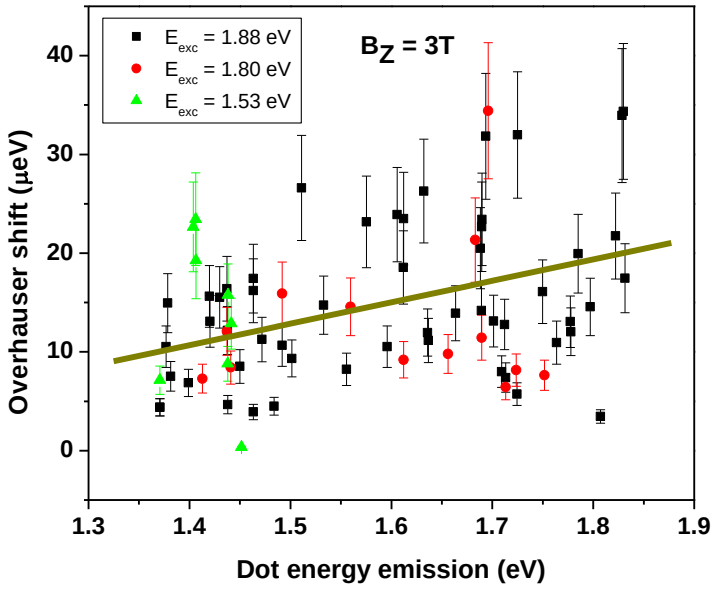

Figure 4.10: Quantum dot emission energy dependence of Overhauser shift at $B_Z = 3$ T using three different optical excitation energies. $E_{exc} = 1.88$ eV (solid squares), $E_{exc} = 1.80eV$ (open circles) and $E_{exc} = 1.53$ eV (solid triangles).

We found that DNP can be induced with any of the three lasers. However, DNP under non-resonant excitation ($E_{exc} = 1.88$ eV) is more efficient. Clear trend of the OHS with QD emission energy can be also observed. Black line in Fig. 4.10 is a guide to the eye. For QDs at low energy $E_{PL} \sim 1.35 - 1.5eV$, we detect values of $OHS \sim 0\mu eV - 47\mu eV$, where more effective nuclear spin pumping is created with $E_{exc} = 1.53eV$ (solid triangles). OHS keeps increasing monotonically for $E_{PL} \sim 1.5 - 1.85eV$ reaching a maximum value of $OHS \sim 35\mu eV$.

Figure 4.11 shows B_N dependence on QD emission energy. The B_N was calculated using the data presented by solid lines giving average values for OHS in fig. 4.10 and g_e in fig. 4.7. and diving by g_e interpolation of the trend average value (fig. 4.7) multiplying for μ_B.

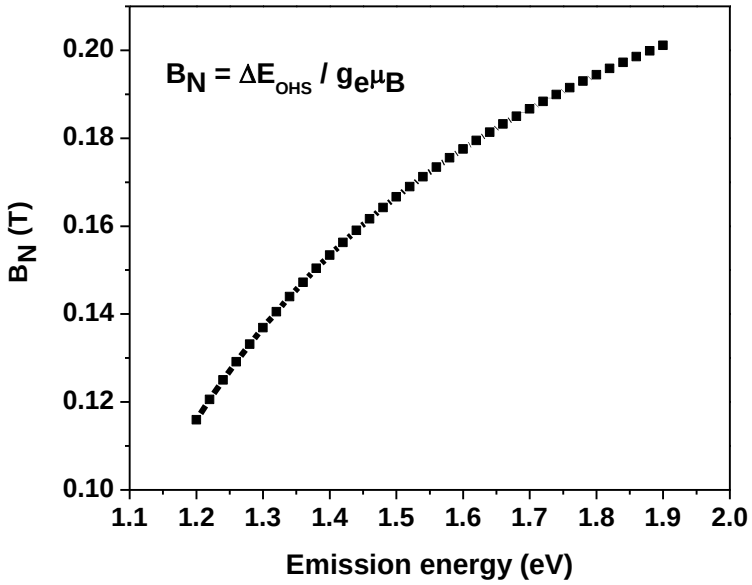

Figure 4.11: Quantum dot emission energy dependence of Overhauser field B_N. Trend of Overhauser shifts (OHS) at $B_Z = 3$ T see fig. 4.10, is divided by Bohr Magneton μ_B and g_e trend, see fig. 4.7.

Values of B_N systematically increase as QD emission energy is increased. The range of B_N values goes from 0.1 at 1.2eV to 0.2T at 1.9eV.

Using the expression $\Delta E_{OHS} = \sum \rho_i A_i I_i S_{N,i}$ we deduce a degree of polarisation of about 15%. $As - atoms$ have spin $I = 3/2$ and $A = 47\mu eV$, $P - atoms$ spin $I = 1/2$ and $A = 36\mu eV$, and $In - atoms$ spin $I = 9/2$ and $A = 56\mu eV$. ρ_i is the material composition, for the sample measured we estimated an As of 40%. However, $In - atoms$ give the main contribution for DNP due to its spin configuration. The degree of polarisation deduced of 15% for our dots shows a not very efficient DNP as reported for InP or InAs separately under non-resonant excitation [21, 26]. Nevertheless, variation of composition in these dots is still unclear and other possible source of depolarisation may be present.

4.5 Conclusions

First optical magneto-spectroscopy studies on single InAsP/GaInP quantum dots have been presented. Dependence of g-factors with energy emission was found. More specifically g_e follows a clear trend from values of 1.0 at low emission energy of 1.3eV up to 1.6 at high emission energy of 1.8eV. We expect the dependence to originate from variation in As concentration. Further analysis of g-factor is in progress and will be published elsewhere. Studies of nuclear spin pumping also reflect a trend of OHS and B_N values with QD energy emission. Degree of polarisation in this InPAs QD systems was found to reach 15%. This reflects not very efficient DNP for our sample, and ways to improve it may be needed. Data presented in this chapter opens the way for further investigation of the influence of *As* on the electronic and optical properties of QDs. Additional to this, dynamic nuclear polarisation found in this system, allows for ODNMR studies which will enable composition and strain investigation as recently reported for InGaAs and InP QDs [7].

References

[1] Mitsuru Sugawara, ed. *Self-Assembled InGaAs/GaAs Quantum Dots*. Vol. 60. Semiconductors and Semimetals. San Diego: Academic Press, 1999 (cit. on p. 73).

[2] D. Bimberg and N. Kirstaedter. "InGaAs-GaAs quantum-dot lasers". In: *Selected Topics in Quantum Electronics, IEEE* 3 (1997), pp. 196 –205 (cit. on p. 73).

[3] J. Shumway and A. J. Williamson. "Electronic structure consequences of In/Ga composition variations in self-assembled InxGa1-xAs/GaAs alloy quantum dots". In: *Physical Review B* 64 (2001), p. 125302 (cit. on p. 73).

[4] D.A. Vinokurov and V.A. Kapitonov. "Self-organized nanosize InP and InAsP clusters obtained by metalorganic compound hydride epitaxy". In: *Technical Physics Letters* 24 (1998), pp. 623–625 (cit. on p. 74).

[5] E. Ribeiro and R.L. Maltez. "Optical and structural properties of InAsP ternary self-assembled quantum dots embedded in GaAs". In: *Applied Physics Letters* 81 (2002), pp. 2953–2955 (cit. on p. 74).

[6] R.L. Maltez and E. Ribeiro. "Controlling alloy composition of InAsP self-assembled quantum dots embedded in GaAs". In: *Journal of Applied Physics* 94 (2003), pp. 3051–3056 (cit. on p. 74).

[7] E. A. Chekhovich, K. V. Kavokin, and J. Puebla. "Structural analysis of strained quantum dots using nuclear magnetic resonance". In: *Nat. Nanotechnology* 7 (2012), 646650 (cit. on pp. 75, 82, 86, 94).

[8] M. N. Makhonin. "Nuclear spin pumping under resonant optical excitation in a quantum dot". In: *Appl. Phys. Lett.* 93 (2008), p. 073113 (cit. on pp. 80, 91).

[9] J. Skiba-Szymanska. "Overhauser effect in individual InP/Ga_xIn_{1x}P dots". In: *Phys. Rev. B* 77 (2008), p. 165338 (cit. on pp. 80, 91).

[10] E. A. Chekhovich. "Direct Measurement of the Hole-Nuclear Spin Interaction in Single InP/GaInP Quantum Dots Using Photoluminescence Spectroscopy". In: *Phys. Rev. Lett.* 106 (2011), p. 027402 (cit. on pp. 80, 86, 87, 91).

[11] E. A. Chekhovich. "Pumping of Nuclear Spins by Optical Excitation of Spin-Forbidden Transitions in a Quantum Dot". In: *Phys. Rev. Lett.* 104 (2010), p. 066804 (cit. on pp. 80, 86).

[12] E. A. Chekhovich. "Light-polarization-independent nuclear spin alignment in a quantum dot". In: *Phys. Rev. B* 83 (2011), p. 125318 (cit. on pp. 80, 88, 91).

[13] W. Heller and U. Bockelmann. "Magnetooptical studies of a single quantum dot:ffExcited states and spin flip of excitons". In: *Phys. Rev. B* 55 (1997), pp. 4871–4874 (cit. on p. 80).

[14] J. J. Finley. "Quantum-confined Stark shifts of charged exciton complexes in quantum dots". In: *Phys. Rev. B* 70 (2004), p. 201308 (cit. on p. 81).

[15] M. Bayer. "Observation of ultrahigh quality factor in a semiconductor microcavity". In: *Phys. Rev. B* 65 (2002), p. 195315 (cit. on p. 81).

[16] A. I. Tartakovskii. "Dynamics of Coherent and Incoherent Spin Polarizations in Ensembles of Quantum Dots". In: *Phys. Rev. Lett.* 93 (2004), p. 057401 (cit. on p. 81).

[17] D. Gammon. "Electron and Nuclear Spin Interactions in the Optical Spectra of Single GaAs Quantum Dots". In: *Phys. Rev. Lett.* 86 (2001), pp. 5176–5179 (cit. on pp. 81, 86).

[18] R. Oulton. "Subsecond Spin Relaxation Times in Quantum Dots at Zero Applied Magnetic Field Due to a Strong Electron-Nuclear Interaction". In: *Phys. Rev. Lett.* 98 (2007), p. 107401 (cit. on p. 81).

[19] I. A. Akimov. "Fine structure of the trion triplet state in a single self-assembled semiconductor quantum dot". In: *Appl. Phys. Lett.* 81 (2002), p. 4730 (cit. on p. 84).

[20] J. G. Tischler. "Fine Structure of Trious and Excitons in Single GaAs Quantum Dots". In: *Phys. Rev. B* 66 (2002), p. 081310 (cit. on p. 84).

[21] E. A. Chekhovich and M. N. Makhonin. "Dynamics of optically induced nuclear spin polarization in individual InP/GaxIn1xP quantum dots". In: *Phys. Rev. B* 81 (2010), p. 245308 (cit. on pp. 86, 93).

[22] Urbaszek Bernhard and Marie Xavier. "Nuclear spin physics in quantum dots: an optical investigation". In: *arXiv:1202.4637* 84 (2012), p. 195305 (cit. on pp. 86, 88).

[23] A. I. Tartakovskii. "Nuclear Spin Switch in Semiconductor Quantum Dots". In: *Phys. Rev. Lett.* 98 (2007), p. 026806 (cit. on pp. 86, 91).

[24] A. Abragam. *The principles of Nuclear Magnetism.* London: Oxford University Press, 1961 (cit. on p. 87).

[25] P. Fallahi. "Measurement of a heavy-hole hyperfine interaction in InGaAs quantum dots using resonance fluorescence". In: *Phys. Rev. Lett.* 105 (2010), p. 257402 (cit. on p. 87).

[26] B. Eble. "Dynamic nuclear polarization of a single charge-tunable InAs GaAs quantum dot". In: *Phys. Rev. B* 74 (2006), p. 081306 (cit. on pp. 88, 91, 93).

[27] C. Latta. "Confluence of resonant laser excitation and bidirectional quantum-dot nuclear-spin polarization". In: *Nature Phys.* 5 (2009), p. 758 (cit. on p. 91).

[28] F. Klotz. "Asymmetric optical nuclear spin pumping in a single uncharged quantum dot". In: *Phys. Rev. B* 82 (2010), p. 121307 (cit. on p. 91).

[29] C. Kloeffel. "Controlling the Interaction of Electron and Nuclear Spins in a Tunnel-Coupled Quantum Dot". In: *Phys. Rev. Lett.* 106 (2011), p. 046802 (cit. on p. 91).

Chapter 5

Conclusions and future work

5.1 Conclusions

In this thesis three main topics were investigated. (i) Charge control in InP/GaInP single quantum dots embedded in Schottky diodes, (ii) Dynamic nuclear polarisation in InGaAs/GaAs quantum dots under non-resonant ultra-low power optical excitation, and (iii) Magneto - spectroscopy and dynamic nuclear polarisation of InAsP/GaInP quantum dots. The key results presented for each topic were the followings:

(i) By realising MOVPE growth of low density InP/GaInP QDs, we have overcome the major hurdle of the presence of high densities of large QDs in this system. We achieve a reproducible and smooth transition in QD size distribution and density by varying nominal InP deposition thickness. Such an achievement has allowed the detection and manipulation of neutral (X_0) and negatively charged (X^{-1}) exciton energy levels in individual QDs by application of vertical electric fields using Schottky devices. X^{-1} binding energies are shown to range from 4 to 7 meV, similar to InGaAs/GaAs QDs. Systematic studies of QD permanent dipole moment and polarisability in a large ensemble of QDs allows for

the characterization of the exciton wavefunction in such system. We argue that due to a relatively higher confinement regime imposed to electrons, the sign of QD permanent dipole moments are mainly determined by the position of the hole wavefunction along the growth direction, which provides insight into the QD composition and strain distribution. Moreover, from the relationship between dipole moment and polarisability, we show that the lateral extent of the exciton wavefunction varies very little from dot to dot. We obtain an average in-plane exciton radius of 7.7 and 5.5 nm for two QD ensembles probed in different samples. Photocurrent technique has been demonstrated, allowing for resonant manipulation and electrical detection of excitons in single InP/GaInP QDs.

(ii) We studied experimentally the dependence of dynamic nuclear spin polarisation on the power of non-resonant optical excitation in neutral InGaAs/GaAs quantum dots. We showed that the recently reported mechanism of nuclear spin pumping in InP/GaInP QDs via second order recombination of optically forbidden ("dark") exciton states in InP/GaInP quantum dots is relevant to the material system considered in this work [1]. In the studied InGaAs/GaAs dots this nuclear spin polarisation mechanism is particularly pronounced due to long non-radiative lifetime of "dark" excitons, resulting in nuclear spin polarisation degree up to $\sim 45\%$ and $B_N = 3.2T$ achieved at optical excitation powers ~ 1000 times smaller than the power required to saturate ground state excitons. Polarisation degrees reported in this work under ultra - low power optical pumping are comparable to those achieved by more demanding techniques such as resonant excitation or optical pumping with high power circular polarised light [2, 3, 4, 5, 6, 7]. Dynamic nuclear polarisation via second - order recombination of "dark" excitons may become a useful tool in single quantum dot applications, where

manipulation of the nuclear spin environment is required.

(iii) First optical magneto-spectroscopy studies on single InAsP/GaInP quantum dots have been presented. Dependence of g-factors with energy emission was found. More specifically g_e follows a clear trend from values of 1.0 at low emission energy up to 1.6 at high emission energy of 1.8eV. We expect the dependence to originate from variation in As concentration. Further analysis of g-factor is in progress and will be published elsewhere. Studies of nuclear spin pumping also reflect a trend of OHS and B_N values with QD energy emission. Degree of polarisation in this InPAs QD systems was found to reach 15%. This reflects not very efficient DNP for our sample, and ways to improve it may be needed. Data presented in this chapter opens the way for further investigation of the influence of As content. Additional to this, dynamic nuclear polarisation efficiency found on this system, allows for ODNMR studies which will enable composition and strain investigation as recently reported for InGaAs and InP QDs [8].

5.2 Future work

Future experiments related to the results obtained in the present thesis which could be of interest.

5.2.1 Coherent control in InP/GaInP quantum dots

Photocurrent technique (PC) has demonstrated to be a powerful experimental tool for coherent control of spin states in quantum dots, specially for InAs/GaAs [9]. With the first demonstration of resonant manipulation and electrical detection of excitons in single InP/GaInP QDs presented in chapter 2, we open the possibility

of engineering InP/GaInP QD structures for coherent control of the hole spin, which has been successfully demonstrated for InA/GaAs [10].

5.2.2 Voltage control of nuclear spin polarisation

The hyperfine interaction of electron-nuclear spins is responsible of nuclear spin polarisation, due to electron spin flip-flop. One of the principal obstacles for more effective nuclear spin pumping is the injection of polarised electron spins effectively into the dot due to Pauli blocking. Hence, the tunneling rate of an electron spin within a QD can be controlled by applying electric fields in a Schottky diode structure. Dependence of nuclear spin with applied voltage has been already reported [11, 12]. Additional to this, significant DNP on singly charge excitons in InAs/GaAs QDs has been probed [3], similar effect could be expected for charge excitons in InP/GaInP. QDs.

5.2.3 Inverse nuclear magnetic resonance for material characterization

NMR provides a non-destructive technique for structural analysis, but has been restricted only to unstrained semiconductor nanostructures [13, 14]. Just recently, a variation of the optically detected NMR has been reported, which allows analysis of individual strained quantum dot [8]. This new ODNMR technique allows to measure strain distribution and chemical compositions of intriguing new QD systems like InPAs/GaInP presented in chapter 4. Additional to this, we could obtain precise control of nuclear spins [15] in the presence of strong quadrupole effects on QD systems with high relatively high degrees of nuclear polarisation

like InGaAs/GaAs presented in chapter 3.

References

[1] E. A. Chekhovich. "Light-polarization-independent nuclear spin alignment in a quantum dot". In: *Phys. Rev. B* 83 (2011), p. 125318 (cit. on p. 100).

[2] D. Gammon. "Electron and Nuclear Spin Interactions in the Optical Spectra of Single GaAs Quantum Dots". In: *Phys. Rev. Lett.* 86 (2001), pp. 5176–5179 (cit. on p. 100).

[3] B. Eble. "Dynamic nuclear polarization of a single charge-tunable InAs GaAs quantum dot". In: *Phys. Rev. B* 74 (2006), p. 081306 (cit. on pp. 100, 102).

[4] J. Skiba-Szymanska. "Overhauser effect in individual InP/Ga_xIn_{1x}P dots". In: *Phys. Rev. B* 77 (2008), p. 165338 (cit. on p. 100).

[5] C.W. Lai. "Knight-field-enabled nuclear spin polarization in single quantum dots". In: *Phys. Rev. Lett.* 96 (2006), p. 167403 (cit. on p. 100).

[6] E. A. Chekhovich. "Pumping of Nuclear Spins by Optical Excitation of Spin-Forbidden Transitions in a Quantum Dot". In: *Phys. Rev. Lett.* 104 (2010), p. 066804 (cit. on p. 100).

[7] C. Latta. "Confluence of resonant laser excitation and bidirectional quantum-dot nuclear-spin polarization". In: *Nature Phys.* 5 (2009), p. 758 (cit. on p. 100).

[8] E. A. Chekhovich, K. V. Kavokin, and J. Puebla. "Structural analysis of strained quantum dots using nuclear magnetic resonance". In: *Nat. Nanotechnology* 7 (2012), 646650 (cit. on pp. 101, 102).

[9] A J Ramsay. "A review of the coherent optical control of the exciton and spin states of semiconductor quantum dots". In: *Semicond. Sci. Technol.* 25 (2010), p. 103001 (cit. on p. 101).

[10] T. M. Godden. "Coherent Optical Control of the Spin of a Single Hole in an InAs/GaAs Quantum Dot". In: *Physical Review Letters* 108 (2012), p. 017402 (cit. on p. 102).

[11] M. N. Makhonin. "Nuclear spin pumping under resonant optical excitation in a quantum dot". In: *Appl. Phys. Lett.* 93 (2008), p. 073113 (cit. on p. 102).

[12] A. Ebbens. "Optical orientation and control of spin memory in individual InGaAs quantum dots". In: *Phys. Rev. B* 72 (2005), p. 073307 (cit. on p. 102).

[13] D. Gammon. "Nuclear spectroscopy in single quantum dots: nanoscopic Raman scattering and nuclear magnetic resonance". In: *Science* 277 (1997), pp. 85–88 (cit. on p. 102).

[14] M.N. Makhonin. "Fast control of nuclear spin polarization in an optically pumped single quantum dot". In: *Nature Mat.* 10 (2011), pp. 844–848 (cit. on p. 102).

[15] Alexander V. Khaetskii. "Electron Spin Decoherence in Quantum Dots due to Interaction with Nuclei". In: *Phys. Rev. Lett.* 88 (2002), p. 186802 (cit. on p. 102).

Appdx A

This appendix contains the description of fabrication of quantum dot Schottky diode structures, and nanoapertures for micro-photoluminescence characterization.

.1 Quantum dot Schottky diode structure

Figure 1 shows schematic of QD Schottky diode structures. Sample A consisted of a QD layer grown on top of a 40 nm thick i-GaInP layer above the n-doped GaInP region (a). Capping was performed with a 160 nm-thickness i-GaInP layer only. Sample B consisted of a QD layer also grown 40 nm above the n-doped GaInP region, but capped by a sequence of undoped GaInP/AlGaInP/GaInP layers with thicknesses of 85, 25, and 50 nm, respectively, in order to create a blocking barrier for holes (b).

Non-resonant optical excitation above the transitions in the QDs create charges, which relax into the dot and then recombine. Charging can be controlled by applying electric field as seen in chapter 2. Resonant optical excitation with the transitions in the QDs create e-h pairs, which tunnel out of the dots under applied electric field and can be detected as photocurrent.

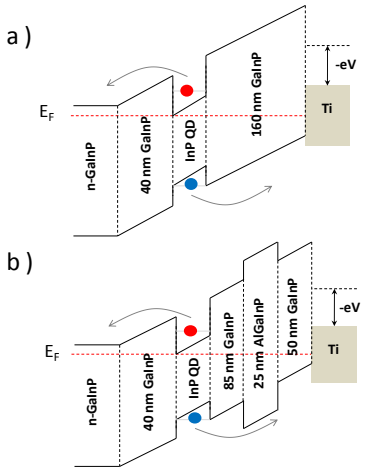

Figure 1: Schematic of quantum dot Schottky diode structures. Sample A used in chapter 2 is presented in top panel (a), and sample B used in the same chapter is presented in bottom panel (b).

.1.1 Device processing

QD dot wafers for samples A and B were processed into Schottky diodes with a combination of (i) optical lithography to define diode structure shapes, (ii) chemical etching to define paths for electric contacts, (iii) metal deposition.

Figure 2 shows a photograph of a fully finished Schottky device. Labels on the photograph show the Ohmic contact (bottom), Schottky contact, Large mesas with rough dimensions of $350\mu m$ x $400\mu m$ and small mesas $150\mu m$ x $250\mu m$. Beneath the Schottky contact and across the mesa a semi-transparent Titanium layer of 8-10nm thick is indicated.

Figure 3 shows nano apertures for micro-PL characterisation. Top panel shows a optic microscope photograph of the array of apertures with sizes from 400 to 1000nm (a). Bottom panel shows a SEM image of one aperture with dimension of about $1\mu m$ (b).

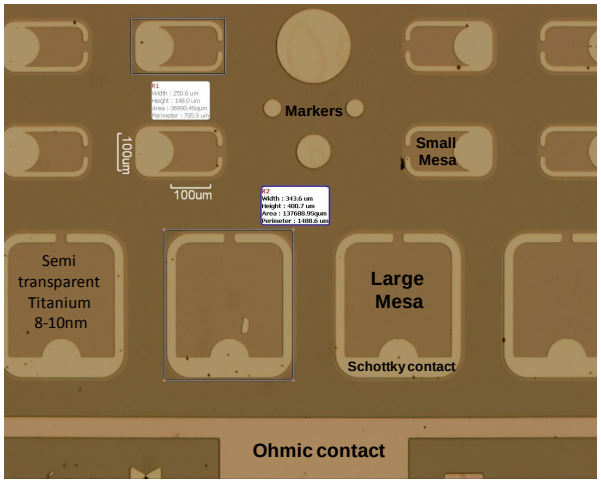

Figure 2: Photograph of fully finished quantum dot Schottky device. Labels indicate the Ohmic contact (bottom), Schottky contact, Large mesas, small mesas. Beneath the Schottky contact and across the mesa a semi-transparent Titanium layer of 8-10nm thick is indicated.

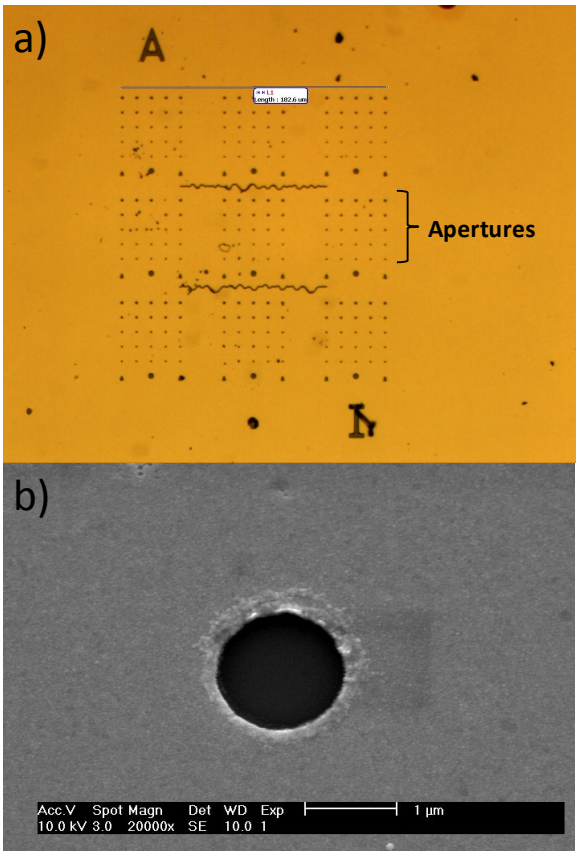

Figure 3: Nano-apertures for micro-PL characterisation. Top panel shows a optic microscope photograph of the array of apertures with sizes from 400 to 1000nm (a). Bottom panel shows a SEM image of one aperture with dimension of about $1\mu m$ (b).

Appdx B

In this appendix we present the technical details of the Charge Coupled Device used for detection in most of the experiments presented in this thesis.

.2 CCD Detection System

The detection system used for the experiments presented in this thesis were carried out with a Spectrum One CCD3000 of Jobin Yvon Horiba company. The CCD is a liquid nitrogen LN_2 cooled system. The most relevant feature for the analysis for our data is the quantum efficiency curves of the detector chips. Figure 4 shows quantum efficiency curves of Spectrum One CCD3000 chips. Top panel shows Q.E. curves for SiTe chips, and bottom panel Q.E. curves for EEV CCD chips.

The Q.E. significantly drops down below 50% after 800nm, which is an important data when analyse PL intensity in our data.

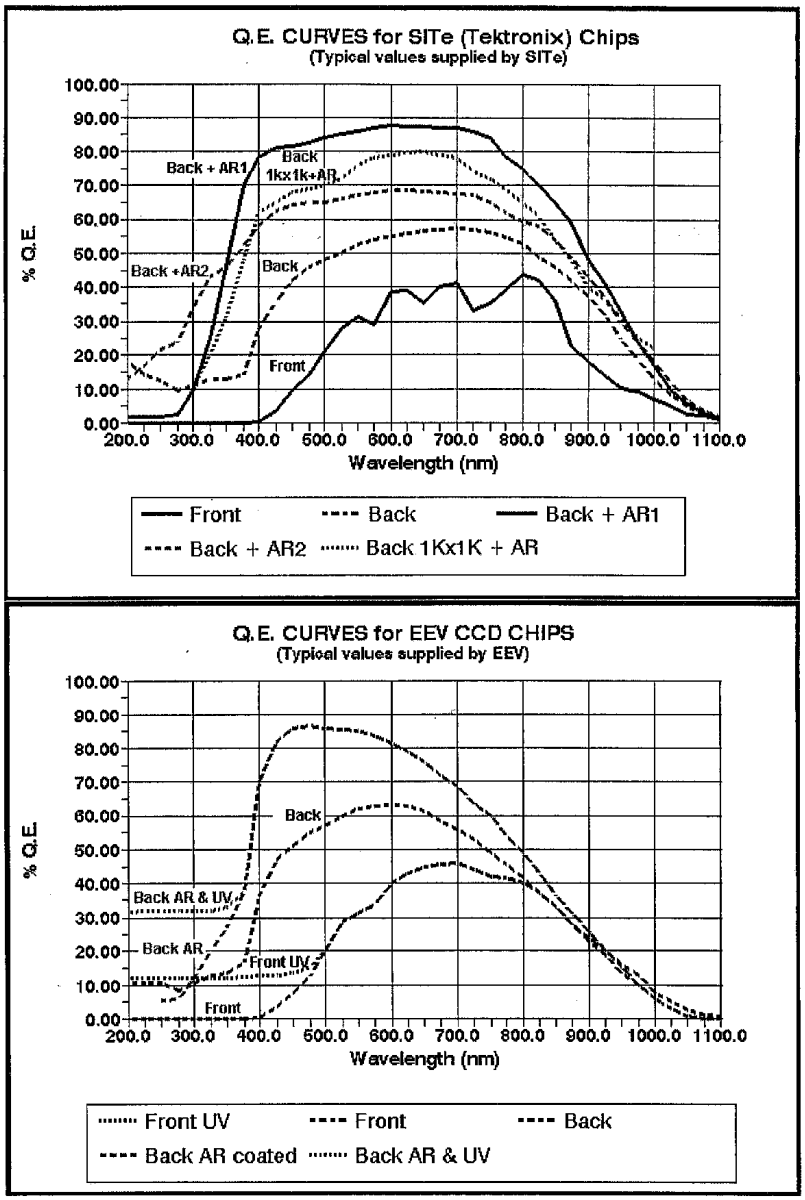

Figure 4: Quantum efficiency curves of Spectrum One CCD3000 chips. Top panel shows Q.E. curves for SiTe chips, and bottom panel Q.E. curves for EEV CCD chips.